Biophysical Force on the T-Cell Receptor Fosters Digital Antigen Responsiveness and Exquisite Specificity during T-Cell Activation

By

Yinnian Feng

Dissertation

Submitted to the Faculty of the

Graduate School of Vanderbilt University

in partial fulfillment of the requirements

for the degree of

DOCTOR OF PHILOSOPHY

in

Chemical Engineering

May 11, 2018

Nashville, Tennessee

Approved:

Matthew J. Lang, Ph.D.

Jamey Young, Ph.D.

John T. Wilson, Ph.D.

Ryoma Ohi, Ph.D.

I dedicate this dissertation to my parents for their love and sacrifices and to my wife for her unwavering support and encouragement.

ACKNOWLEDGMENTS

Shakespeare had his quill-pen, Bernstein had his baton, and I? As a future biophysicist as well as a chemical engineer, I have my own unique "camera". It is truly a common sense that a camera's main function is "creating durable images by recording light". But to me, it is more than taking pictures. Starting out in Vanderbilt is a wonderful journey full of creativity and discovery, which is the source of inspiration for my scientific research.

Science is a kaleidoscope. Just like the wave-particle duality nature of things, science always shows her stunning beauty from different perspectives. I still remember how excited and astonishing I was when I saw an optical trap system. I want to recognize my advisor, Matt Lang, for bring such a gaint but delicate "camera" to me, which lets me unveil the mystery of immunology from the physical perspective. Thank you for your seasoned guidance, infinite patience, and constant encouragement to me who at first had no idea what a T-cell receptor is. You are the reason that I want to pursue my future career as a scientist. Without your support, I wouldn't have been able to be as involved as I have been and my future would certainly look a little different. Thank you for your example and everything you have done for me.

This work would have not been completed without the contribution of my collaborators in the Laboratory of Immunobiology at Dana-Farber Cancer Institute. Here I very appreciate Dr. Reinherz for his great suggestions and help. You are a guiding star for me in the immunology area. I also want to thank Dr. Mallis, Dr. Brazin and Dr. Kobayashi for their experimental supporting on this T-cell mechanosensing project.

Studying in US as an international student is completely a brand-new experience to me. Frankly speaking I was a little freaked out initially. Fortunately, I have this great opportunity to work with talented and supportive lab mates, Dr. Yongdae Shin, Dr. Dibyendu Kumar Das, Dr. Juan Carlos (JC) Cordova, Dr. Sonia K Brady, Dr. Harris Manning, Dr. Dana (Nikki) N Reinemann, Dr. Mark Hilton. Yongdae taught me a lot of basic knowledge

about single molecule biophysics and I had a great time with him to talk about history. Dibyendu is like a big-bro to me and he is the one who broadens my view of science. I greatly thank Sonia for training me all the cell experiment. It is also my great honor to talk with JC and Harris about all ClpXP stuff. I also want to thank Nikki for her great example of hard work and perseverance though it is still a big challenging for me to wake up so early to prepare experiments. Thanks Mark for continuing doing part of my research, I am pretty sure you will do better than me. I also want to thank Zhu Hai for doing experiment with me for a month.

To the rest of my committee, Professors Jamey Young, John Wilson, and Ryoma (Puck) Ohi - thank you for your guidance and support over the last several years. Your great suggestions during the annual meeting are very helpful to my project.

I would be remiss if I did not acknowledge and thank all of you who have put in countless orders for me, made sure I got paid, responded to and fixed things around the lab, offered encouragement, and have brightened every day of my time at Vanderbilt with your smiles and love of life. Mary Gilleran, Rae Uson, Julie James, Angie Pernell, Mark Holmes and Felisha Baquera: THANK YOU! You are so appreciated.

To my ChBE Chinese friends: Guang Feng, Mingjie Wei, Li Wan, Song Li, Lili Gai, Shan Guo, Sichang Lu, Siyuan Yang, Yu Zhang, Xuanli Deng and Yajuan Shi. Thank you for the laughs, hotpot parties, and everything in Nashville. My life and science would be different without you.

I must say that performing single molecule on single immune cell is a very challenging project. As I remembered, I only triggered three T cells in the first two years after I joined Matt's lab. I am grateful for my parents with their stonecutter story they told me when I was a kid:"when nothing seems to help, I go and look at a stonecutter hammering away at his rock perhaps a hundred times without as much as a crack showing in it. Yet at the hundred and first blow it will split in two, and I know it was not that did it-but all that had gone before". It is this sprite that helps me conquer all the difficulties in my research.

Now I can proudly say that I have triggered more than ~500 cells. I also want to thank my wife, Mingwei Li. During the three years, I have realized that how deep the love you have given me. I will probably never be able to repay you, but thank you for your support and encourage.

As I look forward, I am excited to start my Post-doc life at Stanford. Matt gave me the opportunity to pursue my passions and follow my heart to do the RNA-seq but there have been so many others who have helped along the way. So, to everyone who has helped me in pursuing the science, THANK YOU!

TABLE OF CONTENTS

LIST OF FIGURES

CHAPTER 1

INTRODUCTION

*Sections 1.2-1.4 in this chapter are adapted from Yinnian Feng, Ellis L. Reinherz, and Matthew J. Lang, "$\alpha\beta$ TCR mechanosensing forces out serial engagement" under review.

1.1 Overview

The term immunity can be traced back to the Latin word *immunitas*, which originally comes from the Roman Senators with the authority of exempting people of Rome from military service, tax payments or other public services and lawsuit [1]. Nowadays, the meaning of immunity has been evolved to indicate the protection ability of cellular organisms to defense disease while having/building adequate tolerance and resistance to allergy and autoimmune diseases. The immune response, comprised of innate and adaptive immunity, is the reaction we make against infection by potential pathogens as well as dysfunctional cells such as cancer [2]. Innate immunity, as the first line to defense the invaders, responds nonspecifically to the antigen immediately or within hours after its appearance in the body [3]. The second line, termed as adaptive immunity, is a specific immune response towards the pathogens by the cooperation of abundant lymphocytes [4]. The adaptive immunity distinguishes itself from innate immunity with the properties of higher specificity and immunological memory [2]. The antigen must be digested at first, and then the heterogeneous fragment can be presented by the antigen presenting cells (APCs). Once an antigen has been recognized as an "enemy", the ammunition of adaptive immunity will be expanded by creating an army of immune cells that specifically aims and attacks that antigen. Adaptive immunity also includes a "memory" that responds more rapidly and effectively to a pathogen that has been encountered previously, granting long-lasting protection to reinfection with the same pathogen. Thus, it is more sophisticated than the innate immunity. With

these advantages, adaptive immune response has been focused on for most of the immunologists, trying to understand the mechanism in order to design personalized medicines, especially for the cancer therapy [5].

1.2 Adaptive immunity and $\alpha\beta$ T-cell recognition

The adaptive immune response is executed by two key lymphocytes known as B cells and T cells [6]. The former performs their tasks in antibody responses while the latter functions in cell mediated immune response. B Cells are the major cells to secret antibodies that circulate in blood stream and lymph, where they interact specifically to the pathogen to deactivate it or mark it for clearance or destruction [7]. Cell-mediated immunity is comprised of the activation of various immune cells such as macrophages, natural killer cells (NK), helper T-lymphocytes (CD4 T cells), antigen-specific cytotoxic T-lymphocytes (CD8 T cells), and the release of various cytokines in response to an antigen [8].

T-cell recognition of antigen forms the basis of adaptive immunity. Heterogeneous peptide information of the antigen needs to be presented on the surface of the APC and cradled by a cell surface glycoprotein termed as MHC (major histocompatibility complex). Invaders information is submitted to T cells by cell-cell attachment [9]. There are generally two subtypes of T cells involved into the T-cell recognition based on the types of coreceptors on their surface. T cell is termed as CD4 T cell or helper T cell with the expression of CD4 coreceptor on its surface whereas expression of CD8 coreceptor is the hallmark of CD8 T cell or cytotoxic T cell. CD4 and CD8 have the primary function of cooperating with the T cell receptor (TCR) for recognition of antigen-bound MHC. There are also two types of MHC molecules [10]. MHC class I are expressed on the surfaces of all nucleated cells, and class II, which are expressed exclusively on the surfaces of professional APCs such as macrophages, B cells and dendritic cells, presenting foreign antigens to CD4 T cells. The recognition of antigen-MHC II complex forms a TCR-MHC II-CD4 trimer that allows the activation and proliferation of antigen specific CD4 T cells and release of certain

cytokines. TCR on the CD4 T cells then interacts with the antigen-MHC II complex on B cells inducing the proliferation and differentiation of B cells. B cells change into plasma cells which secrete large quantities of antibodies targeting at the foreign agent with great sensitivity and specificity (affinity on nM scale). Infected nucleated cells can also function as Non-professional APCs, which submit antigens originating inside the cell to CD8 T cells. CD8 T cells can then discriminate peptides presented by MHC Class I molecules with the help of MHC I-CD8 coreceptor interaction. Compared to the antibody that deals with extracellular pathogens, CD8 T cells play a critical role in immune defense against intracellular pathogens such as viruses and bacteria as well as in recognition and elimination of cancer cells. When a CD8 T cell recognizes its antigen and becomes activated, it creates major weapons to kill infected or cancer cells, including secretion of cytokines (e.g. TNF-α and IFN-γ), production and release of cytotoxic granules into target cell by destruction of its membrane, and induction of programmed cell apoptosis inside the target cell through Fas/FasL interactions [8].

At the heart of this recognition process is a receptor-ligand interaction between variable domains on the T-cell receptor (TCR) and a peptide cradled in the groove of a major histocompatibility molecule, pMHC (refs. [11, 12] and references therein). A majority of T cells have a TCR composed of two glycoprotein chains called α- and β- TCR chains. There also exists a small subset of T cells that possess a distinct T cell receptor (TCR) on their surfaces. Such TCR is made up of one γ-chain and one δ-chain. This dissertation is focus on the $\alpha\beta$ T cells and omit the $\alpha\beta$ unless specifically mentioning.

T cells specifically recognize "foreign" peptides displayed on infected or otherwise perturbed cells through a process that discriminates with exquisite specificity. In so doing, T cells can discern a single amino-acid difference between two antigens. Antigen presenting cells (APCs) displaying peptide even at single molecule level (~1-3 molecules) can be recognized by T cells [13, 14]. From an equilibrium perspective and our basic understanding of receptor-ligand associations, one expects high affinity like the traditional

antigen-antibody interaction. TCR-pMHC affinities, however, as conventionally measured are in the micromolar range. Given the absence of somatic mutation in T cells, unlike in B cells, poor equilibrium affinity is not unexpected.

Notwithstanding, the paradox that a mere handful of foreign peptides is sufficient for cytotoxic T-lymphocytes (CTLs) to mount a deadly response or helper T cells to activate despite apparent weak affinity was thought to be explained through a concept known as serial engagement [15]. Conceptualized 25 years ago, serial engagement (or serial triggering) recycles a single pMHC through multiple sequential TCR binding events to collectively stimulate a T cell over a time period (seconds to hours) [16]. One ligand with intermediate affinity (K_D=~1-5 μM) on an APC can thus activate in series a number of TCRs on a given T cell where the sum of integrated receptor activation collectively suffices to turn the T cell 'ON' [17]. A fundamental limitation of this model is that it is not based on direct visualization and continuous measurement of the in situ dynamic interactions between TCRs and pMHCs at the live cell membrane, but instead on TCR down-regulation as a parameter of TCR occupancy to hypothesize reutilization of pMHC over a period of hours [18].

1.3 Nonequilibrium property of $\alpha\beta$ T-cell recognition

Physiologically, T cells undergoing immunosurveillance are highly mobile [19]. The polarized cells exhibit directed motion with frequent stops and turns, where, from such global motions, the underlying adhesions experience local stress and directional physical force [20]. Cellular structures such as lamellipodia and microvilli at the leading edge will facilitate T-cell activation [18, 21, 22] as well as the adoption of a scanning behavior that promotes local exploration of the microenvironment to find the strongest antigenic stimulation [23]. Later, T cells cluster their TCRs in the uropod, which is central to the cell and associated with actin retrograde flow [24, 25]. Collectively, immunosurveillance-based cell crawling, microvilli protrusion and cytoskeletal movements can generate forces ranging from pN to nN [26, 27, 28], as shown in Fig. 1.1.

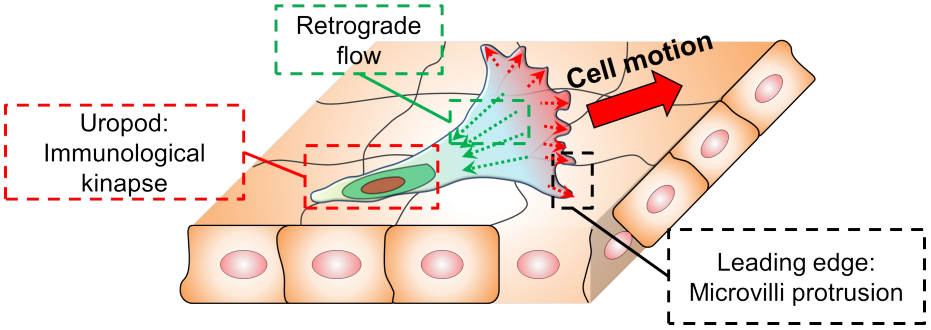

Figure 1.1: **In vivo T-cell immunosurveillance.** Cartoon showing in vivo T-cell immunosurveillance (red arrow) against the surface an epithelium or other interacting cells. Note that substantial mechanical forces are exerted by protrusion of microvilli (dashed red arrows) at the leading edge and the retrograde flow (dashed green arrows) due to cytoskeletal reorganization. The TCRs, initially localizing in microvilli [21, 29], will be transported by retrograde flow to the uropod, forming a kinapse.

After activation, a structure known as an immunological synapse (IS) on stationary cell interaction or a kinapse on motile cell interaction is formed [30]. Internal forces associated with these structures can be directly visualized by traction force microscopy (such as deformation of underlying elastic substrate or PDMS pillars) [31, 32, 33] or by signal changes in tension gauge tethers (TGT) (such as DNA/peptide force sensors) that open under force to emit a fluorescent signal (Fig. 1.2) [34].

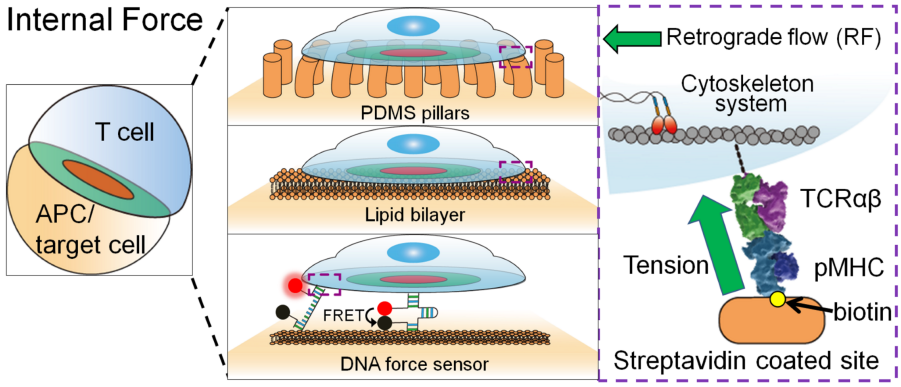

Figure 1.2: **Technologies for measuring and visualizing force generation during immune synapse maturation at the T cell-APC interacting surface.** Traction force microscopy (Polydimethylsiloxane (PDMS) pillar and lipid bilayer) and DNA force sensor are two typical methods. The detailed method descriptions are reviewed in [35]. Such internal forces are mainly driven by retrograde flow through reorganization of cellular cytoskeleton system, as highlighted in the purple box.

Technologies for applying external force and monitoring local stiffness include atomic force microscopy (AFM) [36], biomembrane force probe (BFP) [37, 38, 39], optomechanical actuator nanoparticles (OMA Np) [40], and optical trap/tweezers (OT) among others (Fig. 1.3) [41, 42].

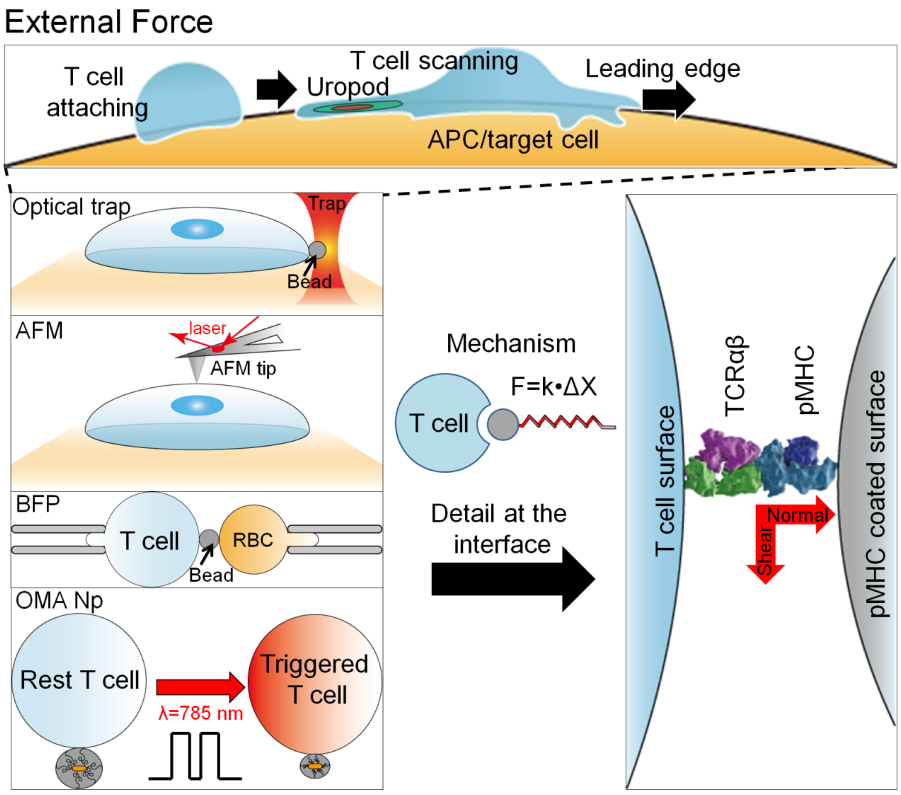

Figure 1.3: **Technologies for generating external force to imitate T-cell scanning APC/-target cell surface.** External force generated at the leading edge during T-cell scanning APC/target cell surface can be imitated by optical trap, AFM, BFP and OMA Np methods. All the methods are based on the spring-like features of the devices/material. With precise directional and distance control, optical traps are a superior technology for testing the mechanosensing of TCR on the T cell surface through a pMHC coated bead.

1.4 Optical trap and fluorescence microscopy

The optical trap, also known as optical tweezer, was first demonstrated and employed in the 1970's and 80's by Arthur Ashkin [43, 44, 45]. An optical trap is formed by tightly focusing a laser beam typically to a diffraction limited, micron sized volume. Light enters

and exits this region in a steep cone forming a gradient of intensities near the focus. The trapping strength and quality can be maximized by expanding the laser beam width to fill the back aperture of a high numerical aperture (NA) objective before being focused to a diffraction-limited point on the specimen. If a tiny object such as a micron sized plastic bead is near the focus, it is moved by photons entering, exiting and scattering off the object in a way that pulls it towards the center axis of the laser beam (Fig. 1.4). Optical

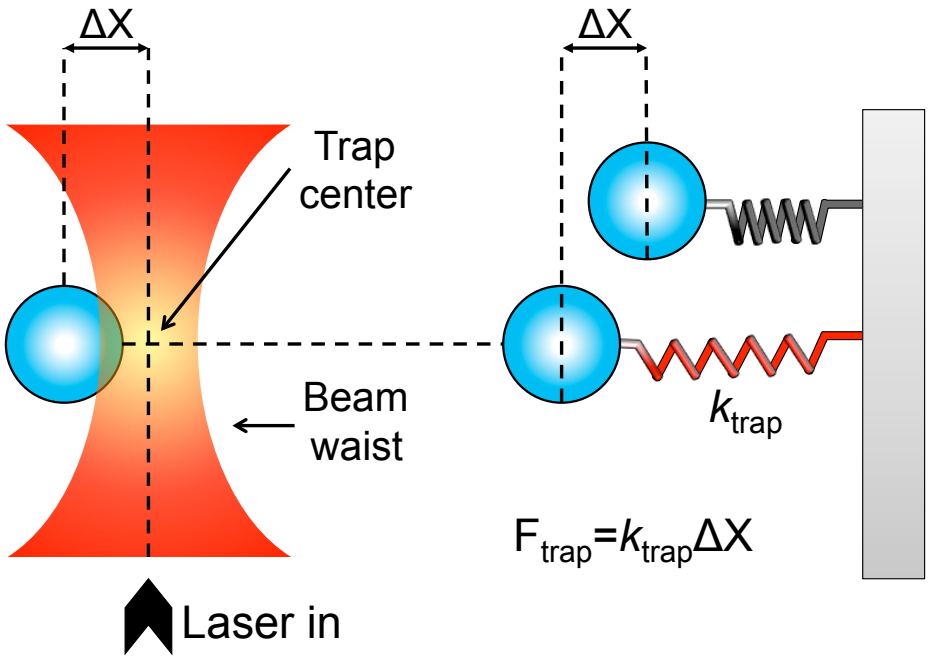

Figure 1.4: **Optical trapping.** An optical trap is formed by a tightly focused laser with a gaussian intensity closed to its diffraction limit by means of a high numerical aperature objective. The trapping phenomenon is usually applied to a dialectic polystyrene bead on a μm size scale. Brownian motion of the trapped particle near the trap center will balance with the restoring force by the trap. Principle of optical trapping has been well elaborated in [46]. The optical trap has a parameter termed as trap stiffness (k_{trap}) that is akin to the spring stiffness so that a trapped bead with ΔX distance from trap center will function as a Hookean spring system.

traps effectively represent a light based 'pick and place' tool for manipulating small objects. If one moves the laser one moves the trapped object. Using position-sensing systems akin to super-resolution methods, one can determine the center location of an object to nanometer level precision. Typically, an optical trapping system can be interlaced with a second laser, termed as a detection laser, to track the position of trapped object relative

to the trap center with precise spatiotemporal resolution [46, 47, 48]. The spatial resolution is generally on the nanometer scale but can be enhanced with resolutions up to 3 $\mathring{A}$ [49, 50]. In our case, position detection is performed by an NIR (near-IR,) laser at low power ($\sim$ 1/10 the power of the trapping laser) with a wavelength (975 nm) slightly below the trapping laser (1064nm) to limit interference with the trap by creating a secondary trap as well as to allow for combination with trapping laser but differentiation of the signals. In addition to exceptional position resolution, the properties of the optical trap for small displacements (~200 nm) are spring like or Hookean. The effective stiffness of the spring can be controlled by changing the power of the laser. An object in the center of the trap will exhibit fluctuations (Brownian motion) due to thermal energy of surrounding water bath kicking the object against the center position of this optical spring. This spread in position has a Gaussian distribution that can be linked to the stiffness of the trap. The trapping property exists when the object has a refraction index larger than the surrounding medium and when the size of the trapped object and wavelength of the trapping laser are close to each other. However, the sizes of many biological species (e.g. soluble protein) ranges from 1 nm to several tens of nm so that direct capture of interest protein becomes less practical as the force that can be applied is limited and they are difficult to visualize as restriction of diffraction limit. The modern super-resolution microscopies (e.g. PALM, STORM, STED and SIM, reviewed in [51]) make the direct observation of proteins possible but still their precise mechanobiology properties are obscure. Therefore, biophysicists use dielectric beads functionalized with certain motor protein or ligand respectively to indirectly apply precise force to visualize the mechanobiological behavior of motor protein or ligand associated receptor. For biological system, the laser heating is a big issue as it may cause some serious disruption due to the absorption [52]. Here we use an 1064-nm trapping laser as light at these wavelengths cause the least absorption in biological samples [53, 54, 55]. The trap stiffness k_{trap} is calibrated based on equipartition method

$$\frac{1}{2}k_BT = \frac{1}{2}k_{trap}(\Delta X)^2$$

in which ΔX is the distance from the center of the trapped particle to the center of the trap, k_B is Boltzmann constant and T is the experiment temperature. If one can track the position variance of a trapped object, then the trap stiffness can be calculated without taking the viscosity of the surrounding medium or the geometry of the object into consideration. Measuring the displacement of the bead from the center of the trap, one multiplies this by the spring constant of the trap k to obtain the force. Force = $k_{trap}\Delta$X. (The trap stiffness is measured straightforwardly and is in typically in units of pN/nm). Optical traps are excellent for exerting forces in the range of sub-pN to ~100 pN.

When a trapped bead binds to an object, the distribution of fluctuations changes due to the system now being effectively coupled to an additional spring. Thus one can observe the width of the distribution to track molecular association, binding and unbinding, and even re-binding events with optical traps (optical tweezers) based single molecule methods. As the TCR-pMHC interaction initiates T-cell recognition that happens in a non-equilibrium process, Chapter 2 of this dissertation will first focus on this interaction under certain load from both single molecule and single molecule on single cell level. The manipulation ability of tweezers paired with the ability to directly visualize binding events also make this an ideal tool for testing serial engagement mechanisms. In Chapter 3, beads that mimic antigen presenting cells, are coated with pMHC at known molecular densities. By using a combination of optical trapping and single cell epifluorescence imaging one can directly visualize the external force induced early T-cell activation. Beads are then trapped and transported to a surface bound cell where associations are actively facilitated. We systematically monitored the ability of forced induced T-cell activation with a range of beads from high molecular densities (non-physiological) to single molecule interactions. Using the same methodology, in Chapter 4 we are focusing on two additional molecules involved in early T-cell activation. Locally, CD3 complex as a TCR signaling transduction com-

ponent may undergo force involved reorganization. Meanwhile during activation, CD45 molecules as an activation inhibitor will segregate away from the T-cell/APC contact area where TCRs are accumulated. The possible biophysical mechanism of such segregation will also be explored.

1.5 Acknowledgement

We thank Vanderbilt University Medical Center Flow Cytometry Shared Resource supported by the Vanderbilt-Ingram Cancer Center (NIH Grant CA68485) and the Vanderbilt Digestive Disease Research Center (NIH Grant DK058404). This work was supported by NIH Grants R01AI100643, R01AI37581, P01GM047467 and R56AI138489 as well as SU2C-AACR-DT13-14.

1.6 Bibliography

[1] Joseph Plescia. Judicial accountability and immunity in roman law. *The American Journal of Legal History*, 45(1):51–70, 2001.

[2] David D Chaplin. Overview of the immune response. *Journal of Allergy and Clinical Immunology*, 125(2):S3–S23, 2010.

[3] Shizuo Akira, Satoshi Uematsu, and Osamu Takeuchi. Pathogen recognition and innate immunity. *Cell*, 124(4):783–801, 2006.

[4] Anne Sperling and Jeffrey A. Bluestone. Acquired immune response. In Peter J. Delves, editor, *Encyclopedia of Immunology (Second Edition)*, pages 13 – 15. Elsevier, Oxford, second edition edition, 1998.

[5] Matthew D Vesely, Michael H Kershaw, Robert D Schreiber, and Mark J Smyth. Natural innate and adaptive immunity to cancer. *Annual review of immunology*, 29:235–271, 2011.

[6] E John Wherry and David Masopust. Adaptive immunity: Neutralizing, eliminating, and remembering for the next time. In *Viral Pathogenesis (Third Edition)*, pages 57–69. Elsevier, 2016.

[7] Harry W Schroeder and Lisa Cavacini. Structure and function of immunoglobulins. *Journal of Allergy and Clinical Immunology*, 125(2):S41–S52, 2010.

[8] Kenneth Murphy and Casey Weaver. *Janeway's immunobiology*. Garland Science, 2016.

[9] Matthias Gunzer, Carsten Weishaupt, Anja Hillmer, Yasmin Basoglu, Peter Friedl, Kurt E Dittmar, Waldemar Kolanus, Georg Varga, and Stephan Grabbe. A spectrum of biophysical interaction modes between t cells and different antigen-presenting cells during priming in 3-D collagen and in vivo. *Blood*, 104(9):2801–2809, 2004.

[10] Jacques Neefjes, Marlieke LM Jongsma, Petra Paul, and Oddmund Bakke. Towards a systems understanding of MHC class I and MHC class II antigen presentation. *Nature Reviews Immunology*, 11(12):823, 2011.

[11] Jia-huai Wang and Ellis L. Reinherz. The structural basis of $\alpha\beta$ T-lineage immune recognition: TCR docking topologies, mechanotransduction, and co-receptor function. *Immunological Reviews*, 250(1):102–119, 2012.

[12] Lei Yin, James Scott-Browne, John W Kappler, Laurent Gapin, and Philippa Marrack. T cells and their eons-old obsession with MHC. *Immunological reviews*, 250(1):49–60, 2012.

[13] Marco A. Purbhoo, Darrell J. Irvine, Johannes B. Huppa, and Mark M. Davis. T cell killing does not require the formation of a stable mature immunological synapse. *Nat Immunol*, 5(5):524–530, 2004. 10.1038/ni1058.

[14] Jun Huang, Mario Brameshuber, Xun Zeng, Jianming Xie, Qi-jing Li, Yueh-hsiu Chien, Salvatore Valitutti, and Mark M Davis. A single peptide-major histocompatibility complex ligand triggers digital cytokine secretion in CD4+ T cells. *Immunity*, 39(5):846–857, 2013.

[15] Salvatore Valitutti. The serial engagement model 17 years after: From TCR triggering to immunotherapy. *Frontiers in Immunology*, 3(272), 2012.

[16] Salvatore Valitutti, Sabina Muller, Marina Cella, Elisabetta Padovan, and Antonio Lanzavecchia. Serial triggering of many T-cell receptors by a few peptide MHC complexes. *Nature*, 375(6527):148–151, 1995. 10.1038/375148a0.

[17] Melita Irving, Vincent Zoete, Michael Hebeisen, Daphné Schmid, Petra Baumgartner, Philippe Guillaume, Pedro Romero, Daniel Speiser, Immanuel Luescher, Nathalie Rufer, et al. Interplay between T cell receptor binding kinetics and the level of cog-

nate peptide presented by major histocompatibility complexes governs CD8+ T cell responsiveness. *Journal of Biological Chemistry*, 287(27):23068–23078, 2012.

[18] Salvatore Valitutti, Daniel Coombs, and Loïc Dupré. The space and time frames of T cell activation at the immunological synapse. *FEBS letters*, 584(24):4851–4857, 2010.

[19] Sarah E. Henrickson, Thorsten R. Mempel, Irina B. Mazo, Bai Liu, Maxim N. Artyomov, Huan Zheng, Antonio Peixoto, Michael Flynn, Balimkiz Senman, Tobias Junt, Hing C. Wong, Arup K. Chakraborty, and Ulrich H. von Andrian. In vivo imaging of T cell priming. *Science Signaling*, 1(12):pt2–pt2, 2008.

[20] Jianping Fu, Yang-Kao Wang, Michael T. Yang, Ravi A. Desai, Xiang Yu, Zhijun Liu, and Christopher S. Chen. Mechanical regulation of cell function with geometrically modulated elastomeric substrates. *Nat Meth*, 7(9):733–736, 2010. 10.1038/nmeth.1487.

[21] Yunmin Jung, Inbal Riven, Sara W Feigelson, Elena Kartvelishvily, Kazuo Tohya, Masayuki Miyasaka, Ronen Alon, and Gilad Haran. Three-dimensional localization of T-cell receptors in relation to microvilli using a combination of superresolution microscopies. *Proceedings of the National Academy of Sciences*, 113(40):E5916–E5924, 2016.

[22] Stephen C Bunnell, David I Hong, Julia R Kardon, Tetsuo Yamazaki, C Jane McGlade, Valarie A Barr, and Lawrence E Samelson. T cell receptor ligation induces the formation of dynamically regulated signaling assemblies. *The Journal of cell biology*, 158(7):1263–1275, 2002.

[23] Hélène D Moreau, Fabrice Lemaître, Kym R Garrod, Zacarias Garcia, Ana-Maria Lennon-Duménil, and Philippe Bousso. Signal strength regulates antigen-mediated

T-cell deceleration by distinct mechanisms to promote local exploration or arrest. *Proceedings of the National Academy of Sciences*, 112(39):12151–12156, 2015.

[24] AlexT Ritter, Yukako Asano, JaneC Stinchcombe, N. M. G. Dieckmann, Bi-Chang Chen, C. Gawden-Bone, Schuyler vanEngelenburg, Wesley Legant, Liang Gao, MichaelW Davidson, Eric Betzig, Jennifer Lippincott-Schwartz, and GillianM Griffiths. Actin depletion initiates events leading to granule secretion at the immunological synapse. *Immunity*, 42(5):864–876, 2015.

[25] Elena V. Tibaldi, Ravi Salgia, and Ellis L. Reinherz. CD2 molecules redistribute to the uropod during T cell scanning: Implications for cellular activation and immune surveillance. *Proceedings of the National Academy of Sciences*, 99(11):7582–7587, 2002.

[26] Revathi Ananthakrishnan and Allen Ehrlicher. The forces behind cell movement. *International journal of biological sciences*, 3(5):303, 2007.

[27] Lin Ji, James Lim, and Gaudenz Danuser. Fluctuations of intracellular forces during cell protrusion. *Nature cell biology*, 10(12):1393–1400, 2008.

[28] Xavier Trepat, Michael R Wasserman, Thomas E Angelini, Emil Millet, David A Weitz, James P Butler, and Jeffrey J Fredberg. Physical forces during collective cell migration. *Nature physics*, 5(6):426–430, 2009.

[29] En Cai, Kyle Marchuk, Peter Beemiller, Casey Beppler, Matthew G Rubashkin, Valerie M Weaver, Audrey Gérard, Tsung-Li Liu, Bi-Chang Chen, Eric Betzig, et al. Visualizing dynamic microvillar search and stabilization during ligand detection by T cells. *Science*, 356(6338):eaal3118, 2017.

[30] Michael L Dustin. T-cell activation through immunological synapses and kinapses. *Immunological reviews*, 221(1):77–89, 2008.

[31] Keenan T. Bashour, Alexander Gondarenko, Haoqian Chen, Keyue Shen, Xin Liu, Morgan Huse, James C. Hone, and Lance C. Kam. CD28 and CD3 have complementary roles in T-cell traction forces. *Proceedings of the National Academy of Sciences*, 111(6):2241–2246, 2014.

[32] Roshni Basu, BenjaminM Whitlock, Julien Husson, Audrey LeFloch, Weiyang Jin, Alon Oyler-Yaniv, Farokh Dotiwala, Gregory Giannone, Claire Hivroz, Nicolas Biais, Judy Lieberman, LanceC Kam, and Morgan Huse. Cytotoxic T cells use mechanical force to potentiate target cell killing. *Cell*, 165(1):100–110, 2016.

[33] King Lam Hui, Lakshmi Balagopalan, Lawrence E. Samelson, and Arpita Upadhyaya. Cytoskeletal forces during signaling activation in jurkat T-cells. *Molecular Biology of the Cell*, 26(4):685–695, 2015. E14-03-0830[PII] 25518938[pmid] Mol Biol Cell.

[34] Yang Liu, Lori Blanchfield, Victor Pui-Yan Ma, Rakieb Andargachew, Kornelia Galior, Zheng Liu, Brian Evavold, and Khalid Salaita. DNA-based nanoparticle tension sensors reveal that T-cell receptors transmit defined pN forces to their antigens for enhanced fidelity. *Proceedings of the National Academy of Sciences*, 113(20):5610–5615, 2016.

[35] Yang Liu, Kornelia Galior, Victor Pui-Yan Ma, and Khalid Salaita. Molecular tension probes for imaging forces at the cell surface. *Accounts of chemical research*, 50(12):2915–2924, 2017.

[36] Kenneth H. Hu and Manish J. Butte. T cell activation requires force generation. *The Journal of Cell Biology*, 213(5):535–542, 2016.

[37] Julien Husson, Karine Chemin, Armelle Bohineust, Claire Hivroz, and Nelly Henry. Force generation upon T cell receptor engagement. *PLoS One*, 6(5):e19680, 2011.

[38] Ya-Chen Li, Bing-Mae Chen, Pei-Chun Wu, Tian-Lu Cheng, Lung-Sen Kao, Mi-Hua Tao, Andre Lieber, and Steve R. Roffler. Cutting edge: Mechanical forces acting on T cells immobilized via the TCR complex can trigger TCR signaling. *The Journal of Immunology*, 184(11):5959–5963, 2010.

[39] Baoyu Liu, Wei Chen, Brian D Evavold, and Cheng Zhu. Accumulation of dynamic catch bonds between TCR and agonist peptide-MHC triggers T cell signaling. *Cell*, 157(2):357–368, 2014.

[40] Zheng Liu, Yang Liu, Yuan Chang, Hamid Reza Seyf, Asegun Henry, Alexa L Mattheyses, Kevin Yehl, Yun Zhang, Zhuangqun Huang, and Khalid Salaita. Nanoscale optomechanical actuators for controlling mechanotransduction in living cells. *nature methods*, 13(2):143, 2016.

[41] Yinnian Feng, Kristine N Brazin, Eiji Kobayashi, Robert J Mallis, Ellis L Reinherz, and Matthew J Lang. Mechanosensing drives acuity of $\alpha\beta$ T-cell recognition. *Proceedings of the National Academy of Sciences*, page 201703559, 2017.

[42] Sun Taek Kim, Koh Takeuchi, Zhen-Yu J Sun, Maki Touma, Carlos E Castro, Amr Fahmy, Matthew J Lang, Gerhard Wagner, and Ellis L Reinherz. The $\alpha\beta$ T cell receptor is an anisotropic mechanosensor. *Journal of Biological Chemistry*, 284(45):31028–31037, 2009.

[43] Arthur Ashkin. Acceleration and trapping of particles by radiation pressure. *Physical review letters*, 24(4):156, 1970.

[44] Arthur Ashkin and JM Dziedzic. Optical levitation by radiation pressure. *Applied Physics Letters*, 19(8):283–285, 1971.

[45] Arthur Ashkin, JM Dziedzic, JE Bjorkholm, and Steven Chu. Observation of a single-beam gradient force optical trap for dielectric particles. *Optics letters*, 11(5):288–290, 1986.

[46] Keir C Neuman and Steven M Block. Optical trapping. *Review of scientific instruments*, 75(9):2787–2809, 2004.

[47] Matthew J Lang, Charles L Asbury, Joshua W Shaevitz, and Steven M Block. An automated two-dimensional optical force clamp for single molecule studies. *Biophysical journal*, 83(1):491–501, 2002.

[48] Thomas T Perkins. Optical traps for single molecule biophysics: a primer. *Laser & Photonics Reviews*, 3(1-2):203–220, 2009.

[49] Joshua W Shaevitz, Elio A Abbondanzieri, Robert Landick, and Steven M Block. Backtracking by single RNA polymerase molecules observed at near-base-pair resolution. *Nature*, 426(6967):684–687, 2003.

[50] Elio A Abbondanzieri, William J Greenleaf, Joshua W Shaevitz, Robert Landick, and Steven M Block. Direct observation of base-pair stepping by RNA polymerase. *Nature*, 438(7067):460–465, 2005.

[51] Bo Huang, Mark Bates, and Xiaowei Zhuang. Super-resolution fluorescence microscopy. *Annual review of biochemistry*, 78:993–1016, 2009.

[52] Leslie Wilson, Paul T Matsudaira, and Michael P Sheetz. *Laser tweezers in cell biology*, volume 55. Academic Press, 1997.

[53] I.A. Vorobjev, H. Liang, W.H. Wright, and M.W. Berns. Optical trapping for chromosome manipulation: a wavelength dependence of induced chromosome bridges. *Biophysical Journal*, 64(2):533 – 538, 1993.

[54] H. Liang, K.T. Vu, P. Krishnan, T.C. Trang, D. Shin, S. Kimel, and M.W. Berns. Wavelength dependence of cell cloning efficiency after optical trapping. *Biophysical Journal*, 70(3):1529 – 1533, 1996.

[55] Keir C. Neuman, Edmund H. Chadd, Grace F. Liou, Keren Bergman, and Steven M. Block. Characterization of photodamage to Escherichia coli in optical traps. *Biophysical Journal*, 77(5):2856 – 2863, 1999.

CHAPTER 2

SINGLE-MOLECULE OPTICAL TRAPPING REVEALS THAT $\alpha\beta$TCR IS A MECHANOSENSOR

*This chapter is adapted from Das et al, "Force-dependent transition in the T-cell receptor β-subunit allosterically regulates peptide discrimination and pMHC bond lifetime" Proceedings of the National Academy of Sciences 112 (5), 1517-1522 (2014) by permission granted under the Liberalization of Proceedings of the National Academy of Sciences (PNAS) copyright policy.

2.1 Summary

The $\alpha\beta$ T-cell receptor (TCR) on each T lymphocyte mediates exquisite specificity for a particular foreign peptide bound to a major histocompatibility complex molecule (pMHC) displayed on the surface of altered cells. This recognition stimulates protection in the mammalian host against intracellular pathogens, including viruses, and involves piconewton forces that accompany pMHC ligation. Physical forces are generated by T-lymphocyte movement during immune surveillance as well as by cytoskeletal rearrangements at the immunological synapse following cessation of cell migration. The mechanistic explanation for how TCRs distinguish between foreign and self-peptides bound to a given MHC molecule is unclear: peptide residues themselves comprise few of the TCR contacts on the pMHC, and pathogen-derived peptides are scant among myriad self-peptides bound to the same MHC class arrayed on infected cells. Using optical tweezers and DNA tether spacer technology that permit piconewton force application and nanometer scale precision, we have determined how bioforces relate to self versus nonself discrimination. Single-molecule analyses involving isolated $\alpha\beta$-heterodimers as well as complete TCR complexes on T lymphocytes reveal that the FG loop in the β-subunit constant domain allosterically

controls both the variable domain modules catch bond lifetime and peptide discrimination via force-driven conformational transition. In contrast to integrins, the TCR interrogates its ligand via a strong force-loaded state with release through a weakened, extended state. Our work defines a key element of TCR mechanotransduction, explaining why the FG loop structure evolved for adaptive immunity in $\alpha\beta$ but not $\gamma\delta$TCRs or immunoglobulins.

2.2 Introduction

Antigen recognition by T lymphocytes is a crucial feature of adaptive immunity. This process requires the interaction of a clone-specific T-cell receptor (TCR) via its membrane distal variable module with a cognate peptide bound to a major histocompatibility complex molecule (pMHC) (refs. [1, 2] and references therein). Foreign peptide antigens derived from infectious or other cell-altering processes including oncogenic transformation are presented either on a surface of the perturbed cell directly or indirectly via cross-presentation on antigen-presenting cells (APC). In either case, ligation of the relevant TCR$\alpha\beta$ heterodimer initiates a cascade of T-cell signaling events following exposure of the immunoreceptor tyrosine-based activation motif (ITAM) elements in the cytoplasmic tail of the noncovalently associated subunits (CD3$\epsilon\gamma$, CD3$\epsilon\delta$, and CD3$\zeta\zeta$) composing the TCR complex in 1:1:1:1 dimer stoichiometry. This accessibility allows the active kinase, Lck, to bind and phosphorylate ITAMs followed by recruitment and activation of a second tyrosine kinase, ZAP-70 [3, 4, 5, 6]. In turn, multiple downstream pathways are engaged, including transcriptional regulators controlling activation and differentiation of T cells [7, 8]. Thymocyte development is also regulated by the TCR-pMHC interaction as it relates to repertoire selection, generating millions of useful TCRs with diverse specifications (reviewed in ref. [9]).

The MHC-bound peptides recognized by T cells are typically 811 amino acids in length with single amino acid substitutions readily sensed and discriminated by a TCR. During immune surveillance, an individual high-avidity T cell has the capacity to detect several

copies of a specific pMHC on the APC that expresses 100,000 chemically similar pMHC molecules. Discrimination of foreign vs. myriad self-peptides is manifest with precision; if this were not the case, then either autoimmunity or immunodeficiency would result. How TCRs are capable of mediating such exquisite specificity and sensitivity has remained a mystery, especially in view of the fact that, unlike with B-cell receptors, there is no somatic hypermutation of TCR genes and monomeric TCR-pMHC affinities are orders of magnitude weaker than high-affinity antibodyantigen interactions [10].

Very recently, it has become clear that the TCR functions as a mechanosensor. Kim et al. provided the first, to our knowledge, direct evidence of the influence of mechanical force in TCR activation [11]. Using an optically trapped bead coated with pMHC or anti-CD3 monoclonal antibody for engaging the TCR, T cells were mechanically triggered by applying an oscillating tangential force to the cell surface while monitoring their activation via intracellular calcium flux. Importantly, piconewton (pN) force application with cognate pMHC but not irrelevant pMHC triggered activation. Additional mechanosensor evidence was provided in subsequent studies by Li using a micropipette to demonstrate shear force associated with activation [12] and by Husson using a biomembrane force probe (BFP) to reveal pushing and pulling associated with T-cell triggering [13]. Triggering was also shown to depend on substrate stiffness [14]. Prediction that a nonlinear mechanical response such as catch bond formation might facilitate TCR-based recognition [11] was elegantly confirmed by Zhu and coworkers using a BFP [15]. Given the complexities of surface-antigen display on an APC and the physical forces associated with cellular migration, specific structural adaptations must exist for the TCR to work in such a chemically and physically noisy environment. Here we use single-molecule (SM) techniques to search for such relevant mechanotransduction features, identifying the TCR$\alpha\beta$ heterodimer as a finely tuned allosteric regulator of force-driven peptide discrimination.

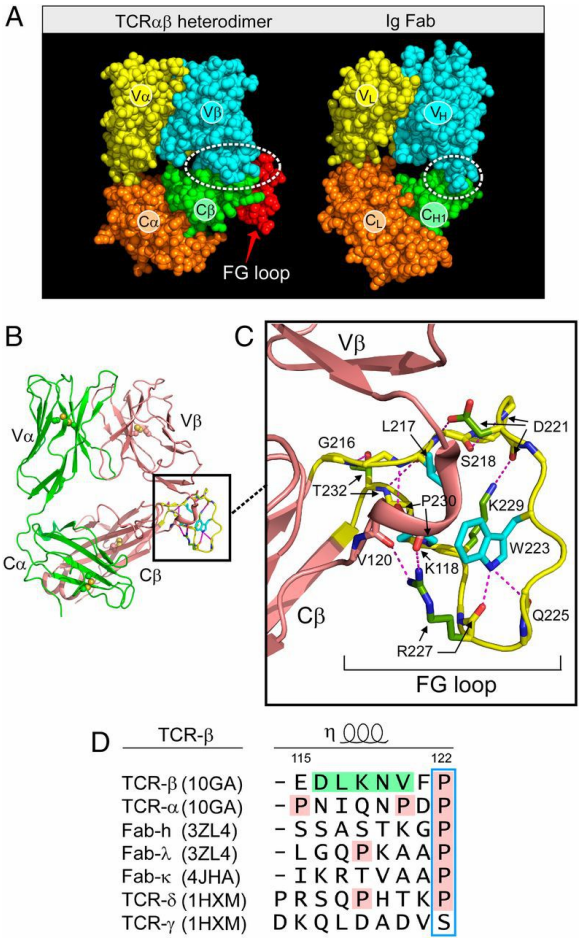

Figure 2.1: **The CβFG loop region includes a structured element expanding the β-subunit interface between its variable and constant domains and an adjacent Vβ-Cβ connector.** (A) Comparison of TCR$\alpha\beta$ heterodimer (1OGA) and Ig Fab (4JFX) fragments with comparable domains delineated in their respectively colored CPK format. (B) Ribbon diagram of TCR$\alpha\beta$ heterodimer with FG loop highlighted in yellow. (C) Magnified view of the CβFG loop region with three conserved hydrophobic loop residues indicated in blue and hydrogen bonds in dashed red. Note the 3_{10} helix in the connector linking Vβ and Cβ domains in brown. (D) Connector sequences of different V-C domains indicated with numbering of sequence according to TCRβ and relevant structural alignment. PDB numbering for each structure is indicated.

2.3 Results

2.3.1 Structural Features of the Cβ FG Loop as a Focus of Single-Molecule Analysis

As shown in Fig. 2.1A, the TCR$\alpha\beta$ heterodimer is very similar in overall topology to an Ig Fab fragment, consisting of a paired variable module (VαVβ vs. V_LV_H) linked to

a constant domain module (CαCβ vs. C_LC_{H1}). Moreover, the overall height and width of these structures are similar [16]. Closer inspection, however, reveals two striking differences. First, the CαCβ module manifests an obvious asymmetry, exposing residues on the ABD β-sheet of the Cβ domain that are buried in the symmetrical Fab (Fig. 2.1B, green). Second, the size of the VβCβ interface is very different from that of the V_HC_{H1} interface. In particular, the buried surface area between Vβ and Cβ domains is 350 Å^2 on each side whereas that between V_H and C_{H1} is only 150 Å^2. This more robust VβCβ interface is contributed to by the CβFG loop (Fig. 2.1A, red), a 12-residue-long insertion unique to mammalian $\alpha\beta$TCRs [17] and accounting for almost one-third of the buried surface area (Fig. 2.2). As shown in Fig. 2.1C, the CβFG loop is well structured. At the middle of the

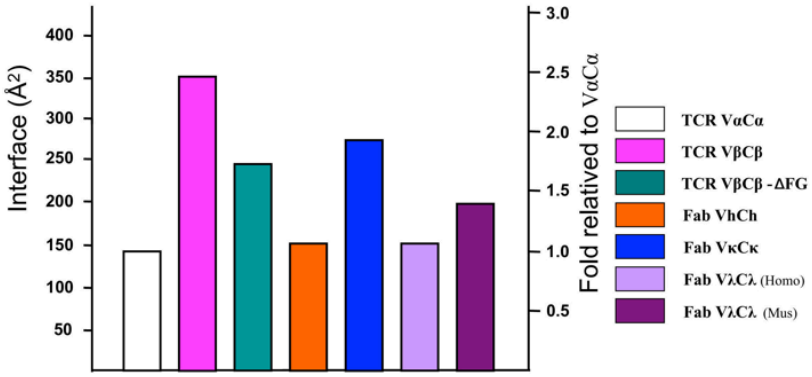

Figure 2.2: **Surface area of each species and its ratio relative to VαCα.**

loop is W223, which uses the NH group at its indole ring to form two hydrogen bonds to the main chain carbonyl oxygen atoms from Q225 and R227. This fixes the W223 residue in a position to serve as the center of a mini-hydrophobic core joined by L217 and P230 (cyan) [16]. In addition, a 3_{10} helix connector between the Vβ and Cβ domains is spatially adjacent to this CβFG loop. This helix is unique to TCRβ (Fig. 2.1D). A 3_{10} helix is an overwound secondary structure and might be induced to extend when subject to a pulling force, as could the CβFG loop, given the absence of disulfide bonds therein to preclude force-driven extension. Because deletion of the CβFG loop attenuated antigen-triggered T-cell function [18, 19], we focused on this $\alpha\beta$TCR feature to determine if it is associated

with mechanotransduction. Note that throughout the designation $\alpha\beta$TCR will be used to refer to the complete TCR complex (i.e., including the associated CD3 subunits) whereas the designation TCR$\alpha\beta$ refers exclusively to the clonotypic heterodimeric component of the complex.

2.3.2 Single-Molecule Assay Isolating the TCR$\alpha\beta$-pMHC Complex

Two single-molecule assays were developed for probing the TCR$\alpha\beta$-pMHC complex under load. The first isolates the N15TCR$\alpha\beta$-pMHC interaction to a coverslip surface (Fig. 2.3A) in a tethered bead configuration. This TCR is specific for the vesicular stomatitis virus octapeptide (VSV8) bound to murine H-2K^b. Biotinylated pMHC molecules (VSV8/K^b) were bound through streptavidin to a PEG-pacified surface containing sparse biotin-PEG molecules. The TCR$\alpha\beta$ heterodimer is fused to an acid-base leucine zipper (LZ) at the C terminus and tethered to an 300-nm-long 1,010-bp DNA molecule covalently bound to the zipper-specific antibody 2H11 and functionalized with digoxygenin on opposite 5 ends. Force is applied to the TCR$\alpha\beta$-pMHC complex through an optically trapped anti-digoxigenincoated bead. To measure the TCR$\alpha\beta$-pMHC bond strength in the isolated SM assay, tethered beads were visualized, centered in the detector laser, and calibrated for position sensing using automated procedures. Lifetime measurements were performed by translating the sample relative to the fixed trap and holding at a fixed position/force until bond rupture, identified as an abrupt snap back of the bead position within the trap. Conformational extensions are seen as upward displacements of the bead within the trap (Fig. 2.3 B and C). In addition to analyzing conformational extensions (Fig. 2.3C), bond lifetime measurements as a function of force were performed using wild-type (WT), CβFG loop-deleted (ΔFG) [18, 19] and H57 Fab-stabilized TCR$\alpha\beta$ heterodimers paired with pMHC molecules (Fig. 2.3D). Note that H57 binds the CβFG loop [16]. The MHC class I H-2 K^b molecules were complexed with the strong agonist peptide VSV8, the weak agonist L4 containing a single valine-to-leucine substitution at the p4 position of VSV8, or the unre-

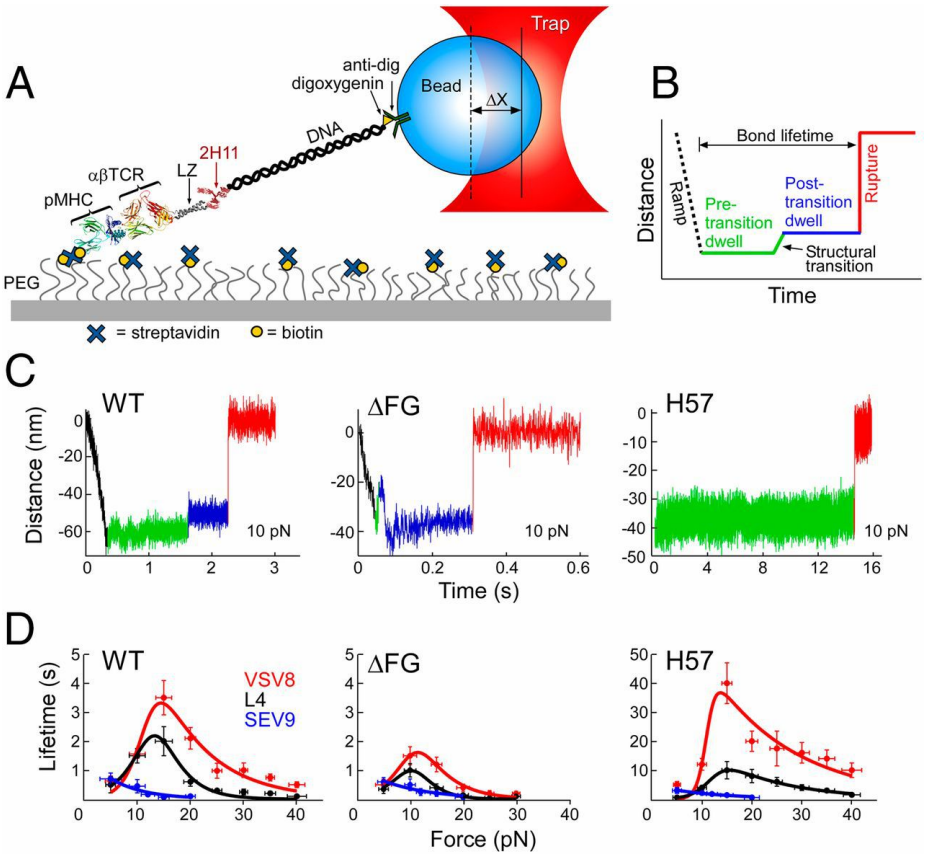

Figure 2.3: **SM studies.** (A) Cartoon showing single-molecule tether assay for probing the lifetime of $\alpha\beta$TCR-pMHC bonds. ΔX denotes displacement of bead out of the center of the trap. (B) Loading profile for measuring bond lifetime. Increase in distance represents greater separation along the system path. An initial ramp phase, indicated by a black dashed line, loads the tether to a fixed force, Pre-transition dwell, indicated by a green line. Frequently, a signature structural transition is observed, indicated by green to blue line, followed by a Post-transition dwell, in blue. Rupture, indicated by red line, is seen as an abrupt upward step. (C) Representative traces at 10 pN for WT, ΔFG, and H57 Fab. The WT trace shows a typical transition and rupture. ΔFG traces typically transition early, here occurring during the initial ramp phase. H57 Fab traces typically show no transition and dwell for longer periods before rupture. Low-amplitude motions in the green baseline (see WT) were also observed. (D) Force-bond lifetime plots for WT, ΔFG, and H57 Fab showing catch bonds for both VSV8 and L4 and slip bond character for SEV9. Catch bonds peak at 15 pN for WT and shift to lower force for ΔFG with significant reduction in bond lifetime. H57 stabilized the FG loop exhibiting dramatic amplification of catch bond lifetimes.

lated Sendai virus nonamer peptide SEV9. SEV9 binds to K^b with comparable affinity to VSV8 but is unable to activate N15TCR-expressing T cells [20]. SM measurements for

the WT-TCR$\alpha\beta$ showed catch bond behavior with peak lifetimes at 15 pN for VSV8, a weaker catch bond character for L4, and a slip bond for SEV9 (Fig. 2.3D). ΔFG shows significantly reduced bond lifetime, shifting the maximal lifetime to a lower force of 10 pN (Fig. 2.3D), and lessens the ability of the TCR to discriminate different ligands bound to the same MHC molecule (see below). In contrast, stabilizing the CβFG loop via H57 Fab ligation amplifies catch bond lifetimes (Fig. 2.3D). By comparison, the Cα-binding antibody H28 only modestly extends bond lifetime (Fig. 2.4).

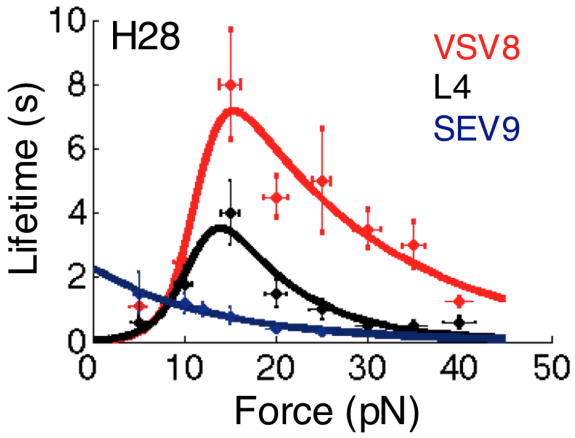

Figure 2.4: **Force-lifetime relationship for wtN15$\alpha\beta$ in the presence of H28.** Effect of H28 on bond lifetime vs Force diagram shows that bond lifetime increases with force up to 15 pN (Catch bond) followed by decrease of lifetime with force for VSV8 (red) and L4 (black). For SEV9 (Blue) the bond lifetime decreases with increment of force. The data are presented along with the fitted curve (solid line).

2.3.3 Conformational Transition Is Linked to the FG Loop

Before rupture, we frequently observed a signature conformational transition spanning 815 nm (Fig. 2.3C). The upward transition represents an extension of the system incorporating rotations of domains, extensions, and potential unfolding. The transition is coupled to the state of the CβFG loop in several respects. First, removing the CβFG loop weakens an energetic barrier, as TCR$\alpha\beta\Delta$FG transitions frequently occurred during the ramp phase (compare Fig. 2.3C, WT vs. ΔFG). Second, stabilizing the CβFG loop with H57 Fab virtually abolished the transition (Fig. 2.3C, H57), suggesting that this loop region controls

access to the transition. Third, ΔFG altered the displacement magnitude, described below.

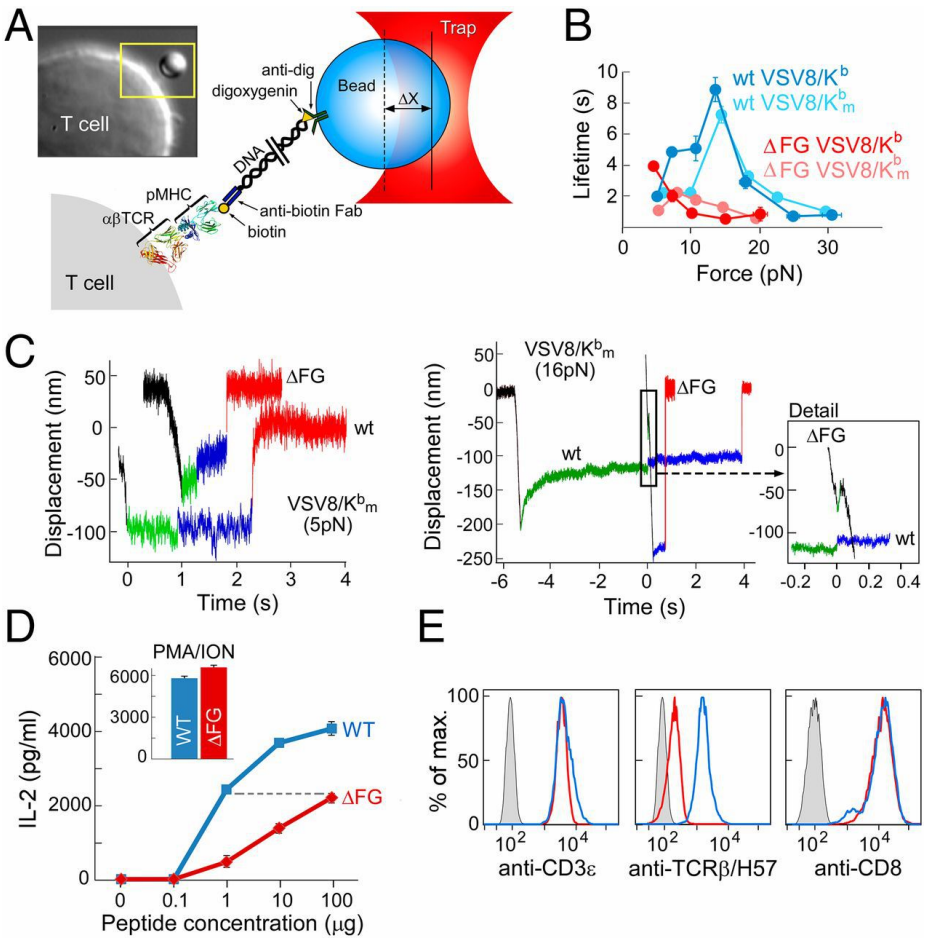

Figure 2.5: **Single molecule on Single-cell studies.** (A) Cartoon showing the SMSC assay along with a photomicrograph of a T cell with tethered bead in the yellow box. (B) Lifetime-force plots comparing N15WT and N15ΔFG T-cell ligation with VSV8/Kb and VSV8/K$^b{}_m$, a mutant pMHC lacking the ability to bind CD8, show catch bonds peaking at 15 pN. (C) Representative traces at low force (5 pN) and high force (16 pN) comparing WT to ΔFG for VSV8/K$^b{}_m$, where the structural transition is clearly visible. ΔFG traces at 16 pN exhibit transitions early on, here during the loading phase of the trace. (D) IL-2 production requires a 2-log-greater VSV8 peptide concentration for ΔFG than WT despite comparable capacity to produce equivalent maximal IL-2 production triggered by phorbal myristate acetate (PMA) plus ionomycin (ION). (E) Flow cytometry confirms similar CD3 and CD8 density and lack of FG loop seen in H57-binding assay. Color code is as in D with gray curve showing background staining.

2.3.4 Single-Molecule Measurements on Isolated Single Cells

Single-molecule measurements on isolated single cells (SMSC), the second assay, corroborate the SM observations (Fig. 2.5). Single tethers on single cells were constructed using anti-digoxygenin beads that linked a digoxygenin-adducted 3,500-bp DNA molecule covalently bound to the thiol group in the hinge domain of a biotin-specific antibody that binds single biotin-labeled pMHC molecules (Fig. 2.5A). SMSC studies were performed by trapping and calibrating a bead, positioning cells to facilitate tether formation, displacing cells to a fixed load, and recording bead position until rupture, as with SM assay. Although the cell system is much more compliant due to the cellular connectivity of the load pathway, the measurements recapitulate a more natural state of the $\alpha\beta$TCR-pMHC complex. As with SM measurements, catch bonds were seen peaking at 15 pN but with generally longer lifetimes (Fig. 2.5B). Dramatic reduction in bond lifetime was seen for N15TCR$\alpha\beta\Delta$FG cells. Despite the gradual creep in position and other displacements as a consequence of membrane compliance and cytoskeletal attachment in single-cell measurements, we were able to identify records displaying the signature conformational transitions found in SM studies (Fig. 2.5C). The N15$\alpha\beta\Delta$FG cells show early transition including some during the ramp phase (Fig. 2.5C). This difference is functionally correlated with a 100-fold reduction in responsiveness to the cognate VSV8 peptide as judged by IL-2 production when stimulated through the TCR, despite comparable surface TCR and coreceptor levels as assessed by anti-CD3 and anti-CD8α mAbs (Fig. 2.5 D and E). CD8$\alpha\beta$ is an important T-cell surface molecule, absent in the SM assay, that functions as a coreceptor by associating with the $\alpha\beta$TCR-pMHC complex via binding to the membrane proximal α3 domain of H-2K^b (reviewed in ref. [1]). To measure the influence of CD8, we performed our assay on cells using a mutant pMHC (VSV8/K$^b{}_m$) unable to bind CD8$\alpha\alpha$ and CD8$\alpha\beta$ dimers (described below). As shown in Fig. 2.5B, a general reduction in bond lifetime was observed, shifting the curve closer to SM and exposing the TCR$\alpha\beta\Delta$FG as forming a weak catch bond. Much of the slip bond character seen in the ΔFG native system

can be attributed to CD8 binding, which masks the diminished pMHC interaction. When

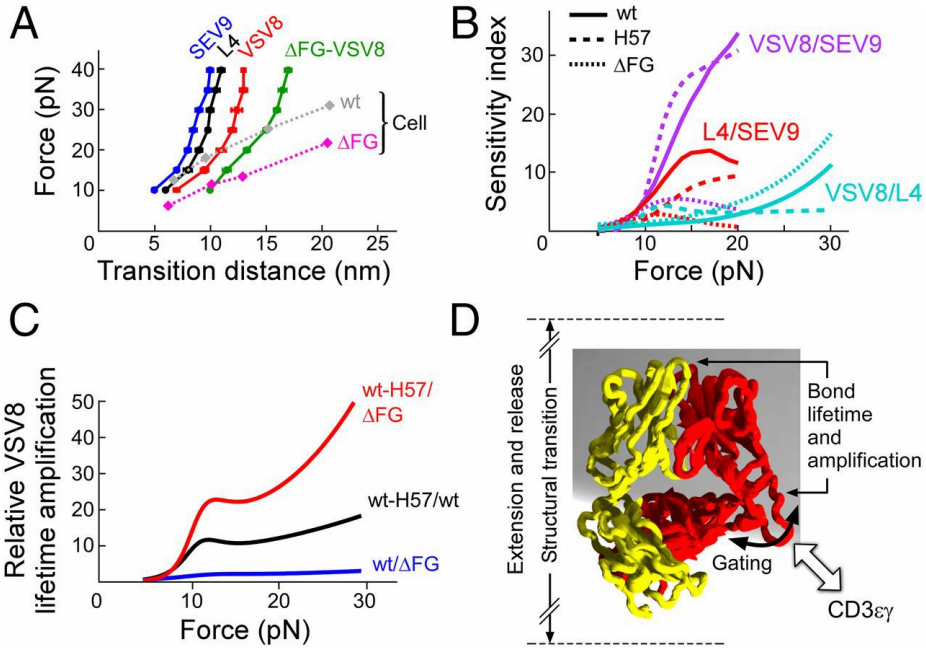

Figure 2.6: **Force-dependent structural transitions, ligand sensitivity, amplification factors and an $\alpha\beta$TCR model.**(A) The major structural transition distance, measured as the difference in bead position before and after the transition, is plotted vs. force for WT-VSV8 cognate peptide (red), -L4 partial agonist (black), -SEV9 irrelevant ligand (blue), and ΔFG-VSV8 (green) showing a ligand dependence with greater ligand potency exhibiting larger structural transition distances in SM systems. Force-transition distance plots for cell systems; SMSC (diamonds with dotted lines) exhibit greater displacement with VSV8 for ΔFG than for WT and are generally larger than the SM transitions. (B) Sensitivity plots comparing lifetime ratios of various antigens for WT (solid), H57 (dashed), and ΔFG (dotted). Plots were constructed from fits in Fig. 2. (C) Amplification factors associated with lifetime enhancement for VSV8 binding including ratios of WT-H57/ΔFG (red), WT-H57/WT (black), and WT/ΔFG (blue). Amplification factors rise abruptly at 10 pN, are greatest with stabilization of the FG loop, and increase generally as a function of force. (D) Model for force-induced motions and gating associated with the CβFG loop region. The FG loop region couples to the binding interface strength and conformational change magnitude. Associations with molecules such as CD3 may dramatically stabilize the CβFG loop, influencing bond lifetime and force transfer response of the loaded $\alpha\beta$TCRpMHC complex system.

comparing transitions, plots of magnitude vs. force (Fig. 2.6A) demonstrate that greater transition displacements are seen for agonists than for nonagonists and in SMSC vs. SM systems. Analysis of the relative response to agonists and nonagonists by comparing ratios of lifetimes for pairs of peptides bound to the same MHC, sensitivity index plots, reveal a

peak for VSV8/SEV9 at 15 pN but minimal, if any, discrimination at low loads (Fig. 2.6B). Plots comparing ratios of lifetimes for VSV8 demonstrate greatest amplification for the stabilized CβFG loop region and with increasing force (Fig. 2.6C).

2.4 Discussion

Using both SM and SMSC assays, we have compared the strength of pMHC interactions with WT-TCR$\alpha\beta$, TCR$\alpha\beta\Delta$FG, and H57 Fab-stabilized WT-TCR$\alpha\beta$. We have found strong evidence for allostery in that the state of the CβFG loop region dramatically modulates the strength of the TCR$\alpha\beta$-pMHC bond. Moreover, we observe a mechanical extension, the displacement of which correlates with ligand potency and the strength of which correlates with the CβFG loop region structure. Single-molecule records are consistent with a model where an unloaded compact TCR binds weakly, a loaded compact TCR binds strongly, and a stabilized CβFG loop region further strengthens binding, whereas release occurs through an extended TCR$\alpha\beta$ heterodimer. The adjacent CD3 ectodomains may stabilize the CβFG loop region, prolonging bond lifetime under force in SMSC relative to SM experiments as detailed below. Our model implies a mechanism whereby the CβFG loop enhances mechanosensor action through force-driven gating of initial access and stabilization of productive pMHC interactions but release of unproductive interactions, thereby controlling catch bond strength and bond lifetime (Fig. 2.6D).

These data confirm that the $\alpha\beta$TCR is a mechanosensor activated by pN forces upon pMHC ligation. More importantly, they show that the CβFG loop region allosterically controls the V domain modules catch bond lifetime and peptide discrimination via force-driven conformational transitions. By contrast, CD8 neither contributes to catch bond formation in mature $\alpha\beta$T cells as shown here nor is a mechanosensor as revealed by earlier data showing an inability of CD8-directed force application to stimulate T-cell activation [11].

The force-induced structural transition observed in SM experiments is large, being on the order of 120 Å(Fig. 2.6A). That said, 40 Åof transition is observed differentially be-

tween VSV8/K^b (agonist) vs. SEV9/K^b (irrelevant) pMHC ligation of the N15$\alpha\beta$TCR heterodimer (Fig. 2.6A). This distance is more than the 15 Åpermitted by simple extension of the Vβ-Cβ connector. In fact, in SM assays, displacements for TCR$\alpha\beta\Delta$FG were greater than WT-TCR$\alpha\beta$ (Fig. 2.6A). Therefore, additional rearrangements, outside of the FG loop, in the TCR$\alpha\beta$ heterodimer-pMHC complex must exist. These might include extension of the long (>20-aa residues) connecting peptides between Cβ and the transmembrane surrogate (LZ) and Cα and LZ or possibly even sliding of the Vβ and Vα domains relative to one another at the hydrophobic interface of the V module. Major motion within individual V and C domains of the TCR heterodimer per se is unlikely, given the existence of intradomain disulfide bonds in each (Fig. 2.1B), but the A and/or G strands nonetheless might be flayed via force. Although our focus has been on the large transition, conformational change was also observed featuring reversible, low-amplitude, 1- to 3-nm motions of the baseline (Fig. 2.5C, WT), suggesting reconfigurations of the $\alpha\beta$TCR-pMHC complex. Single-molecule FRET analysis with fluorophores placed in individual domains can more precisely define the nature of domain extension and twisting in future investigation.

Our prior studies [18, 19] revealed that the CβFG loop facilitates thymocyte development at both CD4CD8 double negative and CD4+CD8+ double-positive stages. The former requires the pre-TCR, a molecular complex involving the same β and CD3 subunits but with the β-chain ectodomain stalk disulfide linked to that of pTα, a surrogate α-chain lacking a V domain. Given the current data, it is tempting to speculate that the CβFG loop-regulated transition observed for the TCR$\alpha\beta$ heterodimer may be applicable to the pre-TCR, but in even greater magnitude in the absence of a Vα pairing constraint. The suggestion that pMHC or other self-ligands could interact with the unpaired Vβ domain [21] is consistent with this possibility and worthy of further investigation.

The Cβ FG loop evolved in mammals at the same time as molecular speciation of CD3 and CD3 genes from a single CD3 precursor gene among Gnathostomata, a group of vertebrates with adaptive immunity involving a recombinatorial system (VDJ) [17]. The

sensitivity of allosteric regulation makes this adaptation highly efficient for antigen recognition. That requirement may be less critical for recognition by TCRs, given the potential for high copy numbers of their less diverse stimulating ligands on APCs [22, 23]. The distinctive CD3 topology adjacent to the CβFG loop can further maximize antigen activation by facilitating force transfer from the TCR$\alpha\beta$ heterodimer to adjacent CD3 [17, 24, 25]. Perhaps force-mediated structural transitions enrich for conformers with the greatest intersubunit ectodomain complementarity, thereby favoring ligation-mediated signaling. That H57Fab prolongs TCR-pMHC bond lifetime (Fig. 2.3H) yet blocks pMHC-triggered T-cell responses [11] is consistent with such a notion. How CD3 may associate with pretransition, intermediate, or posttransition states is unclear. Pretransition binding of CD3 to a compact state might extend the lifetime of the $\alpha\beta$TCR-pMHC bond. During the transition, the bound CD3 heterodimer may participate in the mechanical change, being pushed and pulled to expose sequestered CD3 cytoplasmic tail ITAMs. Posttransition binding to an extended TCR state may also modulate CD3 binding in a positive and/or negative sense in ways that need to be defined.

Mechanotransduction is obviously critical for $\alpha\beta$TCR function, as evident from the above studies. Understanding the structural consequences of pN load will be important to elucidate T-lineage cell biology related to cognate recognition of antigen as well as thymocyte development. Mechanical influence has been established in many systems including stem cell differentiation [26], cell migration and rolling [27], focal adhesion development [28], and integrin adhesion [29]. Single-molecule methods have been pioneered largely through the study of biological motors using classical assays such as our SM system [30], yet there is great opportunity for using single-molecule methods to probe machinery on or within intact cells. The approach presented here bridges the classic isolated single-molecule assays to the more biologically relevant single molecule in a single-cell system. The SMSC system is ideally suited for in situ study of surface membrane-embedded receptors and represents an evolution of single-molecule technology.

Our studies begin to address how it is possible that $\alpha\beta$TCRs, whose affinity in the absence of load (i.e., in solution) is extremely weak, can nevertheless mediate exquisite sensitivity and specificity in a noisy chemical environment on the antigen-presenting cell surface. There, many identically sized peptides are bound to the same type of MHC molecule, forming an array of 100,000 different pMHC complexes. The challenge for any T lymphocyte is to use its clonally endowed 20,000 $\alpha\beta$TCR surface copies to rapidly scan this collection of diverse pMHCs on each cell where a dozen or fewer relevant foreign peptides may be embedded. In this context, load-induced transitions tune $\alpha\beta$TCR-pMHC bond lifetime with high specificity. In particular, maximal nonlinear dynamic bond lifetime is associated with TCR$\alpha\beta$ structural transitions that readily distinguish among peptides, even when differences compose a single residue (VSV8 vs. L4). On the other hand, without force, discrimination is minimal. Hence, during immune surveillance as an $\alpha\beta$TCR is gaffed (i.e., hooked) by its specific pMHC, force is generated, bond lifetime extends, and a structural transition is induced in TCR$\alpha\beta$. These features associated with catch bond formation likely are sufficient to promote further $\alpha\beta$TCR quaternary change, CD3 heterodimer interactions, and transmembrane and cytoplasmic tail segment alterations to foster downstream signaling events [1, 11, 31]. A small number of those productive interactions in time and space will result in quantal T-cell activation that can be further sustained at the immunological synapse [32, 33]. Unlike the cognate peptide, unrelated or variant peptides will not induce either these transitions or extend bond lifetime sufficient to promulgate a signaling event. Remarkably, then, the TCR is able to detect very few side chains of a peptide in the MHC groove even though the majority of recognition surface contacts are shared in common with other pMHC complexes.

That the $\alpha\beta$TCR physically goes through a mechanical transition that prolongs the $\alpha\beta$TCR-pMHC bond lifetime has a number of immediate consequences. First, the extension represents a previously unknown state. As in physical changes observed with integrin $\alpha\beta$ heterodimers, affinities between compact and extended states can be very different.

Interestingly, the mechanical action of the $\alpha\beta$TCR appears to work with a logic opposite to that of the integrins because in the TCR the compact form binds strongly whereas the extended form binds weakly. Leading from an on state as opposed to an off state, as in integrins where ligands are plentiful, may be a consequence of the $\alpha\beta$TCR seeking out rare binding events. Second, the ligand-dependent displacement seen here may differentially couple to mechanisms that critically depend on distance such as TCR-APC intercellular membrane proximity. Third, the mechanical transition in the $\alpha\beta$TCR-pMHC system is regulated via the FG loop region, as observed by H57 Fab stabilization, which may also be occurring through the physiological CD3 associations noted above. This partitioning of function allows the mechanism of discrimination to be conserved within the constant region of the TCR while maintaining near-infinite variability in the ligand-recognition elements in the V-domain module. Fourth, kinetic proofreading mechanisms require working outside of thermal equilibrium and are thus generally energy intensive [31, 34]. Mechanical work through a mechanosensor mechanism can drive such nonequilibrium signaling events, sustaining triggering during immune surveillance and at the immunological synapse while using forces derived via concomitant cell movements.

2.5 Conclusion

The $\alpha\beta$ T-cell receptor (TCR) on mammalian T lymphocytes recognizes intracellular pathogens to afford protective immunity. Detection of various foreign peptides bound to MHC molecules as TCR ligands occurs during immune surveillance where mechanical forces are generated through cell movement. Using single-molecule optical tweezer assays, we show with isolated and complete receptors on single T cells that both sensitivity and specificity of the biological T-lymphocyte response is dependent upon force-based interactions. Our work demonstrates a catch-and-release $\alpha\beta$TCR structural conversion correlating with ligand potency wherein a strongly binding/compact state transitions to a weakly binding/extended state. An allosteric mechanism controls bond strength and life-

time, supporting a model in which quaternary $\alpha\beta$TCR subunit associations regulate TCR recognition under load.

2.6 Methods

2.6.1 $\alpha\beta$ Production and Peptide and Protein Preparation.

TCR N15α and β-subunits were fused to basic and acidic LZ components, respectively, as previously described [35]. They were then separately cloned into the eukaryotic expression vector containing human cytomegalovirus promotor designed for expression of antibody -chain [36] using AgeI/SalI to insert each subunit in-frame, retaining the vector signal sequence while adding a stop codon immediately following the LZ motif. Both WT-TCRα- and β-subunits were expressed simultaneously after transient cotransfection in Freestyle 293F cells (Life Technologies) according to the manufacturers recommendations. A second TCRβ construct wherein the Cβ FG loop was excised as previously described [18, 19], termed N15$\beta\Delta$FG, was used for cotransfection with WT-TCRα to create N15$\alpha\beta\Delta$FG. Proteins were purified from cell supernatants essentially as described [35]. Although yields were lower for the N15$\alpha\beta\Delta$FG than for N15$\alpha\beta$WT, we were able to confirm purification of the N15$\alpha\beta\Delta$FG through SDS/PAGE separation, band excision, trypsin digestion, and identification of both N15α and N15β subunit peptides via electrospray mass spectrometry. Singly biotinylated pMHC were purified [37] and biotinylated [38] as described. Peptides were synthesized by United Biosystems. The monoclonal anti-Cβ antibody H57 was produced as described [35], and Fab fragments were generated and purified using a Pierce Fab Micro Preparation Kit (Thermo Scientific) according to the manufacturers directions.

2.6.2 Single-Molecule Assay

For single-molecule measurements, a complex of N15$\alpha\beta$TCR and pMHC was tethered between a single trapped bead and glass surface. The overall assay geometry included a N15TCR$\alpha\beta$ heterodimer fused to a leucine zipper at the C terminus. A 1,010-bp DNA molecule with anti-leucine zipper antibody (2H11) on one 5 end and a digoxygenin on the opposite 5 end, described below, was used to attach the N15TCR$\alpha\beta$ heterodimer to an anti-digoxygenincoated bead. The DNA served as a spacer between the bead and N15TCR$\alpha\beta$. A biotinylated pMHC complex, VSV8/K^b, was immobilized on a PEG functionalized coverglass surface using biotinstreptavidin chemistry. The schematic diagram of our single-molecule assay is shown in Fig. 2.3. The DNA linker was constructed by PCR of a 1,010-bp region of the M13mp18 plasmid with 5 primers of an amino group and digoxigenin. The 5 amino group was cross-linked to 2H11 using carbodiimide cross-linker strategy (EDC chemistry). A 10-μL flow cell was prepared using two pieces of double-sided sticky tape. Cover-glass surfaces were coated with functionalized PEG silane 99% mixed with 1% biotinPEG silane similar to previously described work [39]. Streptavidin (1 mg/mL) was introduced into the flow cell, incubated for 10 min, and washed with PBS buffer. A total of 20 μL of biotinylated pMHC (1 μg/1 μL) was introduced and incubated for 30 min and washed again with PBS buffer. During this time period, N15TCR$\alpha\beta$ (100 ng/1 μL) and 2H11-DNA-digoxigenin (200 ng/μL), +/H57 or H28 mAb (1mg/mL), were mixed, added to the flow cell, and incubated for 30 min. After washing with 30 μL of PBS buffer, anti-digoxygenincoated (Roche Diagnostics) polysterene beads (Spherotech Inc.) were introduced followed by a 30-μL PBS buffer wash. The flow cell was sealed with nail polish and loaded on the optical-trapping instrument for measurements. Tethers were found by eye, centered using an automated procedure [40], and trapped with typical stiffness of 0.25 pN/nm. Bead positions were sampled at 3 kHz, antialias-filtered at 1.5 kHz, and recorded until rupture. Control experiments where N15$\alpha\beta$TCR was excluded from the assay resulted in no tethers.

2.6.3 Single-Cell Assay

Tethers for SMSC assays were constructed using anti-digoxygenincoated polystyrene beads (1.0 μm in diameter, Spherotech Inc.) to tether the digoxigenin-labeled, 3,500-bp DNA at one end. At the other end, a sulfo-SMCC (Pierce) reaction was used to bind the free thiol group of the half anti-biotin antibody. Finally, biotin-labeled pMHC was linked to the half anti-biotin antibody. Specifically, 0.5 μL 0.25% wt/vol anti-digoxygenin beads were washed two times by PBS buffer (Cellgro) containing 0.02% Tween 20 (PBST) and were incubated with 10 μL of halfanti-biotin functionalized DNA (65 ng/μL). The bead surface was saturated with these 3,500-bp DNA tethers to reduce nonspecific binding between the bead and cell surface. After 1 h of incubation, the DNA-labeled bead was washed three times with PBST buffer and then resuspended in a solution containing 5 μL of 20 pM biotinylated pMHC in PBS buffer for 1 h incubation. After two washes with PBST buffer, the bead slurry was diluted 200-fold for bond lifetime measurements. All of the incubations were performed at room temperature. Cells were cultured in selection medium [complete RPMI medium 1640 (Life Technology) plus 0.1 mg/mL G418 (Life Technology) and 2 mg/mL hygromycin B (Life Technology)] and reached the log phase before the experiments. Cells were washed one time with PBS and then kept in colorless complete RMPI 1640 medium (Life Technology) at 2 million/mL; 20 μL of cells were introduced into the flow chamber, and cells were bound to a poly-L-lysine coverslip prepared as described previously [11]. The coverslip surface was further blocked by 1 mg/mL casein (Sigma-Aldrich) in PBS buffer [11]. After a 10-min incubation at 37 ^{o}C, the pMHC-DNA bead slurry (20 μL) was introduced into the flow cell. The tether-functionalized bead was trapped and brought in the vicinity of N15$\alpha\beta$WT or N15$\alpha\beta\Delta$FG cells to form a stable tether. Tether formation was verified and then loaded by displacing the cell relative to the fixed trap using fine motions of the piezo stage. Bead positions were sampled at 3 kHz, antialias-filtered at 1.5 kHz, and recorded until complete rupture. Assays were performed at 37 ^{o}C.

2.6.4 Production and characterization of N15TCR$\alpha\beta$ and N15TCR$\alpha\beta\Delta$FG T cell lines and IL-2 assay

58 α-β- cells previously transfected to express CD8$\alpha\beta$ and N15TCR$\alpha\beta$wt or the N15TCR$\alpha\beta\Delta$FG mutant (1) were sorted to equivalently match both TCR and CD8 expression levels on the two cell lines. Then R8 (ATCC) cells as APCs were loaded with VSV8 peptide concentrations ranging from 0.1 to 100 μg/ml to stimulate N15 TCR$\alpha\beta$wt and N15$\alpha\beta\Delta$FG expressing cells. Responding cells were added in triplicate at a density of 2x10^5 cells per well in 96 well plates using complete DMEM media supplemented with 1 ng/ml PMA (Sigma). Cells in replicate wells were stimulated with 10 ng/ml of PMA and 500 ng/ml of Ionomycin (Sigma) as a positive control. After 18 h of incubation, plates were centrifuged and 50μl was removed for IL-2 analysis. Conditioned media was analyzed using mouse IL-2 bead assay from (BD biosciences) according to manufacturers protocol on a FACSAria flow cytometer. Anti-CD3 mAb 2C11 and anti-CD8α were used for to quantitate surface TCR complexes and CD8$\alpha\alpha$ andCD8$\alpha\beta$ heterodimers (2). subsectionAntibodies (Abs) and flow cytometric analysis The following mAbs were used: FITC-conjugated anti-Vβ 5.2 (MR9.4) (ebioscience), PE-conjugated anti-TCR Cβ (H57-597) (BD Pharmingen), PE-conjugated anti-CD3 (145-2C11) (ebioscience), APC-conjugated anti-CD8α (CD8a) (Biolegend), FITC-conjugated anti-CD8β (CD8b.2) (Biolegend) and PE-conjugated anti-H- 2K^b antibody (AF6-88.5) (ebioscience). For flow cytometry, single-cell suspensions of wt or ΔFG cells were prepared at 3×10^6 cells/ml in PBS containing 2% FCS. Those cells were single-color stained with the Abs at saturating concentrations. After incubation on ice for 20 minutes, the stained cells were transferred to a falcon tube and characterized by flow cytometry. FACScan (BD Biosciences) and FlowJo software (Tree Star) were used for all samples. Dead cells were excluded from the analysis by forward and side scatter gating. For assessing TCR expression further on both N15$\alpha\beta$wt and N15$\alpha\beta\Delta$FG cells, saturating amounts of FITC-conjugated anti-Vβ5.2 were employed. After 20-minute incubation on ice, the stained cells were subjected to flow cytometry anal-

ysis.

2.6.5 Partial reduction of anti-biotin antibody

Anti-biotin antibodies (Sigma-Aldrich) at 10 mg/ml were dissolved in the reaction buffer (pH=7.4) containing 20 mM sodium phosphate (Sigma- Aldrich), 0.15 M NaCl (Sigma-Aldrich) and 5 mM EDTA (Sigma-Aldrich). A 500-fold molar excess of 2-MEA (Sigma-Aldrich) over the concentration of anti-biotin antibody was added in the solution, followed by 90 minutes incubation at 37^oC. The reaction product was purified using a 30 MBS desalting column (Millipore). Purified product was immediately used for the SMCC reaction.

2.6.6 Covalently coupled half anti-biotin antibody to DNA

A 3500 base-pair DNA linker was constructed by PCR using a M13mp18 plasmid as template with one forward oligonucleotide primer containing a Dig tag at the 5 end (5-Dig-AAT CCG CTT TGC TTC TGA CT-3) and one reverse oligonucleotide primer containing an amino tag at the 5 end (5-NH2-TTG AAA TAC CGA CCG TGT GA-3). Following PCR, the TE buffer in the PCR product was changed to PBS buffer using a 6 MBS desalting column (Millipore). A volume of 30 μl NH2-DNA-Dig solution (conc. 120 ng/μl) was incubated with 30 μl 10 mg/ml freshly made Sulfo-SMCC dissolved in dd-water at 4^oC for 2 hours. A second buffer changing procedure was performed for the DNA-SMCC mixture by changing the PBS buffer to reaction buffer used for partial reduction of anti-biotin antibody. Maleimide-DNA-Dig was incubated with the purified half anti-biotin antibody for 12 hours at 4^oC in order to covalently couple the free thiol group of half anti-biotin antibody to the maleimide group on the DNA. The functionalized DNA can be kept in reaction buffer at -20^oC for 2 months without degradation of function.

2.6.7 H28 measurements

Bond lifetime vs force plots show that, in the presence of H28, bond lifetime increases with force up to 15 pN (Catch bond) followed by decrease of lifetime with force for VSV8 (red) and L4 (purple). Bond lifetime decreases with force for SEV9 (blue). H28 measurement results and fits are found in Fig. 2.4.

2.7 Acknowledgement

We want to acknowledge Dr. Dibyendu Kumar Das for performing all the isolated single molecule experiment. We thank the NIH Tetramer Core Facility at Emory University and Cheng Zhu for providing the VSV8/H2-K^b-α2A2 tetramer. This work is supported by NIH Grants R01AI100643, R01AI37581, and P01GM047467. D.K.D. is a George Russell Chambers postdoctoral fellow. Flow cytometry experiments were performed in the Vanderbilt University Medical Center Flow Cytometry Shared Resource supported by The Vanderbilt-Ingram Cancer Center (NIH Grant CA68485) and the Vanderbilt Digestive Disease Research Center (NIH Grant DK058404).

2.8 Bibliography

[1] Jia-huai Wang and Ellis L Reinherz. The structural basis of $\alpha\beta$ T-lineage immune recognition: TCR docking topologies, mechanotransduction, and co-receptor function. *Immunological reviews*, 250(1):102–119, 2012.

[2] Lei Yin, James Scott-Browne, John W Kappler, Laurent Gapin, and Philippa Marrack. T cells and their eons-old obsession with MHC. *Immunological reviews*, 250(1):49–60, 2012.

[3] Chenqi Xu, Etienne Gagnon, Matthew E Call, Jason R Schnell, Charles D Schwieters, Christopher V Carman, James J Chou, and Kai W Wucherpfennig. Regulation of T cell receptor activation by dynamic membrane binding of the CD3ε cytoplasmic tyrosine-based motif. *Cell*, 135(4):702–713, 2008.

[4] Dikran Aivazian and Lawrence J Stern. Phosphorylation of T cell receptor ζ is regulated by a lipid dependent folding transition. *Nature Structural and Molecular Biology*, 7(11):1023, 2000.

[5] Konstantina Nika, Cristiana Soldani, Mogjiborahman Salek, Wolfgang Paster, Adrian Gray, Ruth Etzensperger, Lars Fugger, Paolo Polzella, Vincenzo Cerundolo, Omer Dushek, et al. Constitutively active Lck kinase in T cells drives antigen receptor signal transduction. *Immunity*, 32(6):766–777, 2010.

[6] Byron B Au-Yeung, Sebastian Deindl, Lih-Yun Hsu, Emil H Palacios, Susan E Levin, John Kuriyan, and Arthur Weiss. The structure, regulation, and function of ZAP-70. *Immunological reviews*, 228(1):41–57, 2009.

[7] Susan M Kaech and Weiguo Cui. Transcriptional control of effector and memory CD8+ T cell differentiation. *Nature reviews Immunology*, 12(11):749, 2012.

[8] Kevin Man, Maria Miasari, Wei Shi, Annie Xin, Darren C Henstridge, Simon Preston, Marc Pellegrini, Gabrielle T Belz, Gordon K Smyth, Mark A Febbraio, et al. The transcription factor irf4 is essential for TCR affinity-mediated metabolic programming and clonal expansion of T cells. *Nature immunology*, 14(11):1155, 2013.

[9] Harald Von Boehmer, Iannis Aifantis, Fotini Gounari, Orly Azogui, Loralee Haughn, Irina Apostolou, Elmar Jaeckel, Fabio Grassi, and Ludger Klein. Thymic selection revisited: how essential is it? *Immunological reviews*, 191(1):62–78, 2003.

[10] Lucia Kato, Andre Stanlie, Nasim A Begum, Maki Kobayashi, Masatoshi Aida, and Tasuku Honjo. An evolutionary view of the mechanism for immune and genome diversity. *The Journal of Immunology*, 188(8):3559–3566, 2012.

[11] Sun Taek Kim, Koh Takeuchi, Zhen-Yu J Sun, Maki Touma, Carlos E Castro, Amr Fahmy, Matthew J Lang, Gerhard Wagner, and Ellis L Reinherz. The $\alpha\beta$ T cell receptor is an anisotropic mechanosensor. *Journal of Biological Chemistry*, 284(45):31028–31037, 2009.

[12] Ya-Chen Li, Bing-Mae Chen, Pei-Chun Wu, Tian-Lu Cheng, Lung-Sen Kao, Mi-Hua Tao, Andre Lieber, and Steve R Roffler. Cutting edge: mechanical forces acting on T cells immobilized via the TCR complex can trigger TCR signaling. *The Journal of Immunology*, 184(11):5959–5963, 2010.

[13] Julien Husson, Karine Chemin, Armelle Bohineust, Claire Hivroz, and Nelly Henry. Force generation upon T cell receptor engagement. *PloS one*, 6(5):e19680, 2011.

[14] Edward Judokusumo, Erdem Tabdanov, Sudha Kumari, Michael L Dustin, and Lance C Kam. Mechanosensing in T lymphocyte activation. *Biophysical journal*, 102(2):L5–L7, 2012.

[15] Baoyu Liu, Wei Chen, Brian D Evavold, and Cheng Zhu. Accumulation of dynamic

catch bonds between TCR and agonist peptide-MHC triggers T cell signaling. *Cell*, 157(2):357–368, 2014.

[16] Jia-huai Wang, Kap Lim, Alex Smolyar, Mai-kun Teng, Jin-huan Liu, GD Albert, Ju Liu, Rebecca E Hussey, Yasmin Chishti, Cole T Thomson, et al. Atomic structure of an $\alpha\beta$ T cell receptor (TCR) heterodimer in complex with an anti-TCR fab fragment derived from a mitogenic antibody. *The EMBO journal*, 17(1):10–26, 1998.

[17] Sun Taek Kim, Maki Touma, Koh Takeuchi, Zhen-Yu J Sun, Vibhuti P Dave, Dietmar J Kappes, Gerhard Wagner, and Ellis L Reinherz. Distinctive CD3 heterodimeric ectodomain topologies maximize antigen-triggered activation of $\alpha\beta$ T cell receptors. *The Journal of Immunology*, 185(5):2951–2959, 2010.

[18] Tetsuro Sasada, Maki Touma, Hsiu-Ching Chang, Linda K Clayton, Jia-huai Wang, and Ellis L Reinherz. Involvement of the TCR cβ fg loop in thymic selection and T cell function. *Journal of Experimental Medicine*, 195(11):1419–1431, 2002.

[19] Maki Touma, Hsiu-Ching Chang, Tetsuro Sasada, Maris Handley, Linda K Clayton, and Ellis L Reinherz. The TCR cβ FG loop regulates $\alpha\beta$ T cell development. *The Journal of Immunology*, 176(11):6812–6823, 2006.

[20] Tetsuro Sasada, Yoseph Ghendler, Ellis L Reinherz, et al. Thymic selection is influenced by subtle structural variation involving the p4 residue of an MHC class I-bound peptide. *European journal of immunology*, 30(5):1281–1289, 2000.

[21] Bo Zhou, Qiang Chen, Robert Mallis, Hongmin Zhang, Jin-huan Liu, Ellis L Reinherz, and Jia-huai Wang. A conserved hydrophobic patch on vβ domains revealed by TCRβ chain crystal structures: Implications for pre-TCR dimerization. *Frontiers in immunology*, 2:5, 2011.

[22] Adrienne M Luoma, Caitlin D Castro, Toufic Mayassi, Leslie A Bembinster, Li Bai, Damien Picard, Brian Anderson, Louise Scharf, Jennifer E Kung, Leah V Sibener,

et al. Crystal structure of vδ1 T cell receptor in complex with CD1d-sulfatide shows MHC-like recognition of a self-lipid by human $\gamma\delta$ T cells. *Immunity*, 39(6):1032–1042, 2013.

[23] Grzegorz Chodaczek, Veena Papanna, M Anna Zal, and Tomasz Zal. Body-barrier surveillance by epidermal $\gamma\delta$ TCRs. *Nature immunology*, 13(3):272, 2012.

[24] Zhen-Yu J Sun, Sun Taek Kim, Il Chul Kim, Amr Fahmy, Ellis L Reinherz, and Gerhard Wagner. Solution structure of the CD3$\varepsilon\delta$ ectodomain and comparison with CD3$\varepsilon\gamma$ as a basis for modeling T cell receptor topology and signaling. *Proceedings of the National Academy of Sciences of the United States of America*, 101(48):16867–16872, 2004.

[25] Zhen-Yu J Sun, Ki Seok Kim, Gerhard Wagner, and Ellis L Reinherz. Mechanisms contributing to T cell receptor signaling and assembly revealed by the solution structure of an ectodomain fragment of the CD3γ heterodimer. *Cell*, 105(7):913–923, 2001.

[26] Adam J Engler, Shamik Sen, H Lee Sweeney, and Dennis E Discher. Matrix elasticity directs stem cell lineage specification. *Cell*, 126(4):677–689, 2006.

[27] Ronen Alon, Daniel A Hammer, and Timothy A Springer. Lifetime of the P-selectin-carbohydrate bond and its response to tensile force in hydrodynamic flow. *Nature*, 374(6522):539–542, 1995.

[28] Armando del Rio, Raul Perez-Jimenez, Ruchuan Liu, Pere Roca-Cusachs, Julio M Fernandez, and Michael P Sheetz. Stretching single talin rod molecules activates vinculin binding. *Science*, 323(5914):638–641, 2009.

[29] Fang Kong, Andrés J García, A Paul Mould, Martin J Humphries, and Cheng Zhu. Demonstration of catch bonds between an integrin and its ligand. *The Journal of cell biology*, 185(7):1275–1284, 2009.

[30] Steven M Block. Real engines of creation. *Nature*, 386(6622):217, 1997.

[31] Arup K Chakraborty and Arthur Weiss. Insights into the initiation of TCR signaling. *Nature immunology*, 15(9):798, 2014.

[32] Yuri Sykulev, Michael Joo, Irina Vturina, Theodore J Tsomides, and Herman N Eisen. Evidence that a single peptide-MHC complex on a target cell can elicit a cytolytic T cell response. *Immunity*, 4(6):565–571, 1996.

[33] Geoff P O'Donoghue, Rafal M Pielak, Alexander A Smoligovets, Jenny J Lin, and Jay T Groves. Direct single molecule measurement of TCR triggering by agonist pMHC in living primary T cells. *Elife*, 2, 2013.

[34] Timothy W Mckeithan. Kinetic proofreading in T-cell receptor signal transduction. *Proceedings of the national academy of sciences*, 92(11):5042–5046, 1995.

[35] Ju Liu, GD Albert, Hsiu-Ching Chang, Jin-huan Liu, Jiahuai Wang, Rebecca E Hussey, Yasmin Chishti, Bruce Rheinhold, Rebecca Spoerl, Stanley G Nathenson, et al. Crystallization of a deglycosylated T cell receptor (TCR) complexed with an anti-TCR fab fragment. *Journal of Biological Chemistry*, 271(52):33639–33646, 1996.

[36] Thomas Tiller, Christian E Busse, and Hedda Wardemann. Cloning and expression of murine Ig genes from single B cells. *Journal of immunological methods*, 350(1-2):183–193, 2009.

[37] Petra S Kern, Mai-kun Teng, Alex Smolyar, Jin-huan Liu, Ju Liu, Rebecca E Hussey, Rebecca Spoerl, Hsiu-Ching Chang, Ellis L Reinherz, and Jia-huai Wang. Structural basis of CD8 coreceptor function revealed by crystallographic analysis of a murine CD8$\alpha\alpha$ ectodomain fragment in complex with H-2K^b. *Immunity*, 9(4):519–530, 1998.

[38] Anne Marie Moody, Yi Xiong, Hsiu-Ching Chang, and Ellis L Reinherz. The CD8$\alpha\,\beta$ co-receptor on double-positive thymocytes binds with differing affinities to the products of distinct class i MHC loci. *European journal of immunology*, 31(9):2791–2799, 2001.

[39] Yongdae Shin, Joseph H Davis, Ricardo R Brau, Andreas Martin, Jon A Kenniston, Tania A Baker, Robert T Sauer, and Matthew J Lang. Single-molecule denaturation and degradation of proteins by the AAA+ ClpXP protease. *Proceedings of the National Academy of Sciences*, 106(46):19340–19345, 2009.

[40] Matthew J Lang, Charles L Asbury, Joshua W Shaevitz, and Steven M Block. An automated two-dimensional optical force clamp for single molecule studies. *Biophysical journal*, 83(1):491–501, 2002.

CHAPTER 3

SYNERGISTIC MECHANOSENSING DRIVES ACUITY OF $\alpha\beta$ T-CELL RECOGNITION

*This chapter is adapted from Feng et al, "Mechanosensing drives acuity of $\alpha\beta$ T-cell recognition" Proceedings of the National Academy of Sciences 114 (39), E8204-E8213 (2017) by permission granted under the Liberalization of Proceedings of the National Academy of Sciences (PNAS) copyright policy.

3.1 Summary

T lymphocytes use surface $\alpha\beta$ T-cell receptors (TCRs) to recognize peptides bound to MHC molecules (pMHCs) on antigen-presenting cells (APCs). How the exquisite specificity of high-avidity T cells is achieved is unknown but essential, given the paucity of foreign pMHC ligands relative to the ubiquitous self-pMHC array on an APC. Using optical traps, we determine physicochemical triggering thresholds based on load and force direction. Strikingly, chemical thresholds in the absence of external load require orders of magnitude higher pMHC numbers than observed physiologically. In contrast, force applied in the shear direction (~10 pN per TCR molecule) triggers T-cell Ca^{2+} flux with as few as two pMHC molecules at the interacting surface interface with rapid positional relaxation associated with similarly directed motor-dependent transport via ~8-nm steps, behaviors inconsistent with serial engagement during initial TCR triggering. These synergistic directional forces generated during cell motility are essential for adaptive T-cell immunity against infectious pathogens and cancers.

3.2 Introduction

The T cell receptor (TCR) expressed on T lymphocytes of the adaptive immune system is a stout and squat (12 nm wide $\times$ 8 nm tall) multi-subunit surface complex whose ligand binding moiety is an $\alpha\beta$ disulfide-linked heterodimer buttressed by the associated invariant CD3 subunits [1, 2, 3]. The $\alpha\beta$ chains are each encoded by V and J gene segments and, in the case of the β, a D segment as well [4]. The clone-specific TCR unique to each T lymphocyte endows mammals with the capacity to detect perturbations in host cellular function resulting from myriad infectious pathogens, physical damage (thermal, irradiation, etc.) or pre-malignant or malignant cellular transformations while averting strong self-reactivities that could induce autoimmunity [5].

Signaling is initiated through ligation of the clonotype by its cognate antigenic peptide cradled in the groove of a major histocompatibility complex molecule (pMHC) and displayed on the surface of antigen presenting cell (APCs) [6, 7]. Ligation impacts disposition and function of the associated CD3 dimers (CD3$\varepsilon\gamma$, CD3$\varepsilon\delta$ and CD3$\zeta\zeta$), as well as the transmembrane domains of the TCR heterodimer and CD3 subunits that interdigitate in the membrane to signal into the cytoplasm [8, 9]. A cascade of intracellular events involving phosphorylation of immunoreceptor tyrosine-based activation motifs (ITAMs) on the CD3 cytoplasmic domains with subsequent ZAP70 activation and downstream signaling follows [10, 11]. Membrane associated CD8 and CD4 coreceptors, marking cytotoxic T lymphocytes (CTL) and helper T cells, respectively, function to bring the membrane anchored Src family tyrosine kinase Lck to the TCR-pMHC complex for the initiation of ITAM phosphorylation. Signaling, in turn, leads to a transient rise of cytosolic Ca^{2+} and other biochemical events resulting in transcriptional activation, ultimately resulting in developmental decisions or effector functions [11, 12, 13].

A CTL must search for and destroy a target expressing a handful of "foreign" (i.e. aberrant) peptides of the relevant specificity displayed among a sea of self-pMHC molecules (~100,000) on the surface of an altered host cell. Confounding immune surveillance is

an apparent weak affinity of TCRs for pMHC, often with micromolar to undetectable affinity in solution, behaviors not reconciled with functional outcomes when examined by 2D-affinity measurements [14]. T lymphocytes do not utilize somatic hypermutation to strengthen TCR affinity as do B cells for generation of high affinity antibodies [15]. Nevertheless, T cells confronting "weakly" interacting ligands are able to sense and discriminate antigens with exquisite specificity, even detecting single amino acid differences between 2 peptides bound to the same MHC allele product [16]. A serial engagement process where a single (or low copy number) antigenic pMHC binds and unbinds multiple receptors (hundreds) on a T cell to amplify and sustain its activation has been proposed to generate signaling through fleeting encounters, including those important for antitumor immunity [17, 18]. The original concept of serial engagement (or serial triggering) was based on reutilization of pMHC over a period of hours that has been recently redefined to encompass shorter cycles of TCR stimulation over a period of seconds [19].

Of note, however, T cells exert physical force on the $\alpha\beta$TCR-pMHC complex at the T cell-APC interface through both internal and external processes that impact the above calculus. During immune surveillance, T cells scan their environment, crawling over tissue components in various organs, adopting elongated shapes typical of polarized cells [20]. Surveillance-based motility generates tensile, shear and compressive stresses over a wide range of forces (pN to nN) [21, 22, 23]. Internally, cytoskeletal machinery drives the relative movements of cell membranes including rearrangement, transport and organization of TCR complex constituents and other cell-surface molecules [24, 25, 26, 27]. As a consequence, the immunological synapse (IS) is formed with TCRs surrounded by segregated clusters of other proteins [28]. The transportation of TCRs to the IS center is due to the centripetal or retrograde actin flow [29, 30].

Experiments directly testing the role of mechanical force in triggering $\alpha\beta$TCRs were first provided using an optically trapped bead to present pMHC to a T cell [31]. Such measurements employed an oscillating shear force with a 50 pN amplitude to trigger T cell Ca^{2+}

flux, with as few as 10 pMHC/bead. Experiments with the same beads but force application normal to the cell surface did not lead to triggering. How T cells might utilize mechanical force and direction for triggering was conceptually proposed to involve nonlinear bonding kinetic mechanisms including conformational change allostery and bond strengthening [32]. This paradoxical extension of $\alpha\beta$TCR-pMHC bound lifetime under force, so-called catch bond behavior, was then observed experimentally [33, 19]. The importance of force on TCR triggering has been confirmed in other work [34, 35, 36, 37, 38, 39, 40]. However, during the initial T cell surface contact, external (scanning) and internal force (retrograde flow) appear to operate in opposing directions [41]. How these directional forces cooperate with each other and orchestrate the TCR triggering is still obscure.

Here, we actively present pMHC-bound beads to T cells, controlling the pMHC surface concentration, force magnitude and direction using an optical trap. A chemical threshold is identified in the absence of trapping force that is well above expected physiological densities for triggering by foreign ligands. In contrast, under proper loading profiles, as few as two pMHC molecules are sufficient to trigger a T cell. Applying force in the shear direction more readily triggers than does application along the normal direction, highlighting the anisotropic feature of this mechanosensor. Rather than serial engagement, during receptor-pMHC ligation, smooth active transport of beads with defined ~8 nm steps through an actomyosin-based mechanism is directly visualized. The regular stepping of this motility process is in direct conflict with features of abrupt unbinding, irregular snapback and multiple binding signatures expected for serial engagement, none of which are observed. Our measurements support a model where force-stabilized pMHC-TCR ligation of as few as two pMHC molecules under a load of 10-20 pN per complex is sufficient for a sustained T cell activation process associated in seconds with processive actomyosin-based displacement. These findings are relevant to establishing signatures of protective T cells arising from natural infection as well as vaccination efforts for eliciting protective CTL-based immunity and tumor immunotherapy.

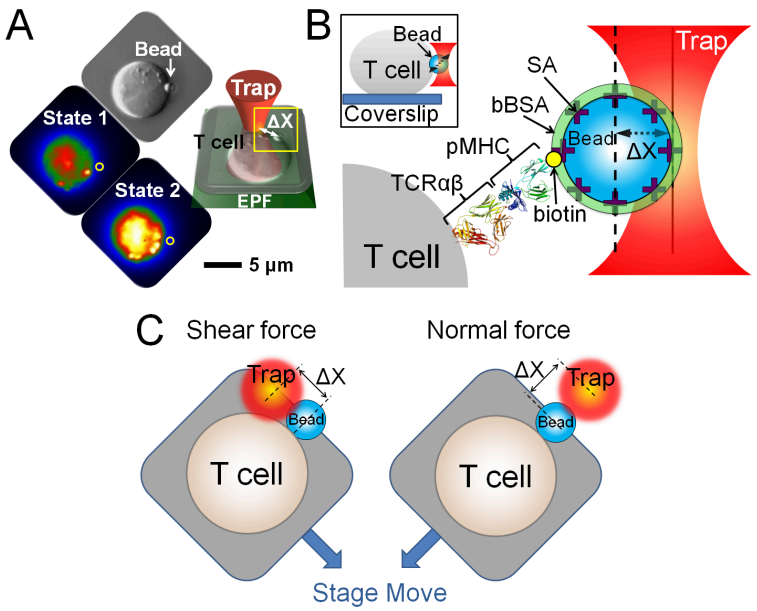

Figure 3.1: **$\alpha\beta$TCR triggering using an optical trap to apply vectoral pN forces over nanometer distances.** (A) Mechanical force is applied using an optical trap. Individual T lymphocytes are immobilized on a coverslip surface. After a trapped ligand-coated polystyrene bead is guided into contact with a T cell, a vectoral one-step force is applied to the bead by moving the piezoelectric stage. ΔX denotes displacement of the bead out of the trap center. The bead abutting the T cell surface is shown in the DIC image indicated by a white arrow and fluorescence image as gray sphere and yellow circle, respectively. The optimal force along the T cell surface triggers a rise in free Ca^{2+} shown in colorization as an increase in yellow intensity (State 2) in comparison to the initial state of the same T cell (State 1). EPF, Epifluorescence. (B) Cartoon detailing the bead-cell contact interface as expanded from the yellow box in A. Optical traps are employed for application of force to a streptavidin (SA)-coated polystyrene bead arrayed with specific biotinylated T cell receptor ligand (pMHC, in this case VSV8/K^b) and then saturated with biotin-BSA (bBSA) to prevent potential non-specific streptavidin binding to cells. The trapped bead was calibrated prior to attachment and the trap force calculated as the product of trap stiffness and ΔX. The molecular model depicts the TCR$\alpha\beta$ heterodimer from 1NFD and the pMHC from 1KPU. For simplicity, only the clonotypic heterodimer in the $\alpha\beta$TCR complex is represented. Inset: Side view of a bead attached T cell. (C) Cartoon showing optimal shear and normal force directions of the bead relative to the cell.

3.3 Results

3.3.1 Antigen presentation assay to mimic cell triggering through optically trapped beads

TCR triggering was investigated using optical tweezers combined with fluorescence visualization that permits pN step force application while simultaneously monitoring Ca^{2+}

flux linked to T cell triggering [31, 42, 43]. Our study employed individual T cells immobilized on the coverslip surface (Fig. 3.1A and Fig. 3.2). Before immobilization, cells

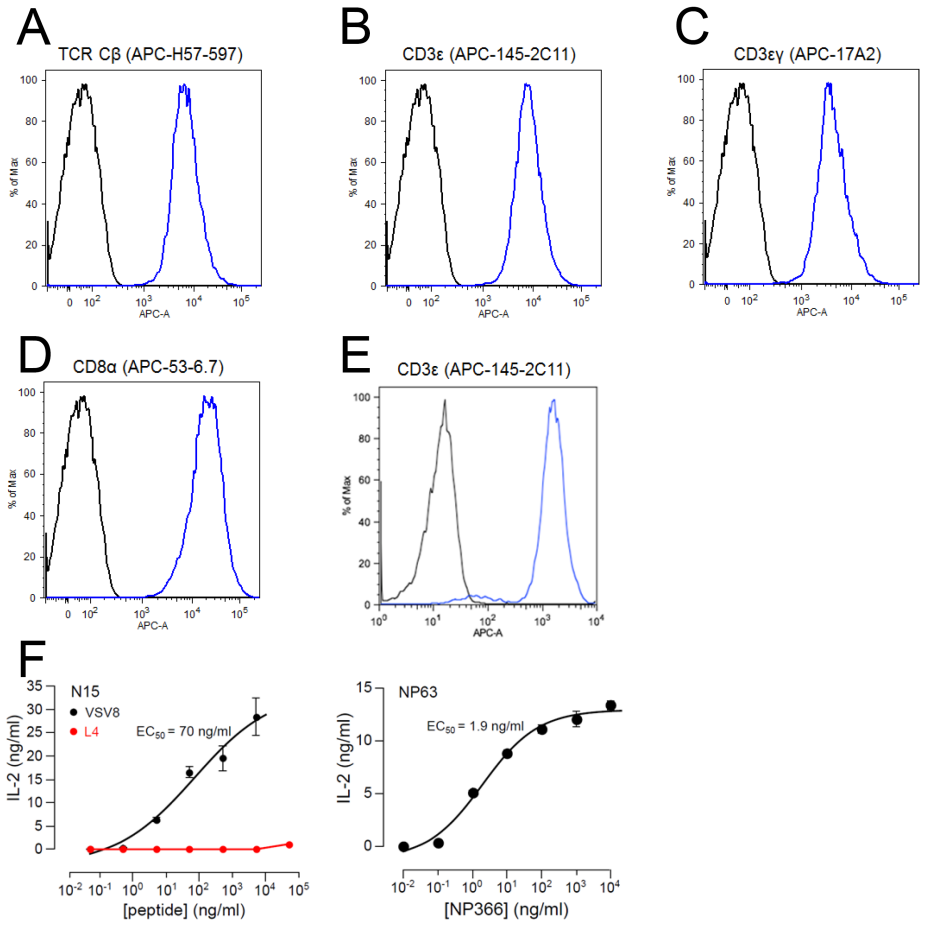

Figure 3.2: **Supplemental analysis of TCR transfectants.** Flow cytometry confirms surface expression of (A) TCR constant domain and (B) CD3ε, (C) CD3$\varepsilon\gamma$ and (D) CD8α on N15 T cells. (E) CD3ε expression of NP63 T cells. Black curves in histograms A-E show background staining of the cells in the absence of antibody. (F) IL-2 production from N15 T cells and NP63 T cells with the indicated peptides as stimulators. Results shown represent mean and standard deviations (SD) of triplicate samples. Note that when the SD is very small, it is not visible in this display. The only L4 concentration stimulating IL-2 production above background is at 50μg/ml (p¡0.001), consistent with prior studies (Refs 9-10 in SI Materials and Methods). EC50 values are given for VSV8/K^b and NP366/Db for N15 and NP63 TCRs, respectively.

were pre-loaded with Quest-Rhod 4 as a Ca^{2+} indicator. Thus, Ca^{2+} flux, an early T cell activation process, could be visualized by fluorescence enhancement. Under bright field illumination, functionalized beads were held by the fixed trap and the surface immobilized

T cell was repositioned using a piezo stage to facilitate bead-cell attachment. Binding

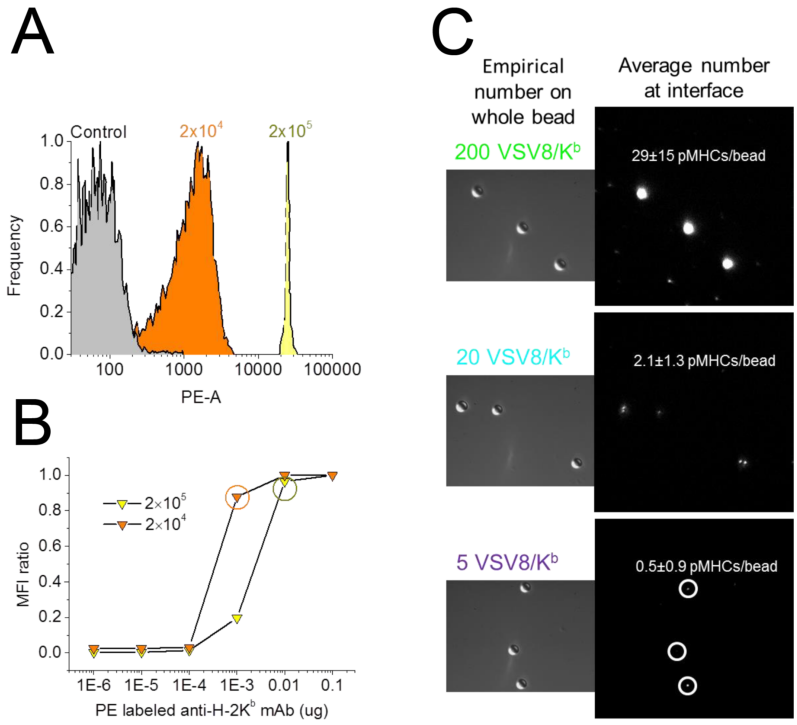

Figure 3.3: **Flow cytometric and single molecule TIRF fluorescence imaging analysis of indicated H-2K^b complexes with different numbers of pMHC molecules immobilized on beads.** (A) FACS fluorescence signals of 2×10^5 and 2×10^4 coated beads (B) Serial dilutions of mAb for measuring the surface copy numbers of 2×10^5 and 2×10^4 VSV8/K^b-coated beads with the inflection points (circled) used to calculate the pMHC numbers as indicated below. MFI: mean fluorescence intensity. (C) Single molecule TIRF fluorescence imaging analysis of beads calculated to display 200, 20 and 5 VSV8/K^b molecules/bead. More than 200 beads were measured and averaged for each empirically determined surface expression analysis. The values in the fluorescence field of view indicate the empirically determined average number +/- SD on the bead-cell contacting surface. Fluorescence signals of background, single dye and bare streptavidin coated beads were also measured. The coupled H-2K^b complexes were quantitated on beads using directly PE-labeled anti-H-2K^b mAb (AF6-88.5) immunofluorescence (anti-Kb-PE). Detailed bead preparation methods are found in Materials and Methods.

was visualized directly and through displacement of the bead out of the trap indicated by changes in signal of our position sensing subsystem, which records the bead position at 3 kHz. After binding, the instrument was transitioned to low light imaging to monitor fluorescence excited by a 532-nm laser with a low light sensitive Andor Ixon camera. Images were recorded at 0.25 Hz for 10 min. Under optimal conditions, triggered cells exhibited

fluorescence levels that steadily increased, whereas non-triggered cells showed a steady drop in fluorescence due to photobleaching. Streptavidin functionalized 1.09 μm beads were coated with biotinylated pMHC (Fig. 2.1B). Methods of quantification of pMHC on the bead are detailed in *Materials and Methods* and Fig. 3.3. Beads were sequentially saturated with biotin-labeled BSA (bBSA) to prevent nonspecific interaction. Vectoral piconewton force was generated by stepping the piezo stage to the desired distance to create a displacement ΔX as shown in Fig. 2.1C. The trapped bead was calibrated at first before the attachment and the trap force was calculated by the product of trap stiffness and ΔX.

Two different TCRs were used in our studies. The first is the N15 TCR specific for a vesicular stomatitis virus nuclear protein octapeptide (VSV8, RGYVYQGL) bound to the H-2K^b molecule (VSV8/K^b). The second is the NP63 TCR specific for influenza A virus PR8 nucleoprotein nonapeptide (NP336, ASNENMETM) bound to the H-2D^b molecule. These TCR epitopes are targets of protective adaptive $\alpha\beta$ T cell immunity against the two viruses. Comparable results with these diverse specificities imply the broadness of the dynamic mechanosensing behaviors we observe.

3.3.2 The chemical threshold for triggering in the absence of external force requires pMHC density exceeding physiological levels

We first tested the sensitivity of triggering N15 T cells using beads displaying different VSV8/K^b copy numbers at the bead-cell interface in the absence of load, beginning with saturating ligand coverage and diluting until activation was no longer observed. Beads were trapped and gently placed on the cell to facilitate attachment. The trap was then immediately turned off. Bead position and fluorescence levels were monitored for 10 minutes. As seen in Fig. 3.4A, a saturated VSV8/K^b -coated bead with ~2×10^4 molecules at the bead-cell interface generated robust TCR triggering (18 of 34 cells)(yellow triangles in Fig. 3.4A). With ~200 molecules at the interface, triggering was reduced (4 of 11 cells) with minimal fluorescence increase (Fig. 3.5B). However, beads with 29 VSV8/K^b at the

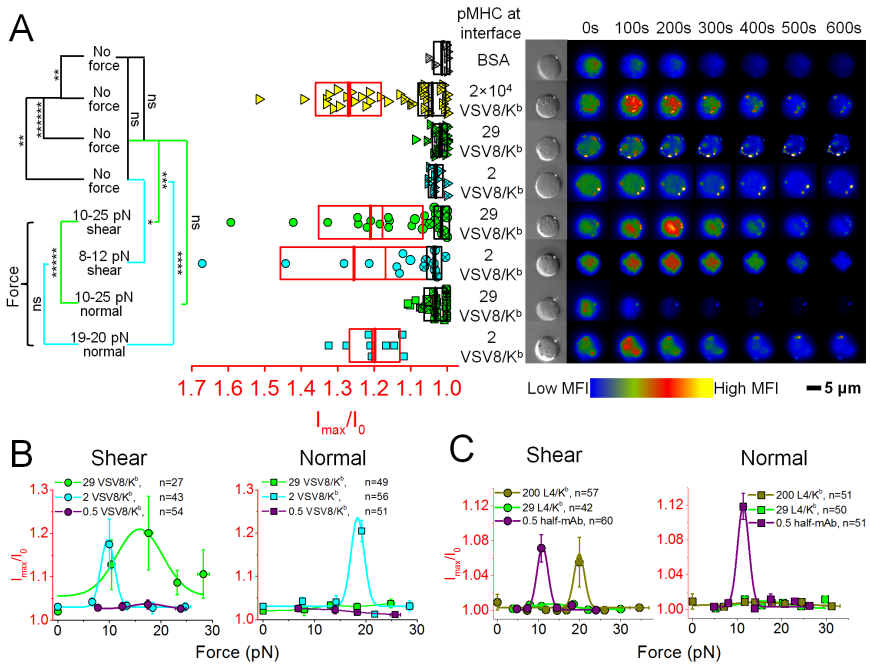

Figure 3.4: **Thresholds for $\alpha\beta$TCR triggering are dependent on both pMHC ligand copy number and directional force.** (A) Ca^{2+} flux was triggered in N15T cells by using either a high density VSV8/K^b copy number at the bead-cell interface (2×10^4) without external force or physiological densities of VSV8/K^b (29 and 2) in conjunction with an optimal vectoral force. Ca^{2+} flux signal is indicated as the ratio of maximum fluorescence intensity (I_{max}) to the initial fluorescence intensity (I_0) of the Ca^{2+} sensitive dye. Width of rectangles illustrates the standard deviation. Mean value and median value are shown in thick line and thin line, respectively. On the right, a rise in intracellular free Ca^{2+} is shown by colorization through an rise in red and yellow intensities at indicated times for representative cells. Boxes with red and black boundaries in the same column were statistically analyzed for triggered T cells (open symbols) and non-triggered T cells (symbols with $\times$), respectively. MFI, Mean fluorescence intensity; $^*P \leq 0.05$; $^{**}P \leq 10^{-2}$; $^{***}P \leq 10^{-3}$; $^{****}P \leq 10^{-4}$; $^{*****}P \leq 10^{-5}$; $^{******}P \leq 10^{-6}$. p-values referring to significant analysis were evaluated using One-Way ANOVA for all the datapoints. (B and C) Directional force vs N15$\alpha\beta$T cell triggering of Ca^{2+} flux under different load and VSV8/K^b (B), L4/K^b (C) or the antiTCR Vβ MR9.4 fragment (C) copies at the interface. Curves represents fitting with Gaussian distribution. Error bars represent SEM. The duration of the increase in calcium for shear and normal directions for VSV8/K^b in (B) and half-mAb in (C) are 269 vs. 132 seconds and 136 vs. 87 seconds respectively.

interface, a pMHC density found physiologically on normal APCs [44], did not trigger (1 of 28 cells)(green triangles in Fig. 3.4A), nor did lower pMHC copies (2 VSV8/K^b) activate the T cells (0 of 10 cells)(cyan triangles in Fig. 3.4A). Measurements on T cells with other pMHC ligands were also tested, including the weak agonist L4 [vesicular stomatitis virus

nuclear protein octapeptide (VSV8) with p4 V to L VSV8 mutation]/K^b and the unrelated Sendai virus SEV9/K^b complexes. With 200 L4/K^b or SEV9/K^b molecules at the interface, no triggering was observed (0 of 17 cells each) (Fig. 3.5A). We also performed controls with BSA-only coated beads (gray triangles in Fig. 3.4A), with fluorescence signals that were used as background for the nontriggered cells without external trapping force. These control beads manifest no cell surface binding and failed to trigger T cells, despite repeated apposition.

3.3.3 External force enhances TCR sensitivity to achieve triggering thresholds with limited numbers of pMHC molecules at the interaction interface

To determine if external force can facilitate TCR triggering at lower pMHC copy number, a step force was applied by actuating the piezo stage to move the cell relative to the fixed trap yielding a desired displacement and force. Measurements on T cells with 29 VSV8/K^b at the bead-cell interface showed robust triggering (16 of 26 cells)(green circles in Fig. 3.4B) under conditions detailed below using specified directional forces ranging from 10 to 25 pN compared with those without external load (Fig. 3.4A and B and Fig. 3.5). Likewise, bead-cell interfaces containing 2 VSV8/K^b molecules yielded 8 of 15 triggered cells at triggering force of 8-12 pN (cyan circles in Fig. 3.4B). In contrast, with an average 0.5 pMHC copy number per interface, where we expect no more than one TCR-pMHC interaction in the bead-cell contacting interface [33], no triggering was observed (Fig. 3.4B, purple circles). Plots of fluorescence increase vs. force show a narrow distribution of triggering forces at the 2 VSV8/K^b pMHC copy number dependent on force application as described below (Fig. 3.4B). L4/K^b shows triggering at 200 but not at 29 copies per interface. To determine whether the TCR can be triggered with a single sustained interaction, we used one-half anti-TCR Vβ MR9.4 mAb fragment at 0.5 molecules per interface, yielding a robust 12 of 18 cell triggering responses (at 8- to 12-pN shear force) (Fig. 3.4C and SI Appendix, Fig. 3.5A, purple).

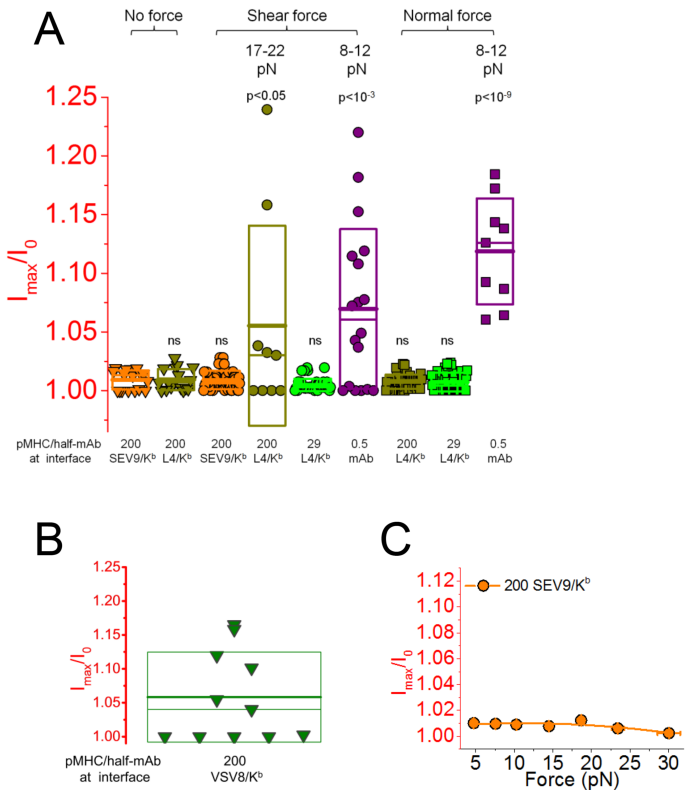

Figure 3.5: **Thresholds for TCR triggering are dependent on ligand species, copy number and directional force.** (A) Ca^{2+} flux was triggered in N15T cells by using either a high L4/K^b copy number at the bead-cell interface (200) with external shear or 0.5 half anti-TCRV antibody (MR9.4) in conjunction with an optimal vectoral force in both normal and shear directions. The other indicated conditions did not trigger. Ca^{2+} flux signal is indicated as the ratio of maximum fluorescence intensity (I_{max}) to the initial fluorescence intensity (I^0) of the Ca^{2+} sensitive dye. The rectangle height illustrates the standard deviation. Mean value and median value are shown in thick and thin horizontal lines, respectively. p-values referring significant analysis were evaluated using One-Way ANOVA for all data points. (B) N15T cell triggering of Ca^{2+} flux with 200 VSV8/K^b at the interface. (C) Directional force vs N15T cell triggering of Ca^{2+} flux with 200 SEV9/K^b as a function of the load at the interface. Fit curves show lack of a distinct peak. Error bars represent SEM.

3.3.4 T cell triggering is anisotropic, preferring shear over normal directionally applied loads

We directly measured the directional dependence of the TCR-pMHC interaction with similar step force and identical pMHC numbers at the cell-bead interface. Whereas step displacements in the shear direction exhibited triggering with as few as 2 pMHC at the

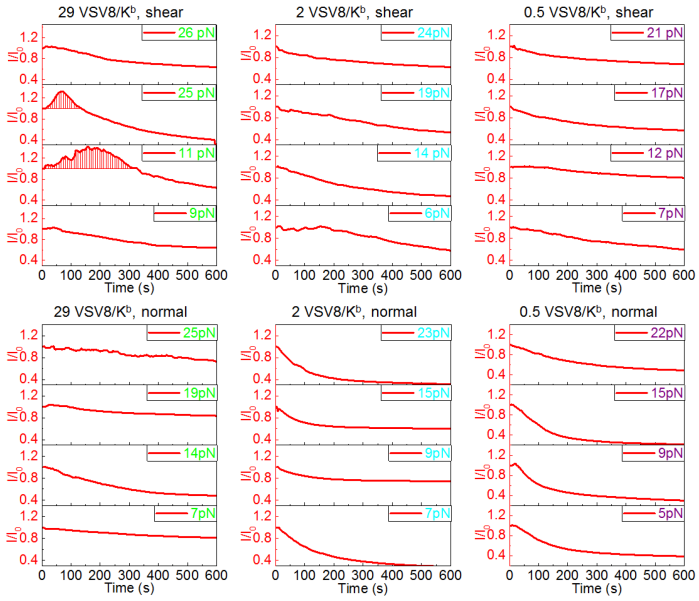

Figure 3.6: **Representative Ca^{2+} signals at indicated force, vectoral direction and VSV8/K^b copies at the bead-T cell interface. Activation is denoted by the area of red bars under the red Ca^{2+} signal curves.**

interface and 10 pN (cyan circles in Fig. 3.4A and B), forces applied in the normal direction required 18 pN (cyan squares Fig. 3.4A and B) to trigger (Fig. 3.4A and B). Ca^{2+} flux durations triggered by 29 and 2 VSV8/K^b molecules at the interface along the shear direction are 250 $\pm$ 92 s (16 cells, $\pm$SD) and 288 $\pm$ 119 s (8 cells), respectively, whereas that stimulated by 2 VSV8/K^b at the interface with optimal normal force is only 132 $\pm$ 43 s (9 cells). Interestingly, beads displaying 29 pMHCs at the interface failed to trigger Ca^{2+} flux with any force application along the normal direction (green squares in Fig. 3.4A and B) but triggered along the shear direction (green circles Fig. 3.4A and B) using a range of forces examined (Fig. 3.4A and B and Fig. 3.6). As with shear (Fig. 3.4B, purple circles), single molecule level pMHC (0.5 VSV8/K^b molecules at the interface) failed to trigger TCR with force applied normal (Fig. 3.4B, purple squares) to the cell surface (Fig. 3.4B, purple square). In contrast, triggering with the very weak agonist L4/K^b was only achieved along the shear direction (Fig. 3.4C). Triggering with the one-half antibody was possible in both shear and normal directions.

3.3.5 T cell triggering is associated with rapid relaxation and large displacements

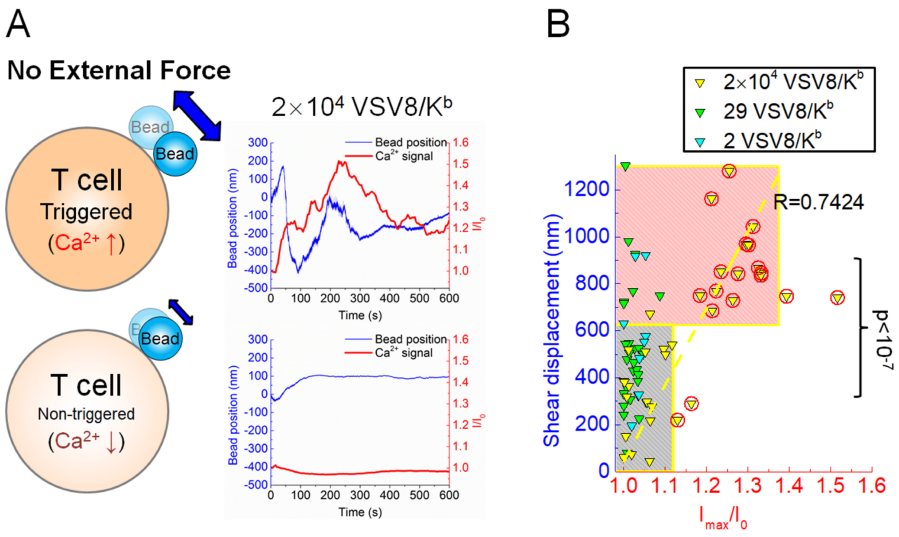

Figure 3.7: **Relationship between TCR triggering and pMHC bead shear displacement in the absence of external force.** (A) Representative 2×10^4 VSV8/K^b bead motion along the shear direction in relationship to contemporaneous measurement of Ca^{2+} signal in a triggered versus a non-triggered T cell, assessed in the absence of external load. (B) 2×10^4 VSV8/K^b bead displacement along the shear direction correlates with Ca^{2+} signal in N15 T cells triggering in the absence of external load (R=0.7427). In contrast, beads with 29 or 2 copies of VSV8/K^b at the contact interface show no correlation. The red and grey box upper limits represent statistical regions (mean+SD) for triggered vs. non-triggered cells respectively, stimulated with 2×10^4 VSV8/K^b bead. 625 nm shear displacement is used as demarcation. The yellow dash line is the correlation analysis between 2×10^4 VSV8/K^b bead shear displacement and Ca^{2+} signal of TCR triggering. Yellow data points with red circles are T cells defined as Triggered, whose I^{max}/I^0 is higher than 1.12, which is the upper limit of the grey box. p-value refers to the significant difference between values in red and grey boxes evaluated using a One-Way ANOVA.

Our measurements in the absence of force simultaneously monitor bead trajectory and Ca^{2+} flux caused by T-cell triggering. In Fig. 3.7A, cells with pMHC-saturated beads ($2\times$ 10^4 VSV8/K^b at the interface) that triggered without force exhibited relatively large displacements (~1000 nm in 200 s) and rapid positional relaxation (peak velocities of 30 nm/s). Note that, during these measurements, the trap is off, only actuated to facilitate the initial bead to cell contact; thus, bead motions originate from the cell. Change in position is contemporaneous with Ca^{2+} rise with peak flux occurring at the end of positional

relaxation and within minutes of the initial bead-cell association. Statistically, unloaded pMHC-saturated beads with limited displacement (below 625 nm) typically did not trigger (Fig. 3.7B). Cells which have fewer pMHC molecules at the interface (29 and 2 VSV8/K^b) show little responsiveness, with no correlation between displacement and Ca^{2+} flux, even for those showing large displacement.

In the presence of shear force, cells exhibit complete positional relaxation as shown in Fig. 3.8A. Here, force increases as a step and steadily decreases as the bead moves back to the trap center. Triggered and nontriggered traces were pooled, normalized and fit to a single exponential decay to extract representative time constants for the average force-displacement transients (Fig. 3.8B) [45]. Force- triggered cells exhibit rapid positional relaxation (Fig. 3.8B, dash lines) followed by a rise in Ca^{2+} signal (Fig. 3.9, red lines).

Traces were also fit individually to map the relation between trigger state, relaxation time and force (Fig. 3.8C). The detailed fitting procedures are illustrated in Fig. 3.10A. Our results illustrate that, for cells stimulated with 29 VSV8/K^b at the interface, triggered cells relaxed more quickly than nontriggered cells, $0.44 \pm 4.65\times10^{-4}$ s compared with $52.42 \pm 8.82\times10^{-3}$ s, respectively, for all measured forces. For T cells stimulated with cognate ligands at identical interface copy number (two pMHCs), triggered cells can be represented by a window centered around 10 pN exhibiting a relaxation width of 10 s compared to nontriggered cells neighboring this window. The subset of particularly fast relaxing, nontriggered cells (average $0.44 \pm 4.89\times10^{-4}$ s) remained bound but was effectively only under load for a fraction of a second (Fig. 3.8B and Fig. 3.10C). A few beads with single molecule-level array (0.5 VSV8/K^b) led to abrupt unbinding, where the bead snapped back to the trap center within 5 ms (n=19) (Fig. 3.10B and C) and failed to trigger. Fig. 3.8C shows clearly that the triggered N15 T cells were centered in the same window irrespective of whether pMHC was competent to bind the CD8 coreceptor (VSV8/K^b) or mutated to abrogate coreceptor binding to the K^b α3 domain (VSV8/$K^b{}_m$). The NP63 TCR-expressing T cells also yielded the same profile using NP366/$D^b{}_m$. Results with triggered N15 and NP63 T cells

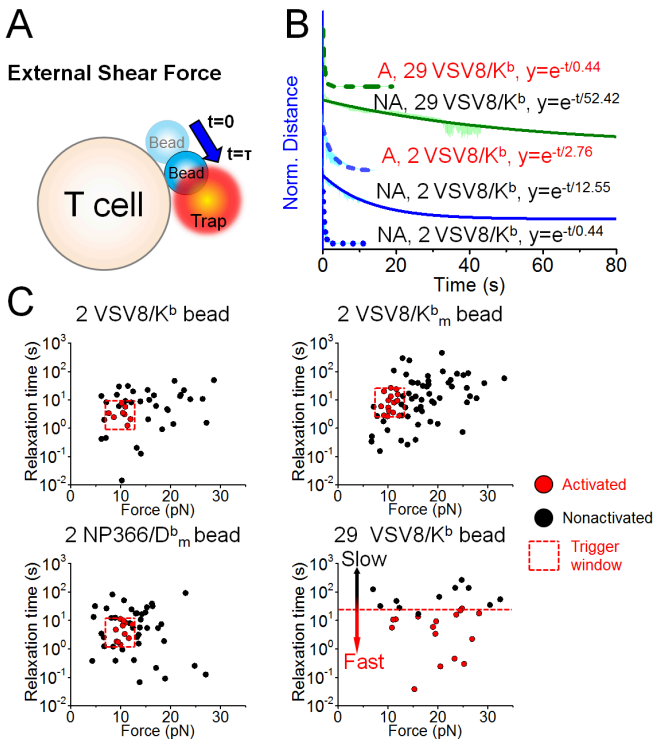

Figure 3.8: **Relationship between $\alpha\beta$TCR triggering and external shear force relaxation.** (A) Cartoon showing shear force relaxation (blue arrow) with characteristic time constant τ after a step displacement of the trap relative to the bead. (B) External force relaxation for different densities of VSV8/K^b bead on the cell surface interface with fits to a single exponential decay profile. External forces were firstly normalized, shifted to the same time zero and then averaged. Traces from top to bottom were averaged from 16 (olive dash), 11 (olive solid), 8 (blue dash), 25 (blue solid), and 10 (blue dot) separate experiments, respectively. A, activated. NA, nonactivated. (C) Scatter plots showing relationship among relaxation rate, external force magnitude and $\alpha\beta$TCR triggering at different pMHC densities for wt VSV8/K^b as well as the mutants VSV8/K$^b{}_m$ and NP366/D$^b{}_m$. For 29 VSV8/K^b, Activated is defined as an I_{max}/I_0 higher than 1.04 (the upper boundary of 29 VSV8/K^b box without external force in Fig. 2*A*). For 2 VSV8/K^b, an I_{max}/I_0 higher than 1.05 (upper boundary of 2 VSV8/K^b box without external force in Fig. 2*A*) is defined as Activated. For 2 VSV8/K$^b{}_m$ and NP366/D$^b{}_m$, I_{max}/I_0 higher than 1.00 (upper boundary of other forces box in *SI Appendix*, Figs. S7*A* and *B*) is defined as Activated. Note the trigger window depicted by dashed lines is the same in VSV8 K$^b{}_m$ and NP366/D$^b{}_m$. In all cases with 2 pMHC at interface, the window spans a force range from 8 to 12 pN.

using VSV8/K$^b{}_m$ and NP336/D$^b{}_m$ beads were pooled and illustrated in Fig. 3.11A and B. A possible triggering mechanism is illustrated in Fig. 3.11C, highlighting that because the pulling direction is shear, TCR-pMHC bonds at the back edge of the bead will sustain the load. TCR-triggered Ca^{2+} flux requires that the magnitude of pulling force on each single

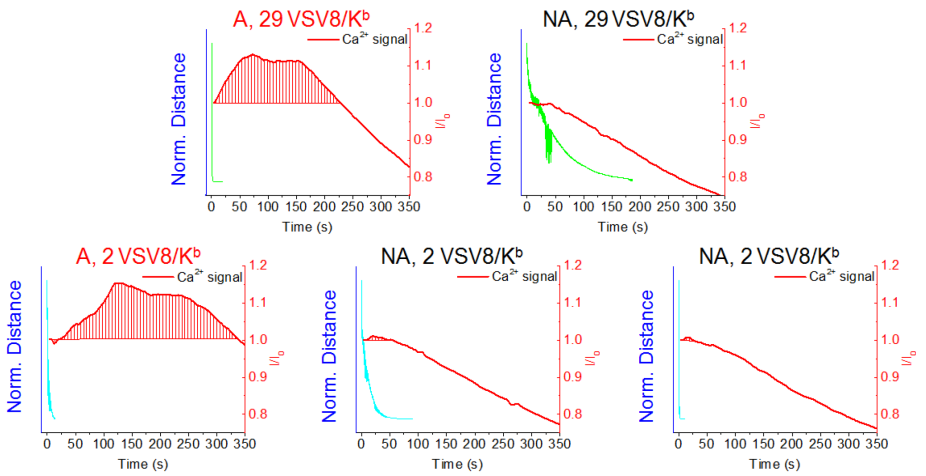

Figure 3.9: **Optimal external trapping force relaxation along the shear direction depicted with concurrent Ca^{2+} signal of a triggered T cell at 29 VSV8/K^b (top row) and 2 VSV8/K^b (bottom row) conditions.** Activated cells are denoted with red bars under the Ca^{2+} signal curves. A, activated. NA, nonactivated.

TCR-pMHC complex achieve a 10-pN physical threshold as well as an optimal relaxation rate. A greater force (i.e. 20 pN) is required for TCR triggering with 29 VSV8/K^b at the interface, because the load is distributed across multiple bonds.

For pulls in the normal direction (Fig. 3.12A), relaxation includes an initial exponential decay and then, a terminal position, where unlike pulling in shear, complete relaxation to the trap center is not achieved (Fig. 3.12B). The initial relaxation portion exhibited exponential time constants (0.1-10 s) similar to shear pulls above. However, unlike pulls in the shear direction, large displacement relaxations in the normal direction were not possible. In Fig. 3.12C, with 2 VSV8/K^b at the interface, the T cell can be triggered and exhibited partial relaxation (n = 9). Bead-cell interface with higher density (29 VSV8/K^b) did not trigger the TCR but exhibited frustrated motion caused by active intracellular processes with a sustained displacement similar to 2 VSV8/K^b. Single-molecule densities (0.5 VSV8/K^b) failed to trigger the TCR because of abrupt unbinding returning to the trap center within 5 ms (n = 16). A possible triggering mechanism along the normal direction is illustrated in Fig. 3.12D. Force, shared evenly by the 2 VSV8/K^b molecules, requires 20 pN to reach the TCR triggering threshold for any single TCR. For 29 VSV8/K^b at the inter-

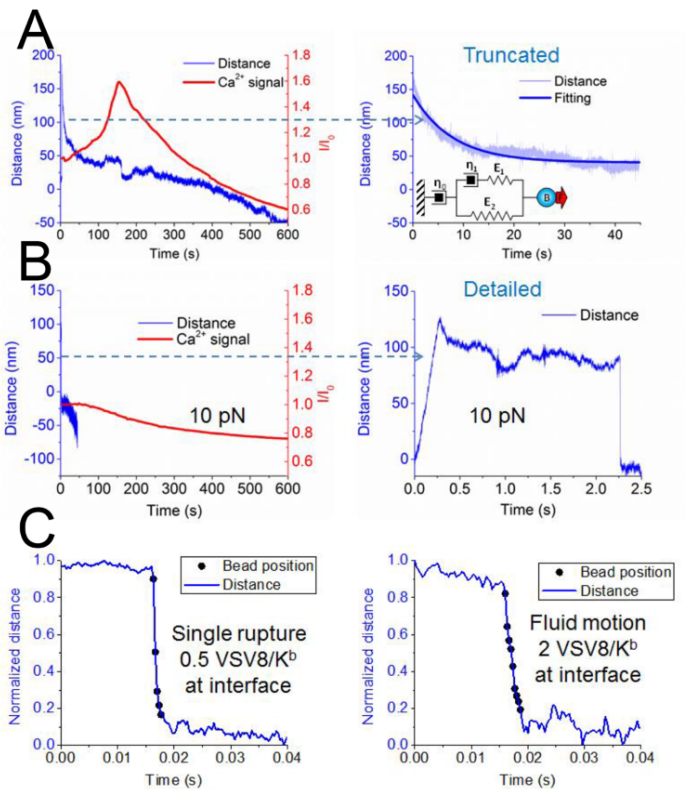

Figure 3.10: **Fitting procedure for force relaxation time calculation and representative traces for T cell triggering under 10 pN shear force and individual VSV8/K^b molecules at the interface.** (A) Original and truncated traces and fitting curve (navy) based on exponential decay equation associated with T cell activation for a bead type with an average of 29 VSV8/K^b at the interface. Detailed fitting steps are: 1) finding the peak position, 2) obtaining the 1st derivative from peak to end, 3) truncating the data which shows the zero derivative and 4) fitting the truncated data to the model: Distance released=A$\cdot$e$^{-t/}$, : relaxation time(s), t: time (s), A: Initial distance between trap and bead (nm) (B) Representative trace for 0.5 VSV8/K^b bead along shear direction showing single bond rupture and no T cell activation. (C) Normalized representative traces for 0.5 VSV8/K^b bead (left) along shear direction showing single bond rupture with five data points and 2 VSV8/K^b bead (right) along shear direction showing fluid-like motion with eight data points and no T cell activation. Data points are separated by 1/3 ms.

face, however, force is distributed among many TCRs, where any single TCR is below the threshold force for triggering. These data and those in Fig. 3.8 also rationalize the distinctions among the vectoral pulling forces required to trigger T-cell activation in Fig. 3.4B. Similar optimal triggering windows were obtained for L4/K^b and one-half antibody shear triggering Fig. 3.13.

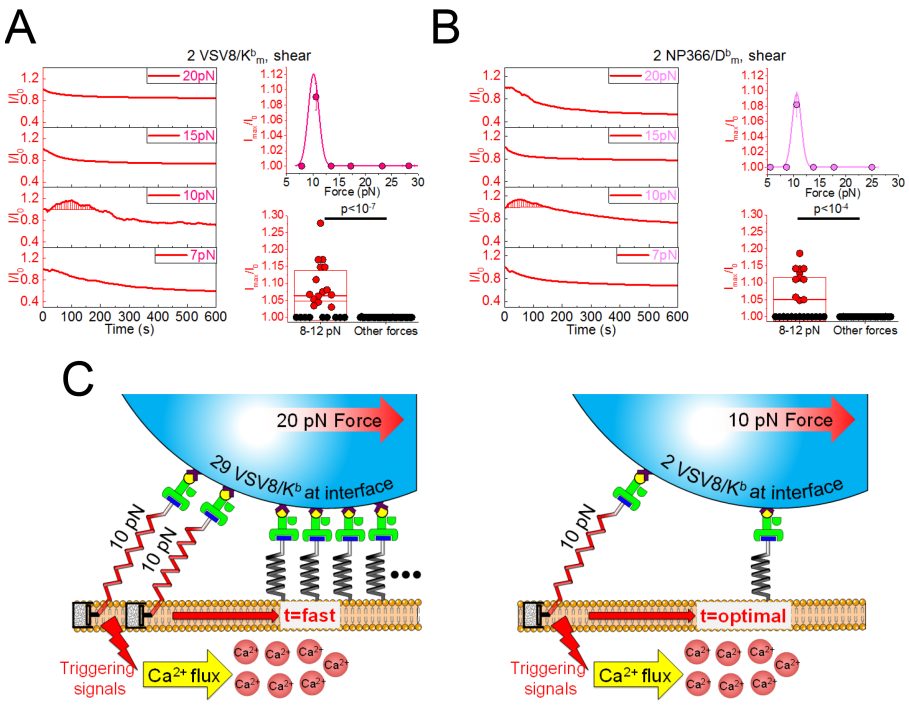

Figure 3.11: **External shear force-induced TCR triggering does not need engagement of the CD8 co-receptor with the same activating pMHC ligand.** (A) N15 TCR triggering in the absence of CD8 co-receptor ligation to 2 VSV8/K^b_m at the bead-T cell interface. p-value referring significant analysis was evaluated using One-Way ANOVA. Triggered and non-triggered cells are represented as red and black circles, respectively. 74 cells in total were used. (B) NP63 TCR triggering in the absence of CD8 co-receptor ligation to 2 NP366/D^b_m at the bead-T cell interface. p-value referring significant analysis was evaluated using One-Way ANOVA. Triggered and non-triggered cells are represented as red and black circles, respectively. 45 cells in total were used. (C) Cartoon of shear force facilitated TCR triggering. The red force arrow illustrates the force vector. Each TCR complex is represented as a spring. Force-loaded TCRs are in red and force-free TCRs are in grey. To simplify, we omit the 23 no force-loaded TCR-pMHC complexes for 29 VSV8/K^b as well as non-bounded TCRs. Along the shear direction, when external force is applied on the bead, the TCRs at the back edge sense most of the pulling force, leading to TCR triggering with 10 pN optimal force and favorable relaxation time.

3.3.6 Regular steps linked to actomyosin machinery rather than TCR serial engagement

Given the prominence of T cell-induced bead motion on TCR-pMHC ligation, we studied these movements in greater detail. Bead motion reveals discrete steps after shear force application at threshold pMHC numbers (2 VSV8/K^b at the interface). The traces are characteristic of single-molecule motility of motor proteins on cytoskeletal filaments [46].

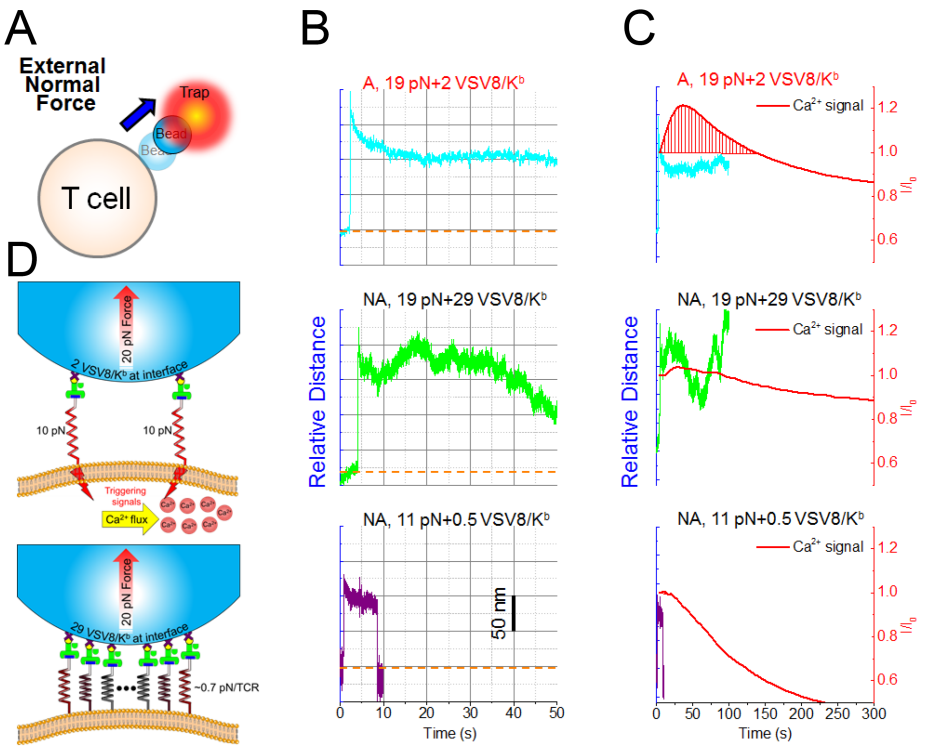

Figure 3.12: **Force facilitated TCR triggering along the normal direction.** (A) Cartoon showing partial normal force relaxation (blue arrow). (B) Representative traces for 2 VSV8/K^b (cyan), 29 VSV8/K^b (green), and 0.5 VSV8/K^b (purple) at the bead-cell contact area. Orange dash line shows the position of the trap center. (C) Bead displacement and Ca^{2+} signal. Optimal external trapping force along the normal direction with concurrent measurement of Ca^{2+} flux in an activated T cell (top) in comparison with absent T cell activation due to insufficient force (middle) and single bond rupture (bottom) at the contacting interface. Activation is illustrated by the area of red bars under the Ca^{2+} signal curves. (D) Cartoon of normal force facilitated TCR triggering. The arrow illustrates the force vector with TCR shown as a spring. Force-loaded TCRs are in red and relatively force-free TCRs are in grey with omission of unbound TCRs. While complete fast relaxation is dispensable, optimal 10 pN force per TCR-pMHC interaction is essential. Thus 20 pN loaded on 2 TCR$\alpha\beta$-pMHC interactions using 2 VSV8/K^b beads offers each TCR a 10 pN force whereas the same force magnitude loaded on 29 interactions distributes too little force (0.7 pN) per complex.

Regular stepping occurs with average displacements and dwells of ~7.7 nm for the primary peak (Fig. 3.14A). Additional step analysis is found in Fig. 3.15A. To rule out steps being caused by sequentially unbinding and rebinding of TCRs, we stabilized the pMHC-TCR interaction with H57 Fab, with a single-TCR binding site on the FG loop of Cβ domain that leads to a 10-fold increase in bond lifetime [33]. H57 Fab-ligated T cells exhibited

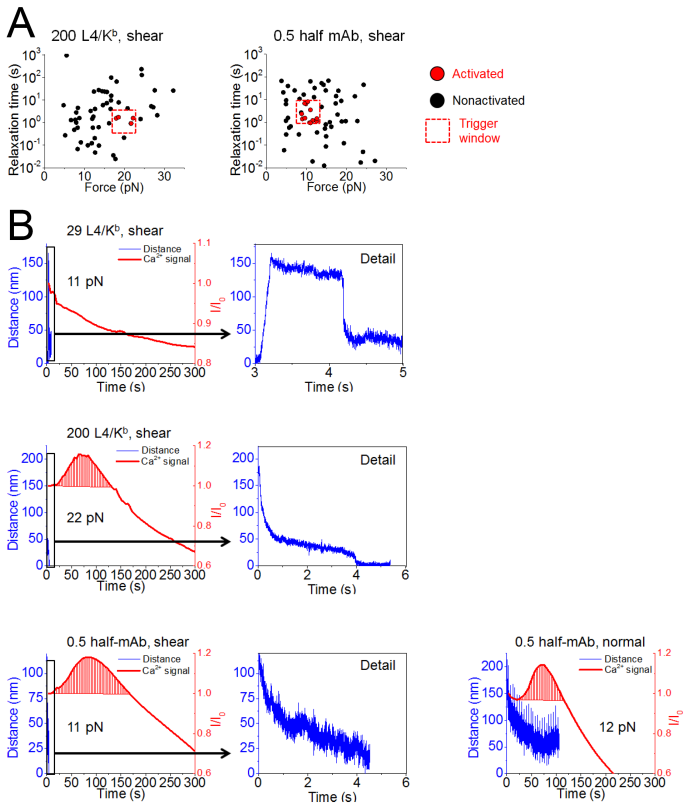

Figure 3.13: **Relaxation vs. force and calcium response of N15 T cells with L4/K^b and half mAb stimulation.** (A) Relationship between activation force and relaxation time for 200 L4/K^b (left) and 0.5 half anti-TCRV antibody (MR 9.4) (right). Note the trigger window for the half mAb is similar to Fig. 3.8C with 2 antigen pMHC coated beads. (B) Typical traces showing bond rupture and no stimulated Ca^{2+} flux when using 29 interfacial L4/K^b (top row), whereas 200 L4/K^b along shear direction (middle row) and 0.5 half anti-TCRV antibody (MR 9.4) along both shear and normal directions (bottom row) induced robust Ca^{2+} flux when optimal forces were applied.

similar step size and dwell times of 8.1 nm (Fig. 3.14B). To unveil the origin of the steps, we challenged the cells with cytoskeletal disrupting drugs, including Nocodazole (Nozo), Cytochalasin D (CytoD), and Blebbistatin (Blebb). Drug studies were conducted using concentrations that significantly disrupt the cytoskeleton but avoid cell toxicities that alter overall cell shape or ability to obtain measurements. Step probability and peak location were unaffected by 10 μm Nozo, a microtubule depolymerizer (Fig. 3.14C) [47]. Nozo blocks Lck phosphorylation [48] but enhances myosin regulatory light-chain phosphorylation, which induces activation of the motor [49]. However, both CytoD, an actin depoly-

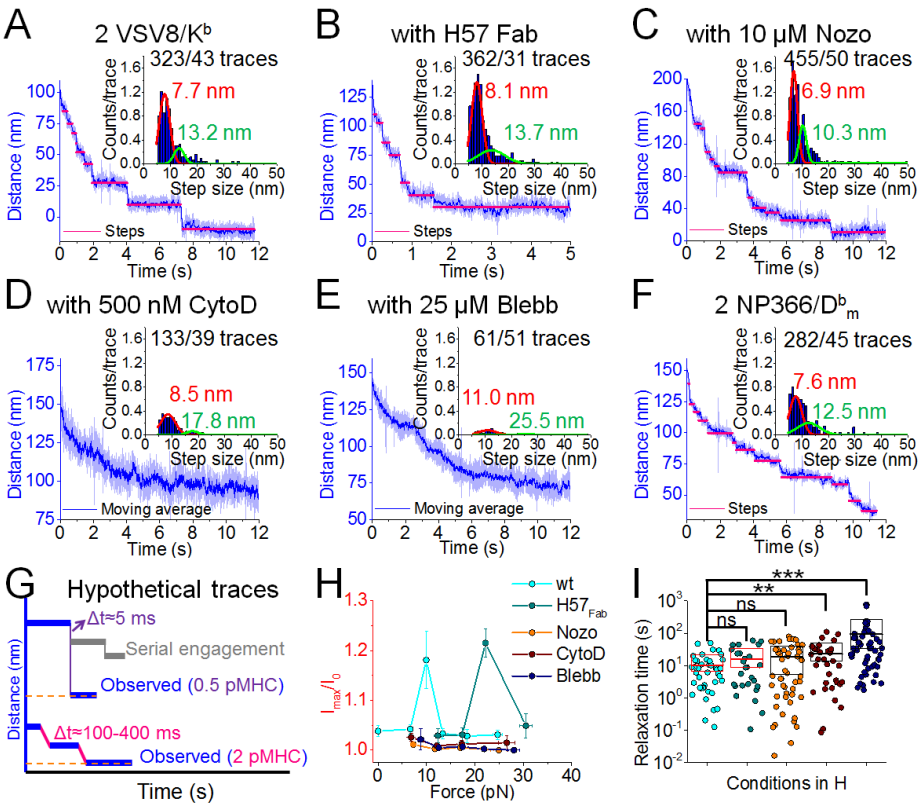

Figure 3.14: **High avidity TCR triggering is a dynamic process requiring actomyosin rearrangement rather than serial engagement.** (A to F) Typical step-wise traces for N15 T cells, treated with H57 Fab, Nocodazole, Cytochalasin D or Blebbistatin with 11-13 pN shear force and 2 VSV8/K^b at the interface. Stepping traces are common for NP63 T cells at 11 pN with 2 NP366/$D^b{}_m$. Insets show relative overall step lognormal distributions with indicated numbers of steps. (G) Hypothetical trace under load of serial engagement (grey) in comparison to the empirically observed completely rupture at 0.5 VSV8/K^b and stepwise trace at 2 VSV8/K^b conditions. Δt between adjacent dwells are averaged from 2 VSV8/K^b at the interface (steps) for the observed regular stepwise trace under shear force. For the hypothetical serial engagement trace, an upper bound of Δt=5 ms is obtained from 0.5 VSV8/K^b bead (single rupture) measurements where unbinding and complete snapback to the trap center is observed. Serial engagement, which is not observed, would either show rebind to a random location or, alternatively, return to baseline within this 5 ms (H) H57 Fab or drug treated N15TCR triggering under load. Mean fluorescence intensities of T cells triggering by external forces were monitored at 2 VSV8/K^b cases through shear direction. Error bars represent SEM. (I) Comparison of relaxation times resulting from the indicated treatments. Box height illustrates standard deviation. Red and black boxes illustrate the triggered and non-triggered conditions, respectively. Mean value is shown in thick line. $^{**}P \leq 10^{-2}$; $^{***}P \leq 10^{-3}$ were determined using One-Way ANOVA.

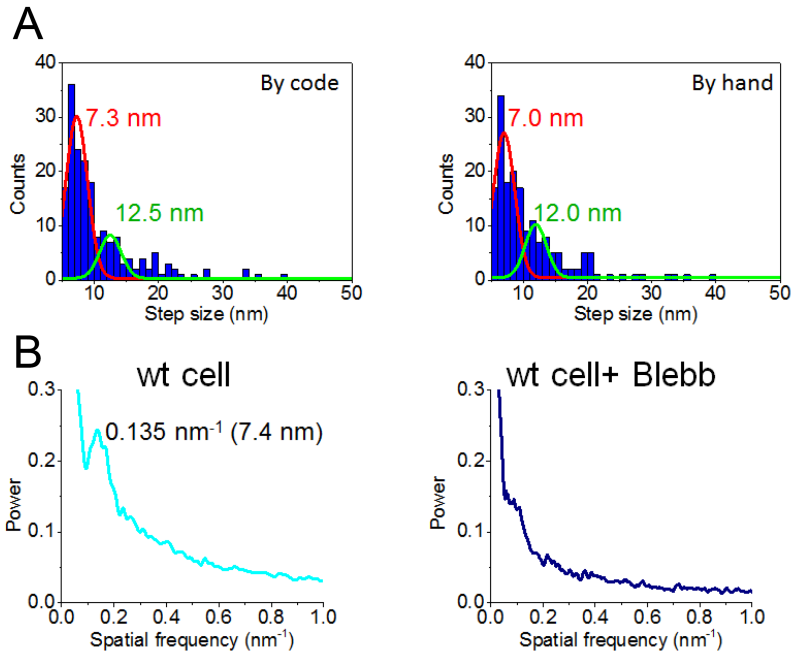

Figure 3.15: **Detailed step distribution characterization for N15 T cell.** (A) Step distribution comparison between step-finding code (left) and hand selection of dwell locations (right) for 18 traces. (B) Power spectrum density analysis for wt N15 T cell and Blebbistatin (Blebb) treated cells under the conditions in Fig. 3.14. Curve of wt N15 T cell shows a visible spatial frequency peak at 0.135 nm-1, which corresponds to 7.4 nm. However, Blebb treatment abolishes distinct peak exhibiting a relatively smooth curve.

merizer at 500 nM, and Blebb, a myosin inhibitor at 25 μM, showed clear reduction in step probability (Fig. 3.14D and E and Fig. 3.15B). Normally, we can extract 7.5 steps per trace, which were reduced to 3.4 and 1.2 steps for CytoD and Blebb, respectively. Blebb also shifted the step size distribution to 11.0 nm and reduced bead velocity returning to the trap center. Regular ~8 nm steps were also visualized for another TCR-pMHC pair (NP63 TCR-NP366/D$^b{}_m$) (Fig. 3.14F). Purified, naïve N15 transgenic CD8$^+$ T cells (Fig. 3.16A) exhibited step-linked triggering (Fig. 3.16B-D). All cells challenged with drugs did not trigger as expected given the significant role of the cytoskeleton in TCR triggering (Fig. 3.14H and Fig. 3.17) [50]. Although H57 typically inhibits triggering (31), at high forces (23 pN), some cells showed an increase in Ca^{2+}-mediated fluorescence but with reduced Ca^{2+} flux: 85$\pm$29 s (8 of 20) above 22 pN. Force relaxation time also shows significant difference when cells are treated with CytoD and Blebb (Fig. 3.14I).

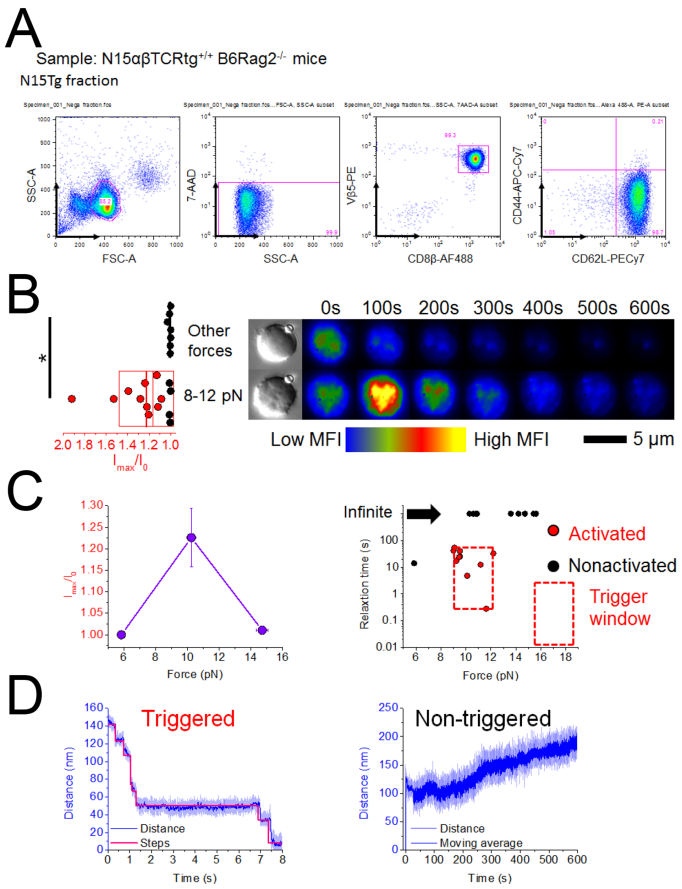

Figure 3.16: **Naïve N15Tg CD8+ T cells from N15tg$^{+/+}$RAG2$^{-/-}$B6 mice show a similar triggering behavior as N15 T cell transfectants with respect to shear load and 2 VSV8/K^b per bead-cell interface.** (A) Naïve N15tg T cells were fluorescently stained with CD8β-AF488 (eBioscience), Vβ 5.1/5.2-PE (BioLegend), CD44-APC-Cy7 (BioLegend), and CD62L-PE-Cy7 (BioLegend) and analyzed by flow cytometry using the BD LSRII. Cell debris and dead cells were excluded from the analysis based on scatter signals and 7-Aminoactinomycin D (BD Biosciences) fluorescence. The Data was analyzed by FlowJo software (Tree Star Inc.). FACS gating analysis was performed from left to right on the delineated populations. Note that essentially all CD8$^+$V5$^+$ tg T cells are naïve (CD44$^-$CD62L$^+$). (B) Ca^{2+} flux was triggered in Naïve N15Tg CD8+ T cells at 9-12 pN. *P $\leq$ 0.05. p-value referring significant analysis was evaluated using One-Way ANOVA. Triggered and non-triggered cells are represented as red and black circles, respectively. (C) T cell activation of Ca^{2+} flux under different load (left) and the relationship between activation force and relaxation time (right). Error bars represent SEM. (D) Typical triggered trace showing fast relaxation via steps (left) whereas non-triggered T cells manifest no relaxation in the trace (right).

The concept of serial engagement was suggested, because very few pMHC ligands on an APC induced loss of hundreds of copies of surface TCRs on the relevant antigen-

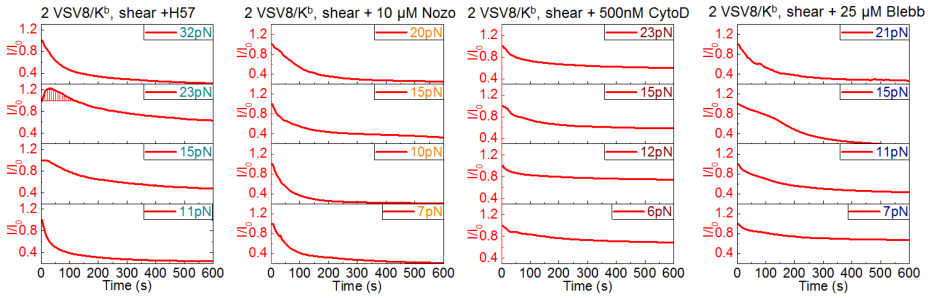

Figure 3.17: **External shear force-induced TCR triggering requires an intact cytoskeleton network.** Representative Ca^{2+} signal for N15 T cells treated with a saturating amount of H57 Fab and or indicated drugs at the specified concentrations when using 2 VSV8/K^b copies at interface. Activation is illustrated by the red bars under the red Ca^{2+} signal curve.

specific interacting T cell over a timeframe of many hours [17]. However, rather than a direct serial single-pMHC ligation of many TCRs at initial TCR triggering, establishment of a network of cytoskeletal interactions might indirectly modulate TCR distribution and/or surface expression. We tested this possibility by developing a two-bead assay, with both beads apposed to a T cell in the absence of external force. One bead is coated with a low copy number of nonactivating anti-CD3$\varepsilon\gamma$ mAb 17A2 [31] to monitor pMHC-unligated TCRs on the cell, while a second bead of different size arrays high density-specific pMHC. As shown in Fig. 3.18, only in activated T cells (i.e. fluxing Ca^{2+}) does the 17A2 bead move a greater distance to become more proximal to the pMHC bead. This phenomenon may relate to activation of motors in the vicinity of the motor ligated to the triggered (Fig. 3.18). The convergence of TCRs is consistent with initiation of IS formation. Hypothetically, serial engagement in the early timeframe (seconds to minutes) would exhibit random dwell displacements caused by sequential bond rupture and rebinding with step time intervals no greater than $\sim$5 ms (Fig. 3.10C, Fig. 3.12B, and Fig. 3.13B), the time measured for a ruptured bead to completely snap back to the trap center, whereas we observed a dwell time between steps ranging from 100- to 400-ms intervals (Fig. 3.14G). Fig. 3.2F shows functional avidity plots of N15 for VSV8 and L4 as well as NP63 for NP366 depicting IL-2 production in response to graded peptide stimulation. Given that the functional avidities

differ by 10,000-fold among these receptor-ligand pairs and no pattern of 5 ms Δt was observed, the phenomenon of serial engagement is not occurring in this timeframe.

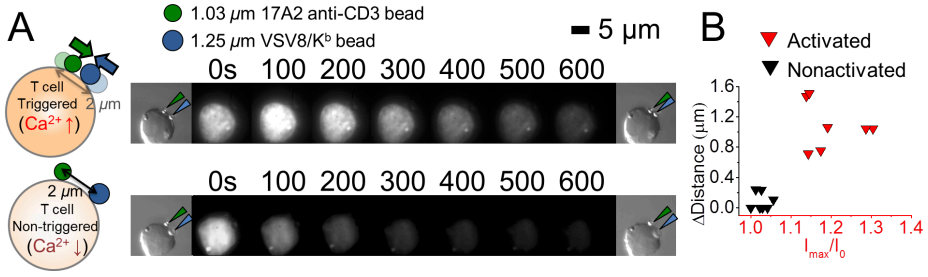

Figure 3.18: **pMHC triggered T cell cluster ligand engaged as well as unengaged TCRs.** (A) During triggering, more N15 $\alpha\beta$TCRs (binding with 1.03 μm bead, olive arrow) translocate to the interface where the pMHC-specific triggering initiates (1.25 μm bead, dark blue arrow, n=7 cells). By contrast, nonactivated cells manifest limited $\alpha\beta$TCR motion (n= 10 cells). (B) Changes of distances between the two beads for activated and non-activated T cells. The two clusters are significantly different at $p \leq 1\times10^{-6}$.

3.3.7 TCR triggering impacted by directional tangential force

Failed TCR triggering associated with slow force relaxation could be rescued by rapidly reversing the pulling direction, resulting in a fast relaxation response. Representative studies were performed on beads presenting 29 VSV8/K^b at the interface with N15 T cells (Fig. 3.19A and Fig. 3.20). Since TCRs are reported to directly link to actin filaments via CD3$\zeta\zeta$ chains [51], the fast- vs. slow-force relaxation could be explained by the assistance or hindrance, respectively, of the optical trap force as shown in Fig. 3.19B. Concordance of force direction resulting from actin motion and optical trap as applied to the TCR could facilitate release of the force-dependent structural transition of the TCR heterodimer-pMHC complex [33, 52]. In contrast, the structural extension would persist in the case of a pMHC-arrayed bead, slowly relaxing back to trap center. This behavior is consistent with that of a T cell performing immune surveillance on an APC surface; force loaded on the TCR through one direction (e.g. cell moving/spreading direction or microvilli protrusion [53, 54, 55]) may be quickly released by the motion along the other direction (e.g. actin retrograde flow), as shown in Fig. 3.19C [41]. Although N15 T-cell triggering rescue is hard to

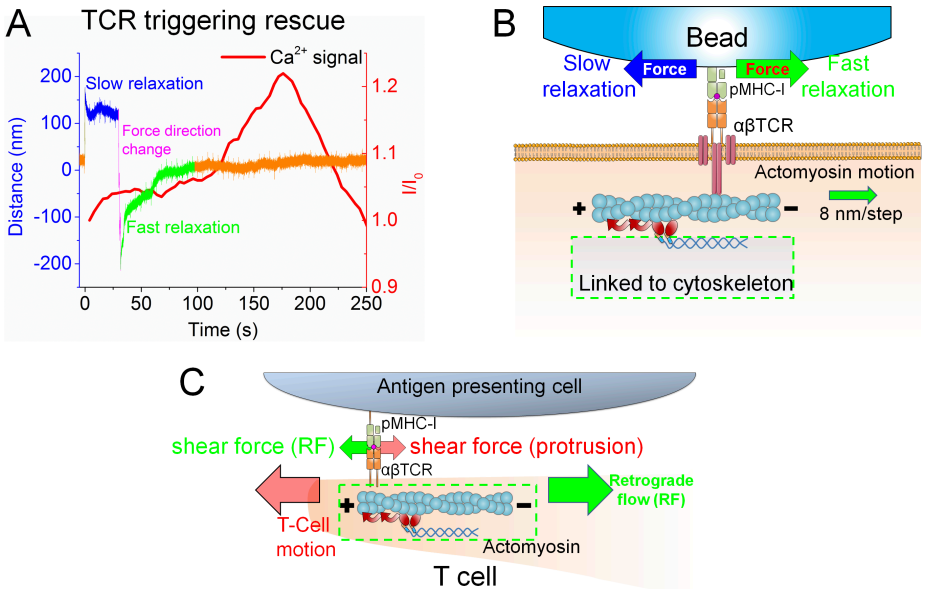

Figure 3.19: **External force in the direction of retrograde flow synergizes with actomyosin motion to facilitate $\alpha\beta$TCR triggering.** (A) Preference in external pulling force direction revealed by optical trap analysis. Failed $\alpha\beta$ TCR triggering by 29 VSV8/K^b beads after a slow relaxation (blue) lacking Ca^{2+} flux (red curve) can be rescued by quickly switching pulling force direction (magenta). This directional change induces fast relaxation (green) and attendant Ca^{2+} flux (red curve) without altering pulling force magnitude. The portion of the trace in orange represents the position of the trap center. (B) Possible actomyosin motion when rapid trapping force relaxation initiates along the tangential direction. Polarization of F-actin is indicated by plus and minus marks. Relative motion of F-actin is indicated by the green arrow. Different external force directions are indicated by blue and green arrows, which correspond to slow and fast relaxation, respectively. The actomyosin motion will facilitate force relaxation and steps when pulled in the green direction generated by myosin II pulling (gradient red arrows). In contrast, pulling in the blue direction will exhibit a tug of war that results in a slow relaxation, such that the TCR cannot be triggered, despite application of identical force magnitude. (C) Cartoon of synergistic shear forces-facilitated TCR triggering during T cell-APC contact; CD3 components were omitted for clarity. A T cell scans an APC surface in search of specific pMHC. Shear force could be generated either by cell motion (as drawn) or actin retrograde flow (RF, green arrow). Scanning force (red arrow) loaded on the TCR caused by T-cell motion (large red arrow) may be quickly released by the force generated by local actomyosin stepping (red curved arrows). Synergy between these two forces may foster TCR molecular recoil to facilitate T-cell activation and recruit more TCRs to the uropod. Note that the actin cortex is a much more complex array of actin and myosin filaments but simplified here for illustration.

actuate for 2 VSV8/K^b at the interface, hallmarks distinguishing fast relaxation from slow relaxation are evident when the position of VSV8/K^b-coated bead is close to trap center

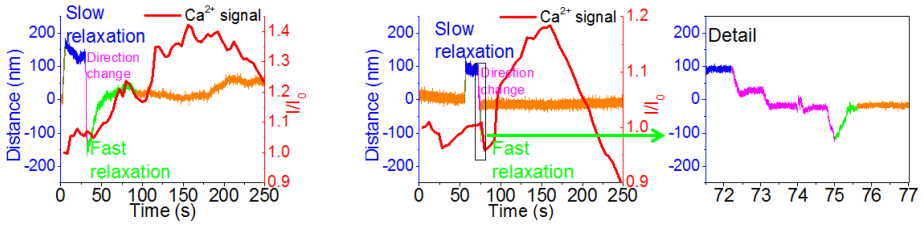

Figure 3.20: **Examples of triggering rescue through switching the direction of applied force from the optical trap.** Pulling started at the orange portion at time zero that represents the trap center, followed by a failed TCR triggering by 29 VSV8/K^b beads after a slow relaxation (in blue) lacking Ca^{2+} flux (red curve). The event can be rescued by quickly switching the pulling force direction (in magenta). This directional change induces fast relaxation (in green) and attendant Ca^{2+} flux (red curve). A detail blowup of the second example is shown in the far right panel.

(Fig. 3.21). There, bead traces exhibiting fast relaxation smoothly return to the trap center (Fig. 3.21A and B). However, slow trajectories exhibit fluctuations and even step against the trap at low displacements (Fig. 3.21C). Collectively, these results reveal a clear force vector directionality linked to successful TCR triggering by pMHC at the single-molecule level.

3.4 Discussion

T cells executing surveillance motions orchestrate a complex process that operates on many length scales. The cells leading edge, microvilli, uropod and trailing elements exhibit extensions and retractions as adhesions are formed and broken, exerting nanonewton forces to deform the underlying substratum [56]. Within the cell, actin structures cycle through states of polymerization, depolymerization and flow mediated by motors and actin binding proteins that couple filaments, sever filaments, generate branches, cap ends, and facilitate depolymerization (reviewed in [57]). T cells cluster their TCRs in the uropod, which is central to the cell and tied to actin structure undergoing retrograde flow [58, 59]. T cells exhibit frequent periods of persistent motion but with intermittent stops and turns. The underlying adhesions result in pulling and dragging motions, where shear forces similar in

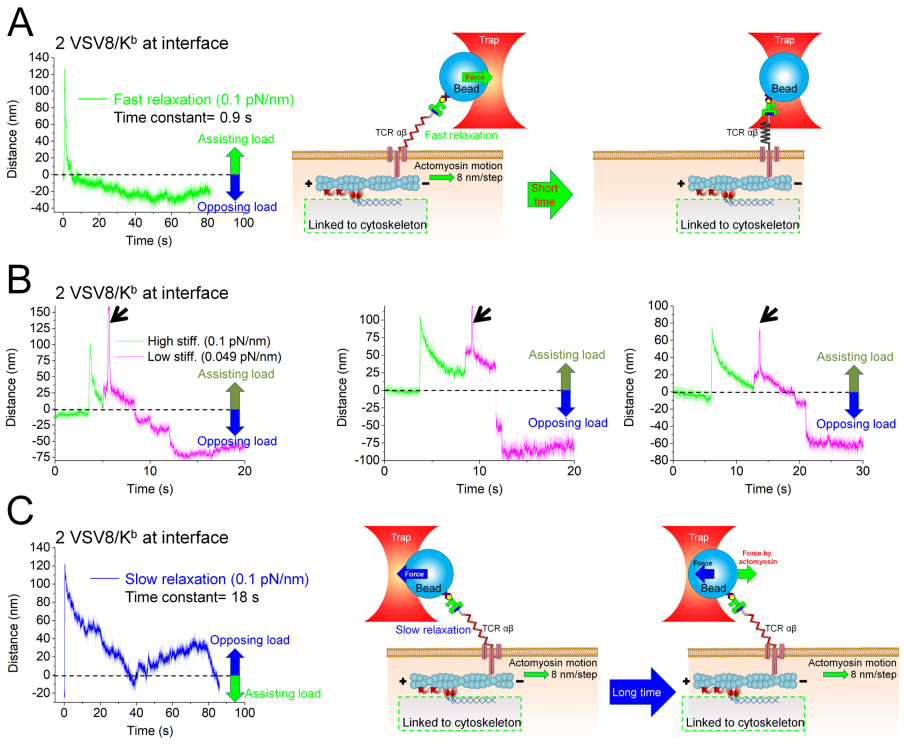

Figure 3.21: **Representative traces for force relaxation and a possible mechanism linked to T cell functional activation when using ∼2 pMHC copies are at interface.** Black dash in each trace represents trap center. (A) Fast relaxation at 0.1 pN/nm stiffness. When force direction (in green) is consistent with the actomyosin motion (in green), the TCR may be extended initially but is then restored to its original geometry as the bead rapidly returns to trap center due to actomyosin motion. Note the bead continues moving against the opposing load and stalls at ∼3.7 pN. (B) Representative traces showing possible active transport of the bead with longer displacement against the opposing load when lowering down the trap stiffness (black arrow) after the cell activation. The stall force is still ∼3.7 pN. In these experiments cells were triggered at higher trap stiffness (0.1 pN/nm, green) and then the trap force was reduced to a lower stiffness (0.049 pN/nm, pink). Note that there is a spike soon after the trap stiffness change due to a brief period where the acoustic-optic deflector amplitude is adjusting to the new setting. In the presence of the weaker trap, the system transitions to an opposing load geometry and pulls the bead out of the trap. In these cases the magnitude of displacement is larger showing directed motion still continues against the trap force. The maximum displacements are consistent with measured stall force. (C) Slow relaxation at 0.1 pN/nm stiffness. In this case force direction (in blue) is against the actomyosin motion (in green) so that the initially extended TCR remains extended with the bead returning slowly to the trap center. Note at the trap center (∼0 nm distance) the bead moves in the other direction, stalling at 3.77±0.50 pN (n=30) due to the tug of war between actomyosin motion and trapping forces.

magnitude and direction to those in our experiments can be generated (Fig. 6*C*). Our data show that the native environment of the TCR mechanosensor exploits direct coupling to the cell motility machinery for its performance. Cell motions provide the energy to activate the ~10-nm $\times$ 10-pN conformational change, where the equivalent of 100 pNnm of work is done on the system [33].

At physiological pMHC densities, triggering requires external load (Fig. 3.4A and B). We observe a triggering preference for shear vs. normal-directed forces as occur when T cells perform their scanning functions (Fig. 3.8, Fig. 3.6 and Fig. 3.12) [60, 59]. Stresses were applied experimentally via loading through our optical trap system, delivering on average, ~10 pN per TCR-pMHC interaction. The anisotropic response can be explained, in part, by geometrical factors. TCR triggering along the normal direction shares the load equally among each interfacial TCR-pMHC complex (Fig. 3.12D) and thus, requires a greater overall pulling force for any one of them to breach the ~10-pN conformational change threshold [33]. On the contrary, shear motion distributes the force unevenly at the bead-cell interface, concentrating it where fewer TCRs engage (Fig. 3.11C). Thus, for shear pulls, triggering is seen at both 29 pMHC and 2 pMHC interfacial molecules.

Without load, the TCR can be triggered when 2×10^4 VSV8/K^b molecules are present at the bead-cell interface (Fig. 3.4A). We expect that the high densities provide a stabilizing interface to create multiple points against which internal cytoskeletal forces can pull to activate TCR-pMHC mechanosensors [40, 61]. Consistent with this notion, triggered cells are associated with large bead displacements along the shear direction (Fig. 3.7). Such high-density array is relevant to exogenously loaded APCs under in vitro conditions but rarely, if at all, to naturally processed viral antigens [62].

In addition to force, direction impacts coupling of the mechanosensor to the underlying actin machinery. Shear pulls permit motility of TCRs along actomyosin structure, even at low pMHC copy number (2 pMHC) at the interface (Fig. 3.14A and F). Pulling in the normal direction directs the TCR away from membrane-associated actin. Our results are

consistent with this anisotropic phenomenon, as a much stronger Ca^{2+} flux is seen with shear over normal pulls (Fig. 3.9 and Fig. 3.12C).

Bead trajectories for cells that trigger reveal processive active transport in the direction of applied shear force. Although visually the bead positional relaxation appears smooth, the high spatiotemporal resolution of our instrument allows discrete stepping of the TCR coupling to the actin machinery to be detected. Although the step size (8 nm) suggests microtubule-based transport, drug inhibition studies and stall force (3.8 pN) measured here (Fig. 3.14A and F and Fig. 3.21) are consistent with myosin-based transport (and steps sizes) on actin filaments [63, 64, 65]. We cannot formally rule out that the transients originate from bulk contraction of actomyosin networks, release of actin cross-linkers or other attachments, or encountering of other obstacles in the cell. Notwithstanding, Fig. 3.21 shows motion against the trap force, revealing that active transport contributes to bead behavior after an activating manipulation.

Unlike the rapid and relatively long distance bead motion observed in triggered cells, bead trajectories of most non-triggered cells show a slow return to the trap center (Fig. 3.8B and Fig. 3.9). The slow relaxation further suggests that a strong linkage connects the TCR to cytoskeleton. In contrast, a fluid-like microenvironment, with TCR uncoupled to the underlying actin structure, results in fast bead relaxation to zero displacement as the large trap force easily overcomes the relatively small drag force of the TCR complex within the membrane (Fig. 3.8B, dotted blue line). Fluid-like relaxation is directly seen in some traces, which exhibit distinctly faster timescales relative to observed active motility (Fig. 3.8B and Fig. 3.10C). In fact, while naïve cells that triggered showed stepping, those that failed to trigger did not relax to zero displacement (Fig. 3.16D). Moreover, rapid fluid-like relaxation is not observed. This is consistent with the greater densities of TCR and associated actomyosin on the surface of the ~4 μm diameter naïve cell.

Direct coupling to underlying cytoskeleton is a desirable feature underpinning our mechanosensor model as TCR activation requires a sustained load. The direct connection

to actin (i.e. a load sustaining pathway) is likely through a single active motor, because discrete steps are observed. If multiple motors were transporting the TCR, then that discreteness would be blurred, and the single-molecule nature of the stepping lost because of averaging over an ensemble of motors. Our rescue experiments (Fig. 3.19A) also support the model that motility is linked to actomyosin and a single or small number of motors and only permitted in a direction aligned with the polarity of the underlying actin cytoskeleton. Triggered T cells manifest actomyosin motion in the direction of force application; thus load is in a direction that assists motility (Fig. 3.21A). Force in the opposite direction works against motility and opposes transport, setting up a tug of war between the trap and motor leading to a stall. Myosin II stall forces have been reported in the range of 3.4 $\pm$ 0.9 pN, consistent with lack of motion against the ~10-20 pN trap forces applied here (Fig. 3.21C) [66]. If a handful of motors were engaged and activated, collectively, they would likely overcome the opposing trap force and displace the bead. Trajectories of non-triggered cells under load exhibit small amplitude displacements above the thermal noise distribution of the trapped bead, likely driven by TCR linked actomyosin machinery.

Given that the $\alpha\beta$TCR-pMHC complex has a wide base, optical trap shear load applied parallel to actin structures, analogous to forces at work during immune surveillance motion, will torque the mechanosensor apparatus. The pushing and pulling on signaling structures drives T cell activation. Although we observe some bead motion at low force, TCR activation correlates with activation of cytoskeleton motility [40]. A number of mechanisms may drive the latter, including phosphorylation, Ca^{2+} increase, and mechanically triggering activation. Motors within the neighboring microenvironment may be able to receive these signals and activate their associated TCRs to amplify the signaling cascade [67]. In two-bead experiments, a pMHC array-saturated bead was used to trigger the cell, while a second bead coated with a nonstimulatory anti-CD3$\varepsilon\gamma$ mAb [31] showed motion towards the triggered bead. This motion was not observed in cases where the pMHC-coated bead failed to trigger the cell, suggesting that the triggering event activates neighboring motors.

Thus, during T cell activation, the neighboring, nonengaged TCRs will accumulated at the contact site [68] by direct active transportation of F-actin-coupled TCRs and assembly of initial non-coupled TCRs to F-actin through ERM (ezrin/radixin/moesin) proteins [69].

In contrast, without direct connection to the cytoskeleton to sustain load and drive force generation, the TCR-pMHC bond simply unbinds or displaces within the fluid-like membrane, never achieving critical load thresholds required for mechanosensor-based activation, including bond strengthening, conformational change, and other push and pull motions [33, 52]. A fluid-like microenvironment does not have the densely organized actin machinery of a motile cell, and thus, second wave signaling after TCR-pMHC triggering is muted. Similarly, load in the normal direction pulls the TCR away from membrane-associated actin. We underscore that mechanosensor activation requires a physical anchor, namely the underlying actin cytoskeleton. Fortunately, our pulling geometry capitalizes on cell surface attachment to the coverslip where an organized actin structure is created (Fig. 3.1B, inset) [70], similar to that of T cells scanning a cellular substratum. Beads are placed on the side of the cell adjacent to this structure where TCRs are engaged with actin machinery.

Biomembrane force probe analysis has been used to investigate early T-cell activation events [19] by applying load through pMHC to the distal pole of the T cell, typically opposite the holding micropipette location, where organized actin structure is sparse or lacking [70]. Repeat pulls are required to activate individual T cells with force direction normal to the cell surface (which we have shown here is less efficient than shear force). Ligated TCRs likely form a locus to organize actin machinery, permitting actomyosin-mediated motility and neighboring TCR signaling. Because signal buildup independent of those originating from a single TCR contributes to T-cell activation, the process is empirically conceptualized as cumulative bond lifetime [19].

The threshold studies on three different systems show a very similar window for triggering requirements centered at ~ 8-12 pN (Fig. 3.8C), force ranges and relaxation times

consistent with myosin stepping. Forces below this region do not permit catch bond formation necessary to create an energized TCR-pMHC bond [33, 19]. On the other hand, higher force regimes also fail to trigger. Although we believe these TCR-pMHC molecular interactions are capable of supporting conformational change, they may either rapidly rupture or not allow repetitive hopping back and forth between conformational states seen in our single molecule experiments [52]. Actomyosin-based transport acts as a force regulator, maintaining the TCR-pMHC system within this window optimal for conformational transitioning. Oscillating conformational changes in single TCRs likely foster signal transmission by altering membrane lipids, inducing transmembrane segment conformational change, or exposing interfacial cytoplasmic tail segments for downstream modifications [9]. Our triggering of single cells is quite robust, with ~ 53.3 % of T cells triggered by the lowest pMHC density studied here using optimally applied force. This frequency is remarkable, assuming a 50:50 chance of applying the correct pulling direction relative to actin polarity.

Supported lipid bilayer (SLB) experiments investigating TCR activation are performed at high pMHC densities, where the T cell is able to elicit signals without an apparent external force and in geometries initially devoid of organized actin [71]. T cells are then placed on the bilayer surface establishing fluid-like areas in which TCRs-pMHC bonds move freely flanked by rigid supports, where their motion is blocked. Force across the TCR can only be sustained against those supports or within internal cellular actomyosin structures. The triggering chemical thresholds are very high for SLB experiments, 0.2 pMHC per 1 m^2, which corresponds to ~16 pMHC beneath the cell [28]. At least 4 pMHC within a single TCR cluster spanning 400 $\times$ 400 nm^2 and containing 18-100 TCRs, is sufficient to induce the Ca^{2+} flux [72]. TCR-pMHC clusters form and begin to organize actin machinery, eliciting transport and IS formation with distal, peripheral and central supramolecular activation clusters. Triggering is not immediate but requires sufficient ligand density and time (minutes) to generate motions and forces necessary for clustering and

triggering. A mature IS contains all of the features of our mechanosensor-based activation, including shear motions and the ability to generate force across a TCR-pMHC bond, processive motility, and activation and transport of neighboring TCRs. These IS structures are reflective of uropod actin organization for mediating rapid Ca^{2+} flux and motor activation featured by our experiments.

Earlier studies have suggested that only a single or very few pMHC molecules per APC/ target cell are required to stimulate T cell activation [73, 74, 75]. Although our lowest pMHC densities capable of triggering cells involve two pMHC molecules at the interface, the bead trajectories with nanometer-scale resolution suggest that a single interaction is sustaining the load. Perhaps the second molecule serves to stabilize the interaction along a line, defined by two points. This finding is consistent with adhesion activation studies requiring two ligands in related systems [76]. While our assay geometry recreates many of the elements found in cells undergoing surveillance, it lacks APC adhesion molecules such as CD58/48, that are known to be important for cognate recognition by pairing with CD2 on the T cell to enforce the relevant intermembrane spacing between cells forming conjugates [77]. Thus, in the context of a T cell-target cell or T cell- APC conjugate, one TCR-pMHC bond is probably sufficient to trigger. Triggering with single molecules of the MR9.4 mAb fragment supports this notion.

Serial engagement is a leading model for T cell activation based on a concept of sequential binding and unbinding of a single pMHC molecule to multiple TCRs [17]. The model rests on evidence that many TCRs on a single T cell are down-regulated in the presence of small numbers of pMHC molecules. Serial engagement has morphed over years to incorporate arguments germane to 2D vs. 3D apparent binding kinetics [78], rationalizing the requirements for optimal TCR affinity to avoid interactions that are too strong or too weak to achieve repeat binding and sustained T-cell signaling [18]. Liu et al. [19] suggested that serial engagement is occurring through early and rapidly accumulated bond lifetimes.

Multiple observations made here are in direct conflict with serial engagement as being

critical for initial TCR activation over seconds to minutes as opposed to hours. First, we observe immediate and direct stepping in trajectories of beads triggering cells. These findings indicate a rapid, sustained, systematic and strong connection to the actomyosin based machinery (Fig. 3.14A). Second, in the presence of H57 Fab, which extends the N15 TCR-VSV8/K^b bond lifetime 10-fold, where any unbinding probability is further reduced [33], we observe a similar stepping signature, suggesting the TCR-pMHC maintains a single bond throughout the trajectory (Fig. 3.14B). Third, given known estimates for 2D densities of pMHC and TCRs at the bead-cell interface, the probability in our system of pMHC rupturing and binding a second TCR is less than 1% [78, 79] at the single molecule level (0.5 VSV8/K^b at interface). Thus we would expect to see only a single binding event during the trace. In fact, for experiments where we observe unbinding, beads return to the trap center within 5 ms (Fig. 3.10C), a time window extremely short with respect to requirements for serially engaging a second receptor. If serial engagement were occurring, we would observe a single short dwell followed by a single rupture and snap back to the center of the trap position (Fig. 3.14G). Rather we observe regular discrete steps (Fig. 3.14A). This is also consistent with single pMHC tracking experiments, showing that re-entrapment of the same pMHC with multiple TCRs nearby is unlikely once it is disengaged from the TCR [80]. Fourth, conditions expected to severely reduce serial engagement, such as pulling in the normal force direction where pMHC is moved away from the cell surface, reducing the probability for repeat binding, still allow triggering (Fig. 3.12). Fifth, a wide array of ligand affinities was investigated here, where weaker binding L4 showed reduced triggering over VSV8. In contrast, sustained binding through a single one-half antibody was capable of triggering cells at the single-molecule level. Sixth, we can directly show clustering of pMHC-triggered and pMHC-untriggered TCRs in two-bead experiments (Fig. 3.18). Our two-bead measurements suggest that serial engagement is not required for initiation of IS formation in this timeframe.

The translational implications of our findings are significant. T cell activation requires

recognition of but a handful of specific pMHC ligands on a given target cell. This sensitive TCR signal transduction apparatus is dependent on external mechanical force resulting from cell movement and coordinated intracellular retrograde cortical actin flow similarly directed. A correlate is that foreign antigens derived from infectious pathogens or non-synonymous mutations in tumor exons need not be displayed at more than a few copies on the target because the TCR functions as an exquisitely sensitive anisotropic mechanosensor. Highly potent CTL for adoptive immunotherapy may be most effectively stimulated in vitro on relevant pMHC molecule arrays using pN shear forces to train and expand CTL for subsequent in vivo use. Chimeric antigen receptor T cells (CAR-T) consisting of an antibody antigen-binding fragment of predefined specificity as an ectodomain linked to an intracellular T cell activation domain originally proposed by Eshhar in 1989 [81] have shown great clinical promise recently [82]. The new understanding of the molecular features of TCR mechanobiology revealed here should be exploited to optimize the synthetic biology of CAR-T design to confer heightened potency as well as intrinsic regulation features.

3.5 Conclusion

T-lymphocyte activation during immune surveillance begins with recognition by its $\alpha\beta$ T-cell receptor (TCR) of a peptide ligand bound to an MHC molecule (pMHC) on infected or otherwise altered cells. Using optical traps, we show that activation is fostered at the single-molecule level through synergy between external load on the TCR-pMHC bond and internal, sustained stepping via motor-dependent transport. Chemical thresholds in the absence of load require much higher pMHC density than observed physiologically. With load, however, T lymphocytes can be reliably activated with ~10 pN per TCR molecule, mimicking native shear motions involving a mere two pMHCs at the interaction surface. Initial TCR triggering sensitivity results from synergistic mechanosensing rather than previously postulated serial engagement.

3.6 Materials and Methods

3.6.1 External Mechanical Force applied on the T cell using optical traps

Various external mechanical force applications using optical traps. A single pMHC-functionalized bead (d=1.09 μm) was trapped with a 1,064-nm laser (stiffness 0.06-0.13 pN/nm) and placed alongside a surface-bound T cell with an automated piezoelectric stage. The bead position relative to the trap was monitored so that contact could be achieved with minimal pushing force (<5 pN). After T cell-bead contact was verified, DIC images were taken to calculate the contact area between bead and cell membrane. The contact area was calculated as the surface area of a zone of a spherical cap with its height, which was controlled during the course of the experiment by viewing the position signal along the normal direction. A shear or normal force was then applied to the bead by displacing the bead-attached cell relative to the fixed trap using fine motions of the piezo stage. The force on the bead was determined by measuring the trap stiffness prior to cell-bead contact by the equipartition method, and by measuring the displacement of the bead from the trapping center via post-processing of experiment videos. Distances between bead and trap center were sampled at 3 kHz, antialias-filtered at 1.5 kHz, and recorded for 10 min. Simultaneously, T cells were excited using a 532-nm laser to monitor Ca^{2+}-sensitive Quest Rhod-4 fluorescence every 4 s right after force application. Assays were performed at 37 ^{o}C. All of these experiments were done using an automated custom-built optical trap designed for simultaneous force and fluorescence experiments at the single molecule and single cell scales [42].

3.6.2 Two-bead assay

A single 17A2 antibody functionalized fluorescently labeled bead (d=1.03 μm) was firstly trapped with a 1,064-nm laser and then placed alongside a surface-bound T cell with an automated piezoelectric stage. Secondly, a saturated VSV8/K^{b} -coated bead (d=1.25

μm) was trapped and placed at a position 2 μm distal to the antibody-coated bead. This distance ensures that the trap does not interfere with the antibody-coated bead. Immediately following attachment of the the saturated VSV8/K^b -coated bead to the T cell membrane, the trap laser was turned off and T cells were excited using a 532-nm laser to monitor Ca^{2+} sensitive Quest Rhod-4 fluorescence every 4 s. Two DIC images were also taken before and after the 10-min fluorescence recoding. Assays were performed at 37 ^{o}C.

3.6.3 Cell culture

Cell lines were maintained in high glucose DMEM medium (Sigma-Aldrich) supplemented with 20 % (v/v) fetal bovine serum (FBS) (Sigma-Aldrich), 100 U/ml penicillin, 100 U/ml streptomycin (Life technology), 2 mM glutamine (Life technology), 1 % (v/v) Non-essential amino acid (Life technology), and 0.1 % (v/v) 2-mercaptoethanol (Life technology) and reached the log phase of growth prior to performing the triggering experiment. Naïve T cells from mice were isolated and used shortly post-purification as described below.

3.6.4 Production and characterization of N15 and NP63 T cell lines and their IL-2 production

The BW5147.3 cell line was obtained from ATCC and plasmids CD3WT pMIY and TCR pMIG were a kind gift from the D. Vignali (St. Jude Children's Research Hospital, Memphis, Tennessee). The wildtype mouse CD3 and N15 TCR genes in each plasmid were constructed using the viral 2A-linked system [83] to generate multicistronic vectors for co-transfection of all of the CD3 and TCR genes. The CD8 and genes [84], the CD3WT and N15 TCR plasmids were first transfected into Pheonix-Eco packing cells for the production of CD3 and TCR retroviruses. The virus supernatants were harvested and then used to retrovirally transduce the BW5147-CD8cells to incorporate the CD3 and TCR genes in that order to create the N15TCR^+ $CD8^+$ CD8 $^+$BW5147.3 cell line (N15 T cells). For a

second T cell line, NP63, a similar approach was employed. The NP63 TCR is an influenza A PR8 virus NP366-374/H-2D^b-specific TCR cloned from PR8 virus infected mice, as shall be detailed in a subsequent paper. Briefly, however, CD8$^+$ NP366-374/H-2DD^b tetramer$^+$ cells from spleen of influenza infected mice were single-cell sorted and TCR and cDNAs were amplified from individually sorted cells by single-cell RT-PCR method [85, 86]. Both N15 and NP63 T cell lines were sorted by FACS for stable TCR expression at copies representative of normal naïve or memory T cells (~20,000-40,000 copies per cell).

The T cell activation assay was carried-out in triplicate in a 96 well plate using 1-2$\times 10^5$ R8 cells irradiated at 3000 rads prior to use with 1-2$\times 10^5$ N15 or NP63 T cells in each well. Varying concentrations of the stimulatory peptides VSV8, L4 or NP366 were added to each well ranging from 0-10g/ml. An optimal combination of PMA (25 ng/ml)/ionomycin (2.5 μg/ml) was used as a positive control. The peptide stimulated cells and the negative and positive controls were incubated for 16-18 hours overnight at 37 ^{o}C. Following incubation, the cell supernatants were harvested for IL-2 ELISA assay. Where indicated, the EC50 of the IL-2 producing cells was calculated using a 4-parameter logistic model [87].

The IL-2 ELISA assay was completed using the mouse IL-2 DuoSet and ancillary reagent kit 2 (R&D systems). The T cell supernatants were diluted in media such that the O.D. 450 nm readings fall within the standard curve for the assay due to the high level of IL-2 production in the presence of the VSV8 peptide. The assay was then carried out following the kit instructions. The negative control values were subtracted from each sample point and concentrations in pg/ml were calculated from the standard curve.

3.6.5 Preparation of naïve N15Tg CD8$^+$ T cells

Four 9-16 week old homozygous N15 TCR transgenic (tg) mice on the B6Rag2$^{-/-}$ background were used for the isolation of naïve T cells [88]. Mice were maintained and bred under specific pathogen-free conditions in the animal facility of the Dana-Farber Cancer Institute under a protocol reviewed and approved by the Animal Care and Use Commit-

tee. The naïve $CD8^+$ N15 T cells were purified by magnetic sorting using naive $CD8^+$ isolation kit (Miltenyl Biotec) containing mAbs against CD4, CD11b, CD11c, CD19, CD45, CD49b, CD105, Ter-119, MHCII, CD44 and TCR from spleen of N15 TCRtg Rag2/ mice according to the manufacturer's instructions. Post-purification by negative selection, the naïve $CD8^+$ N15 T cells were used without prior stimulation.

3.6.6 Antibodies (Abs) and flow cytometric analysis

The following monoclonal antibodies (mAbs) were used: FITC-conjugated anti-Vβ 5.2 (ebioscience), APC-conjugated anti-Vβ 5.2 (MR9.4) (ebioscience), FITC-conjugated anti-TCR Cβ (H57-597) (Biolegend), APC-conjugated anti-TCR Cβ (H57-597) (Biolegend), APC-conjugated anti-CD3 (145-2C11) (ebioscience), APC-conjugated anti-CD3 (17A2) (ebioscience), APC-conjugated anti-CD8 (53-6.7) (Biolegend), APC-conjugated anti-CD8 (53-5.8) (Biolegend) and PE-conjugated anti-H-$2K^b$ antibody (AF6-88.5) (ebioscience). For flow cytometry, single-cell suspensions of the T cells were prepared at 3×10^6 cells/ml in PBS containing 2% FBS. Those cells were single-color stained with the mAbs at saturating concentrations. After incubation on ice for 20 minutes, the stained cells were washed, transferred to falcon tubes and analyzed by flow cytometry immediately using a 3-laser BD LSRII. Dead cells were excluded by forward and side scatter gating. For determining TCR expression, FITC-conjugated anti-Vβ and/or H57 mAb were utilized. Mean fluorescence intensities (MFI) were calculated based on the fluorescence method by FACS and the average number of TCRs per cell is ~2-4$\times10^4$ [89].

3.6.7 pMHC coated beads

The vesicular stomatitis virus nuclear protein octapeptide (VSV8, RGYVYQGL) which is the cognate antigen (in complex with H-$2K^b$) for the N15 TCR was bound to recombinant H-$2K^b$ containing a C-terminal biotinylation tag (GGGLNDIFEAQKIEWH) [90]. In addition to the strong agonist peptide VSV8, the weak agonist L4, which contains a sin-

gle valine-to-leucine substitution at the p4 position of VSV8, or the unrelated Sendai virus nonamer peptide SEV9 was also used to complex with the recombinant H-2K^b. SEV9 binds to Kb with comparable affinity to VSV8 but is unable to activate N15TCR-expressing T cells [91, 92]. The streptavidin (SA)-coupled polystyrene beads (1.09 μm diameter, Spherotech) were washed with PBST buffer (1X PBS without calcium (cellgro) with 0.02% (v/v) Tween-20 (Sigma-Aldrich)) three times. To create sample beads with distinct pMHC densities, different concentrations of biotinylated VSV8/K^b solutions were added to the SA-coupled polystyrene bead solution and gently rotated for 1h at room temperature and then wash three times by PBST. For 2×10^5 VSV8/K^b molecules/bead sample, 5μl of 10 M of H-2K^b complexes were used for coupling to 5μl 0.01% w/v streptavidin polystyrene beads. For 2×10^4, 200, 20 and 5 VSV8/K^b molecules/bead samples, 1 μM, 100 nM, 10 nM and 2.5 nM concentrations of H-2K^b complexes were used for coupling to 5 μl 0.1% w/v streptavidin polystyrene beads. For T cell triggering, bead surfaces were blocked by adding 5 mg/ml 20 μl biotin-BSA (ThermoFisher) in the pMHC coated bead slurry for 1 h at room temperature and then wash three times by PBST. The BSA on the bead surface eliminates potential non-specific binding of the bead to the cell membrane [93]. For the assays with two beads, the SA-coupled polystyrene beads (1.25 μm diameter, spherotech) were used following the same coating procedure as above. The biotinylated wild type VSV8/H-2K^b, L4/H-2K^b and SEV9/H-2K^b and the biotinylated mutant VSV8/H-2K$^b{}_m$ and NP366/H-2D$^b{}_m$ molecules whose CD8 coreceptor binding sites were eliminated (both mutants obtained from the NIH Tetramer Core Facility) were used in identical bead-coating procedures.

3.6.8 Quantitation of pMHC on the bead surface

Quantitative immunofluorescence was used to determine the densities of pMHC on the bead surface [89]. When the number of VSV8/K^b on the bead surface is above 500, different amounts of PE-conjugated anti-H-2K^b antibody (AF6-88.5) was added into the bead

solution. After 1-hour gentle rotation, the stained beads were examined by flow cytometry with Mode values of mean fluorescence recorded and normalized by dividing the maximum fluorescence signal using 0.1 μg antibody. It is estimated that the interacting surface between the bead and the cell represents up to 10% of the bead surface area and 10% was used when the surface expression is at 2×10^5 pMHC/bead [94].

Flow cytometry reached its limitation of distinguishing the pMHC bead signal from the background if the surface expression is equal to or lower than 500 pMHC/bead. Accordingly, at low density we used the single molecule total internal reflection fluorescence (smTIRF) microscopy method with a penetration depth of 400 nm easily able to sample the relevant interface contacting the cell surface. Saturated amount of PE-conjugated anti-H-2K^b antibody (AF6-88.5) was added into the bead solution, gently rotated for 1-hour. The stained beads were washed with PBST three times, resuspended in 1X PBS buffer and then examined by smTIRF microscopy. The methodology for calculating the pMHC copies at the interface is as follows with 200 pMHC coated bead used as a representative example. A flow cell containing two separate channels was created where one channel was loaded with 200 pMHC copy- coated beads labeled with PE-conjugated anti-H-2K^b antibody (AF6-88.5) and the other channel loaded with streptavidin beads labeled with the same antibody to calibrate the non-specific binding between antibody and SA. After loading the beads, each channel was washed with 1X PBS five times. Fluorescence signals of single PE-conjugated anti-H-2K^b antibody and background were obtained from bead images. The following three equations are used in calculations where I represents the mean fluorescence intensity:

$$I_{200\ pMHC/bead} = n \times I_{single\ PE-mAb} + I_{nonspecific\ binding\ between\ SA\ bead\ and\ mAb} + I_{Background} \quad (1)$$

$$I_{nonspecific\ binding} = I_{nonspecific\ binding\ between\ SA\ bead\ and\ mAb} + I_{Background} \quad (2)$$

$$I_{PE-mAb} = I_{single\ PE-mAb} + I_{Background} \quad (3)$$

The same region of interest was selected to include pMHC coated bead ($I_{200\ pMHC/bead}$), SA-bead ($I_{nonspecific\ binding}$), PE-conjugated anti-H-2K^b antibody (I_{PE-mAb}), or the background ($I_{Background}$) and the mean fluorescence intensities were determined, i.e. the left parameters in all three equations. n is the number of pMHC molecules at the interface. Expressions of and in eq 1 can be obtained from eq 2 and 3 and then by introduction of the value, one derives

$$n = \frac{I_{200\ pMHC/bead} - I_{SA\ bead}}{I_{PE-mAb} - I_{Background}} \tag{4}$$

From eq 4, the average numbers of VSV8/K^b at the interface are 29, 2 and 0.5 VSV8/K^b based on different seeding amounts of VSV8/K^b despite coating number estimates of 200, 20 and 5, respectively.

3.6.9 Half-antibody coated beads

The half-anti-TCRVβ5.2 (MR9.4) mAb was produced as previous described [33]. After desalting and changing the buffer to 1 X PBS (cellgro, pH=7.4), 0.1 mg of the digestion product was incubated with Biotin-maleimide (Sigma-Aldrich) in 20-fold molar excess. The solution was retained and rotated at 4 ^{o}C overnight. The reaction was terminated by desalting and a biotin tag was added to the hinge region of the half-antibody. The half-antibody solution was further diluted to the desired concentration to make the half-antibody coated beads. Identical procedures described above for preparation of VSV8/K^b coated beads were used to prepare beads coated with 5 half-antibody molecules to get a 0.5 molecules per cell-bead interface number.

3.6.10 Antibody-coated fluorescence beads

5 μl SA-coupled polystyrene beads (0.1% w/v, 1.03 m diameter, spherotech) were washed by PBST buffer three times. 10 nM biotin-conjugated anti-CD3 (17A2) (Biole-

gend) were added in the bead slurry and gently rotated for 1h at room temperature and then washed three times by PBST. 2 μl 10 mg/ml dextran with tetramethylrhodamine (TT) and biotin (MW=3 kDa, ThermoFisher) was added to the antibody coated bead slurry and gently rotated for 1h at room temperature and then washed three times by PBST. The negatively charged dextran inhibits nonspecific binding between the cell membrane and the bead.

3.6.11 Ca^{2+} flux dye loading

Because TCR signaling is associated with elevations in intracellular free calcium, the Quest Rhod-4, AM (AAT Bioquest, Inc.) was used to stain the T cell and observe the characteristic intracellular calcium flux during T cell triggering [95]. Briefly, cells were washed, resuspended at 2 million cells/ml in either colorless DMEM medium (Sigma-Aldrich) for cell lines or colorless RPMI 1640 (Life technology) for naïve cells, and loaded with Quest Rhod-4 at 2 μM for 40 min in the presence of 3% (v/v) FBS, 0.02% (v/v) Pluronic F-127 (Sigma-Aldrich) in PBS at 37 ^{o}C. Cells were gently pipetted every 10 min. T cells were then washed by 1 ml colorless DMEM medium, resuspended in 800 μl colorless DMEM (cell line) or colorless RPMI 1640 (naïve cell) with 3% (v/v) FBS and transferred to a cover glass flow cell for 1 h incubation at 37 ^{o}C, 5% CO2 to allow for cell attachment to the cover glass surface. After coating the surface with blocking buffer containing 5 mg/ml BSA (Sigma-Aldrich) in colorless DMEM medium for 10 min, pMHC-coated beads in blocking buffer were flowed into the sample. After 1 h incubation at 37 ^{o}C, 5% CO_2, the slide was ready for manipulation using an optical trap combined with fluorescence.

3.6.12 Estimation of Ca^{2+} concentration change during TCR triggering under load

Estimating the Ca^{2+} concentration change during TCR triggering was difficult due to nonlinearities and saturation of fluorescence signal of the Andor camera. Traditionally the method involves the following calculation: $[Ca^{2+}] = K_d \times (F - F_{min})/(F_{max} - F)$ where F is

the fluorescence of the indicator at experimental calcium levels, F_{min} is the fluorescence in the absence of calcium and F_{max} is the fluorescence of the calcium-saturated probe. Quest Rhod-4 has a K_d equal to 525 nM. In our case, the precise value of the positive control to obtain F_{max} cannot be determined due to saturation of the fluorescence signal of the Andor camera.

However, we obtained F_{min} from the Andor camera with identical excitation laser power (532 nm) and camera gain to our measurements. Using an identical procedure for sample preparation and Ca^{2+} dye loading as in our experiments, we changed our imaging buffer to a 1X PBS containing 3% FBS and 2 mM EDTA (sigma). This permitted measurement of the average fluorescence levels in cells loaded with the Ca^{2+} chelating agent resulting in an intensity 0.8 times the basal signal (n=50 cells). Given the original concentration of Ca^{2+} is 50 nM [96], F_{max} is calculated to be 3.1 times higher than the basal fluorescence. Since signal changes for T cells in our measurements were 1.2 times on average (Fig. 3.4A and B) we estimate a concentration of 111 nM Ca^{2+} is present in stimulated T cells under optimal load using pMHC coated beads.

3.6.13 Antibody and drug treatment of T cells

For the H57 Fab treated experiment, 0.5 μl 1 mg/ml H57 Fab was added into the cell slurry after the 40-min dye-loading procedure and kept at 37 ^{o}C, 5% CO_2 for 20-min before loading slurry into flow cell. H57 Fab was always present at a concentration of 4.5 μg/ml (i.e. 1000-fold excess of TCR number).

For drug treatment experiments, reagent was firstly dissolved in DMSO (Sigma-Aldrich) and then dilute to its final concentration in the blocking buffer containing 5 mg/ml BSA. The final concentrations of drugs are 500 nM Cytochalasin D (Santa Cruz Biotechnology), 10 μM Nocodazole (Sigma-Aldrich) and 25 μM (S)-(-)-Blebbistatin (Santa Cruz Biotechnology). After 1h incubation at 37 ^{o}C, 5% CO2, the slide was ready for manipulation using a trapping beam (1064 nm). Drugs were always present in the slides at their final concen-

trations during the triggering experiment. The DMSO amount in the final solution is lower than 0.2% (v/v) to maintain the cell viability and functionality.

3.6.14 Cell loaded slide preparation

Slides were prepared by first creating a 110 μl flow cell using two layers of double-sided sticky tape. The flow cell is then loaded through capillary action with the final calcium dye loaded cell solution. In all cases the cell is nonspecifically immobilized on the coverslip surface by maintaining the loaded chamber at 37 ^{o}C, 5% CO_2 (~1 h). We note that these measurements are in the low Reynolds number regime where viscous forces dominate over inertial forces. Relative motions are slow with maximum speeds of the piezo stage 2 μm/s. Given these speeds, viscosity of the medium (DMEM medium is 0.78×10^{-3} N·s/m^2), density of the fluid (1.0×10^{3} kg/m^3) and length scale of the channel (179 μm tall channel and 1 μm diameter bead) we conservatively estimate the Reynolds number is $<5\times10^{-4}$ and drag on the bead below 0.015 pN. Control measurements using beads with no pMHC but coated with BSA executed the similar relative motions of bead and cell apposition and showed no triggering.

3.6.15 Calculation of elastic moduli and viscosities from force relaxation experiment

Fig. 3.10A shows the viscoelastic model used to represent the cells behavior. In this model the strain can be split into the sum of three terms:

$$\varepsilon_T = \varepsilon_0 + \varepsilon_{D1} + \varepsilon_{S1} \tag{1}$$

Also we have the following equations for all the stresses in this model:

$$\sigma = \sigma_0 = \sigma_1 + \sigma_2 \tag{2}$$

$$\sigma_0 = \eta_0 + \dot{\varepsilon}_0 \tag{3}$$

$$\sigma_1 = \eta_1 \dot{\varepsilon}_{D1} = E_1 \varepsilon_{S1} \tag{4}$$

$$\sigma_2 = E_2(\varepsilon_{D1} + \varepsilon_{S1}) \tag{5}$$

Substituting eq 5 into eq 1 and then differentiating once this equation we can get the following equation:

$$\dot{\varepsilon}_T = \frac{\sigma}{\eta_0} + \frac{\dot{\sigma} - \dot{\sigma}_1}{E_2} \tag{6}$$

Differentiating once eq 4 and after substituting it into eq 6 we can obtain the following two equations:

$$\dot{\varepsilon}_T = \frac{\sigma}{\eta_0} + \frac{\dot{\sigma} - \eta_1 \ddot{\varepsilon}_{D1}}{E_2} \tag{7}$$

$$\dot{\varepsilon}_T = \frac{\sigma}{\eta_0} + \frac{\dot{\sigma} - \eta_1 \ddot{\varepsilon}_{S1}}{E_2} \tag{8}$$

For the stresses, we can substitute eqs 4 and 5 into eq 2 and then differentiate once this equation. The equation would be:

$$\dot{\sigma} = E_1 \dot{\varepsilon}_{S1} + E_2(\dot{\varepsilon}_{S1} + \dot{\varepsilon}_{D1}) \tag{9}$$

Then the expression of would be obtained in the form as:

$$\dot{\varepsilon}_{S1} = \frac{\dot{\sigma} - E_2 \dot{\varepsilon}_{D1}}{E_1 + E_2} \tag{10}$$

Plugging eq 10 into eq 8 we can get the following equation:

$$\dot{\varepsilon}_T = \frac{\sigma}{\eta_0} + \frac{\dot{\sigma} + E_1 \dot{\varepsilon}_{D1}}{E_1 + E_2} \tag{11}$$

We can get $\dot{\varepsilon_{D1}}$ and then we take its second derivative form into consideration:

$$\ddot{\varepsilon}_{D1} = \frac{E_1 + E_2}{E_1}(\ddot{\varepsilon}_T - \frac{\sigma}{\eta_0}) - \frac{\ddot{\sigma}}{E_1} \tag{12}$$

On the optical trap side, we can get the total stress as:

$$\sigma = k_{trap}(x_0 - \varepsilon_T) \tag{13}$$

where k_{trap} is the stiffness of trap and x_0 is the initial distance between bead and trap center. We consider its first and second derivative form:

$$\dot{\sigma} = -k_{trap}\dot{\varepsilon}_T \tag{14}$$

$$\ddot{\sigma} = -k_{trap}\ddot{\varepsilon}_T \tag{15}$$

Substituting eqs 12, 13, 14 and 15 into eq 7 we can obtain a linear homogeneous ordinary differential equation with constant coefficients

$$\left[\frac{\eta_1(E_1+E_2)}{E_1E_2k_{trap}} + \frac{\eta_1}{E_1+E_2}\right]\ddot{\sigma} + \left[\frac{\eta_1(E_1+E_2)}{\eta_0E_1E_2} + \frac{1}{k_{trap}} + \frac{1}{E_2}\right]\dot{\sigma} + \frac{\sigma}{\eta_0} = 0 \tag{16}$$

The general solution to the homogeneous equation $A\ddot{\sigma} + B\dot{\sigma} + C\sigma = 0$ is given by $\sigma(t) = C_1e^{-t/\tau_1} + C_2e^{-t/\tau_2}$. We also have two time boundary conditions at t=0 and t=t_f. The latter is the time when bead snapping back to the trap center. During the fitting process, the fitting equation should be restricted by the two conditions $C_1 + C_2 = \sigma(0)$ and $C_1e^{-t/t_f} + C_2e^{-t/t_f} = 0$. We also found out one part of this expression can be neglected as absolute value of either C_1 or C_2 is extremely close to zero and its associated decay constant is at least 10000 times greater than the other one. Therefore, the fitting equation can be simplified to:

$$\sigma(t) = Ce^{-t/\tau} \tag{17}$$

When normal force is applied to the system, the model would be changed to Zerners model and usually the bead never goes back to the trap center as shown in Fig. 3.12B. The general solution to this model was well described in Moreno-Floress paper [97]. Basically, it has the expression as $\sigma(t) = C_0 + C_1 e^{-t/\tau_1} + C_2 e^{-t/\tau_2}$. Detailed discussion on all the parameters is beyond the content of this dissertation but can be provided by requesting information from the author.

3.6.16 Data Analysis

The step finding script was modified from a previous version within the lab and based on a sliding Students t-test that detects the edges of each step to prescribe a dwell and allows for varied step sizes [98]. A dwell was defined as a period of constant position between bursts of motion (steps). Specifically, a dwell is identified if the change in the moving average of position is less than 5 nm (the minimum step-size threshold). This threshold was chosen as a result of step finding optimization. Dwell locations were determined through averaging all points within the dwell period. After dwell optimization, starting and ending times of each dwell were recorded and plotted with the dwell location. It is also noted that step analysis for each trace was visually inspected for accuracy. The same analysis conditions were used for all traces in a data set. In some cases, steps were not always identified as commonly observed for Blebbistatin treated cells. Less frequently, other treatments revealed step loss due to the low signal to noise level. However, these traces are still used to calculate the average number of steps per trace. To avoid the differences of pulling distance for each condition (H57 Fab, drugs or NP366/$D^b{}_m$), the total pulling distances for every condition were normalized to the distances of N15 T cell with 2 VSV8/K^b at interface. In order to confirm the existence of the discrete steps ~8 nm in wt T cells and the reduction in Blebbistatin (Blebb) treated cells, point to point pairwise distance differences were calculated followed by spatial frequency analysis. Five representative traces were selected and individually fit to an exponential decay to remove extension

due to compliance in the trace. The residual of each trace was calculated to remove the decay and the pairwise distance differences function of the subtract trace was calculated. The power spectrum derived from each pairwise function [99, 100], was normalized and pooled to create an average power spectrum.

3.7 Acknowledgements

We thank the NIH Tetramer Core Facility at Emory University for the VSV8/H2-K^b-α2A2 and NP336/H2-D^b-α2A2 monomers. This work was supported by NIH Grants R01AI100643, R01AI37581, P01GM047467 and SU2C-AACR-DT13-14 from the SU2C-Farrah Fawcett Foundation. Flow cytometry experiments were performed in the Vanderbilt University Medical Center Flow Cytometry Shared Resource supported by The Vanderbilt-Ingram Cancer Center (NIH Grant CA68485) and the Vanderbilt Digestive Disease Research Center (NIH Grant DK058404). We also thank Sonia K. Brady for helpful discussions and Rebecca E. Hussey for technical assistance.

3.8 Bibliography

[1] Jamie Rossjohn, Stephanie Gras, John J. Miles, Stephen J. Turner, Dale I. Godfrey, and James McCluskey. T cell antigen receptor recognition of antigen-presenting molecules. *Annual Review of Immunology*, 33(1):169–200, 2015.

[2] Markus G. Rudolph, Robyn L. Stanfield, and Ian A. Wilson. How TCRs bind MHCs, peptides, and coreceptors. *Annual Review of Immunology*, 24(1):419–466, 2006.

[3] Jia-huai Wang and Ellis L. Reinherz. The structural basis of $\alpha\beta$ t-lineage immune recognition: TCR docking topologies, mechanotransduction, and co-receptor function. *Immunological Reviews*, 250(1):102–119, 2012.

[4] Mark M. Davis and Pamela J. Bjorkman. T-cell antigen receptor genes and T-cell recognition. *Nature*, 334(6181):395–402, 1988.

[5] Ellis L. Reinherz. $\alpha\beta$ TCR-mediated recognition: Relevance to tumor-antigen discovery and cancer immunotherapy. *Cancer Immunology Research*, 3(4):305–312, 2015.

[6] Paul A. Roche and Peter Cresswell. Antigen processing and presentation mechanisms in myeloid cells. *Microbiology Spectrum*, 4(3), 2016.

[7] Lawrence J. Stern and Don C. Wiley. Antigenic peptide binding by class I and class II histocompatibility proteins. *Structure*, 2(4):245–251, 1994.

[8] Kristine N. Brazin, Robert J. Mallis, Chen Li, Derin B. Keskin, Haribabu Arthanari, Yuanwei Gao, Shiaw-Lin Wu, Barry L. Karger, Gerhard Wagner, and Ellis L. Reinherz. Constitutively oxidized CXXC motifs within the CD3 heterodimeric ectodomains of the T cell receptor complex enforce the conformation of juxtaposed segments. *Journal of Biological Chemistry*, 289(27):18880–18892, 2014.

[9] Chenqi Xu, Etienne Gagnon, Matthew E. Call, Jason R. Schnell, Charles D. Schwieters, Christopher V. Carman, James J. Chou, and Kai W. Wucherpfennig. Regulation of T cell receptor activation by dynamic membrane binding of the CD3ε cytoplasmic tyrosine-based motif. *Cell*, 135(4):702–713, 2008.

[10] Arup K. Chakraborty and Arthur Weiss. Insights into the initiation of TCR signaling. *Nat Immunol*, 15(9):798–807, 2014.

[11] Jennifer E. Smith-Garvin, Gary A. Koretzky, and Martha S. Jordan. T cell activation. *Annual Review of Immunology*, 27(1):591–619, 2009.

[12] Susan M. Kaech and Weiguo Cui. Transcriptional control of effector and memory CD8+ T cell differentiation. *Nat Rev Immunol*, 12(11):749–761, 2012.

[13] Yubin Zhou, Paul Meraner, Hyoung T. Kwon, Danya Machnes, Masatsugu Oh-hora, Jochen Zimmer, Yun Huang, Antonio Stura, Anjana Rao, and Patrick G. Hogan. STIM1 gates the store-operated calcium channel ORAI1 in vitro. *Nat Struct Mol Biol*, 17(1):112–116, 2010.

[14] Lindsay Edwards, Veronika Zarnitsyna, Jennifer Hood, Brian Evavold, and Cheng Zhu. Insights into T cell recognition of antigen: Significance of two-dimensional kinetic parameters. *Frontiers in Immunology*, 3(86), 2012.

[15] Joyce K. Hwang, Frederick W. Alt*, and Leng-Siew Yeap. Related mechanisms of antibody somatic hypermutation and class switch recombination. *Microbiology Spectrum*, 3(1), 2015.

[16] Tetsuro Sasada, Yoseph Ghendler, Jia-huai Wang, and Ellis L Reinherz. Thymic selection is influenced by subtle structural variation involving the p4 residue of an MHC class I-bound peptide. *European journal of immunology*, 30(5):1281–1289, 2000.

[17] Salvatore Valitutti, Sabina Müller, Marina Cella, Elisabetta Padovan, and Antonio Lanzavecchia. Serial triggering of many T-cell receptors by a few peptide MHC complexes. *Nature*, 375(6527):148–151, 1995.

[18] Salvatore Valitutti. The serial engagement model 17 years after: from TCR triggering to immunotherapy. *Frontiers in immunology*, 3:272, 2012.

[19] Baoyu Liu, Wei Chen, Brian D Evavold, and Cheng Zhu. Accumulation of dynamic catch bonds between TCR and agonist peptide-MHC triggers T cell signaling. *Cell*, 157(2):357–368, 2014.

[20] Sarah E. Henrickson, Thorsten R. Mempel, Irina B. Mazo, Bai Liu, Maxim N. Artyomov, Huan Zheng, Antonio Peixoto, Michael Flynn, Balimkiz Senman, Tobias Junt, Hing C. Wong, Arup K. Chakraborty, and Ulrich H. von Andrian. In vivo imaging of T cell priming. *Science Signaling*, 1(12):pt2–pt2, 2008.

[21] Revathi Ananthakrishnan and Allen Ehrlicher. The forces behind cell movement. *International journal of biological sciences*, 3(5):303, 2007.

[22] Lin Ji, James Lim, and Gaudenz Danuser. Fluctuations of intracellular forces during cell protrusion. *Nature cell biology*, 10(12):1393–1400, 2008.

[23] Xavier Trepat, Michael R Wasserman, Thomas E Angelini, Emil Millet, David A Weitz, James P Butler, and Jeffrey J Fredberg. Physical forces during collective cell migration. *Nature physics*, 5(6):426–430, 2009.

[24] Antonio Lanzavecchia, Giandomenica Iezzi, and Antonella Viola. From TCR engagement to T cell activation: a kinetic view of T cell behavior. *Cell*, 96(1):1–4, 1999.

[25] Zhengyu Ma, Kim A Sharp, Paul A Janmey, and Terri H Finkel. Surface-anchored

monomeric agonist pMHCs alone trigger TCR with high sensitivity. *PLoS Biol*, 6(2):e43, 2008.

[26] Thomas D Pollard and John A Cooper. Actin, a central player in cell shape and movement. *Science*, 326(5957):1208–1212, 2009.

[27] Christoph Wülfing and Mark M Davis. A receptor/cytoskeletal movement triggered by costimulation during T cell activation. *Science*, 282(5397):2266–2269, 1998.

[28] Arash Grakoui, Shannon K. Bromley, Cenk Sumen, Mark M. Davis, Andrey S. Shaw, Paul M. Allen, and Michael L. Dustin. The immunological synapse: A molecular machine controlling T cell activation. *Science*, 285(5425):221–227, 1999.

[29] Jason Yi, Xufeng S. Wu, Travis Crites, and John A. Hammer. Actin retrograde flow and actomyosin II arc contraction drive receptor cluster dynamics at the immunological synapse in jurkat T cells. *Molecular Biology of the Cell*, 23(5):834–852, 2012.

[30] Cheng-han Yu, Hung-Jen Wu, Yoshihisa Kaizuka, Ronald D. Vale, and Jay T. Groves. Altered actin centripetal retrograde flow in physically restricted immunological synapses. *PLoS ONE*, 5(7):e11878, 2010.

[31] Sun Taek Kim, Koh Takeuchi, Zhen-Yu J Sun, Maki Touma, Carlos E Castro, Amr Fahmy, Matthew J Lang, Gerhard Wagner, and Ellis L Reinherz. The $\alpha\beta$ T cell receptor is an anisotropic mechanosensor. *Journal of Biological Chemistry*, 284(45):31028–31037, 2009.

[32] Sun Taek Kim, Yongdae Shin, Kristine Brazin, Robert Mallis, Jim Sun, Gerhard Wagner, Matthew Lang, and Ellis Reinherz. TCR mechanobiology: Torques and tunable structures linked to early T cell signaling. *Frontiers in Immunology*, 3(76), 2012.

[33] Dibyendu Kumar Das, Yinnian Feng, Robert J Mallis, Xiaolong Li, Derin B Keskin, Rebecca E Hussey, Sonia K Brady, Jia-Huai Wang, Gerhard Wagner, Ellis L Reinherz, et al. Force-dependent transition in the T-cell receptor β-subunit allosterically regulates peptide discrimination and pMHC bond lifetime. *Proceedings of the National Academy of Sciences*, 112(5):1517–1522, 2015.

[34] Keenan T. Bashour, Alexander Gondarenko, Haoqian Chen, Keyue Shen, Xin Liu, Morgan Huse, James C. Hone, and Lance C. Kam. CD28 and CD3 have complementary roles in T-cell traction forces. *Proceedings of the National Academy of Sciences*, 111(6):2241–2246, 2014.

[35] Roshni Basu, Benjamin M Whitlock, Julien Husson, Audrey Le Floch, Weiyang Jin, Alon Oyler-Yaniv, Farokh Dotiwala, Gregory Giannone, Claire Hivroz, Nicolas Biais, Judy Lieberman, Lance C Kam, and Morgan Huse. Cytotoxic T cells use mechanical force to potentiate target cell killing. *Cell*, 165(1):100–110, 2016.

[36] Kenneth H. Hu and Manish J. Butte. T cell activation requires force generation. *The Journal of Cell Biology*, 213(5):535–542, 2016.

[37] King Lam Hui, Lakshmi Balagopalan, Lawrence E. Samelson, and Arpita Upadhyaya. Cytoskeletal forces during signaling activation in jurkat T-cells. *Molecular Biology of the Cell*, 26(4):685–695, 2015.

[38] Julien Husson, Karine Chemin, Armelle Bohineust, Claire Hivroz, and Nelly Henry. Force generation upon T cell receptor engagement. *PLoS One*, 6(5):e19680, 2011.

[39] Ya-Chen Li, Bing-Mae Chen, Pei-Chun Wu, Tian-Lu Cheng, Lung-Sen Kao, Mi-Hua Tao, Andre Lieber, and Steve R. Roffler. Cutting edge: Mechanical forces acting on T cells immobilized via the TCR complex can trigger TCR signaling. *The Journal of Immunology*, 184(11):5959–5963, 2010.

[40] Yang Liu, Lori Blanchfield, Victor Pui-Yan Ma, Rakieb Andargachew, Kornelia Galior, Zheng Liu, Brian Evavold, and Khalid Salaita. DNA-based nanoparticle tension sensors reveal that T-cell receptors transmit defined pN forces to their antigens for enhanced fidelity. *Proceedings of the National Academy of Sciences*, 113(20):5610–5615, 2016.

[41] Erdem Tabdanov, Sasha Gondarenko, Sudha Kumari, Anastasia Liapis, Michael L. Dustin, Michael P. Sheetz, Lance C. Kam, and Thomas Iskratsch. Micropatterning of TCR and LFA-1 ligands reveals complementary effects on cytoskeleton mechanics in T cells. *Integrative Biology*, 7(10):1272–1284, 2015.

[42] Ricardo R. Brau, Peter B. Tarsa, Jorge M. Ferrer, Peter Lee, and Matthew J. Lang. Interlaced optical force-fluorescence measurements for single molecule biophysics. *Biophysical Journal*, 91(3):1069–1077, 2006.

[43] Matthew J Lang, Polly M Fordyce, Anita M Engh, Keir C Neuman, and Steven M Block. Simultaneous, coincident optical trapping and single-molecule fluorescence. *Nature methods*, 1(2):133–139, 2004.

[44] Karine Bernardeau, Sébastien Gouard, Gaëlle David, Anne-Lise Ruellan, Anne Devys, Jacques Barbet, Marc Bonneville, Michel Chérel, and François Davodeau. Assessment of CD8 involvement in T cell clone avidity by direct measurement of hla-a2/mage3 complex density using a high-affinity TCR like monoclonal antibody. *European journal of immunology*, 35(10):2864–2875, 2005.

[45] Pradeep Ramesh, Younes F. Baroji, S. Nader S. Reihani, Dimitrios Stamou, Lene B. Oddershede, and Poul Martin Bendix. FBAR Syndapin 1 recognizes and stabilizes highly curved tubular membranes in a concentration dependent manner. *Scientific reports*, 3:1565, 2013.

[46] Haguy Wolfenson, Giovanni Meacci, Shuaimin Liu, Matthew R. Stachowiak,

Thomas Iskratsch, Saba Ghassemi, Pere Roca-Cusachs, Ben Oshaughnessy, James Hone, and Michael P. Sheetz. Tropomyosin controls sarcomere-like contractions for rigidity sensing and suppressing growth on soft matrices. *Nat Cell Biol*, 18(1):33–42, 2016.

[47] Dong Sun, An Huang, Sansar Sharma, Akos Koller, and Gabor Kaley. Endothelial microtubule disruption blocks flow-dependent dilation of arterioles. *American Journal of Physiology-Heart and Circulatory Physiology*, 280(5):H2087–H2093, 2001.

[48] Russell DJ Huby, Arthur Weiss, and Steven C Ley. Nocodazole inhibits signal transduction by the T cell antigen receptor. *Journal of Biological Chemistry*, 273(20):12024–12031, 1998.

[49] Michael S Kolodney and Elliot L Elson. Contraction due to microtubule disruption is associated with increased phosphorylation of myosin regulatory light chain. *Proceedings of the National Academy of Sciences*, 92(22):10252–10256, 1995.

[50] Noah Joseph, Barak Reicher, and Mira Barda-Saad. The calcium feedback loop and T cell activation: how cytoskeleton networks control intracellular calcium flux. *Biochimica et Biophysica Acta (BBA)-Biomembranes*, 1838(2):557–568, 2014.

[51] Yair Klieger, Osnat Almogi-Hazan, Eliran Ish-Shalom, Aviad Pato, Maor H. Pauker, Mira Barda-Saad, Lynn Wang, and Michal Baniyash. Unique ζ-chain motifs mediate a direct TCR-actin linkage critical for immunological synapse formation and T-cell activation. *European journal of immunology*, 44(1):58–68, 2014.

[52] Dibyendu Kumar Das, Robert J Mallis, Jonathan S Duke-Cohan, Rebecca E Hussey, Paul W Tetteh, Mark Hilton, Gerhard Wagner, Matthew J Lang, and Ellis L Reinherz. Pre-TCRs leverage Vβ CDRs and hydrophobic patch in mechanosensing thymic self-ligands. *Journal of Biological Chemistry*, pages jbc–M116, 2016.

[53] Yunmin Jung, Inbal Riven, Sara W Feigelson, Elena Kartvelishvily, Kazuo Tohya, Masayuki Miyasaka, Ronen Alon, and Gilad Haran. Three-dimensional localization of T-cell receptors in relation to microvilli using a combination of superresolution microscopies. *Proceedings of the National Academy of Sciences*, page 201605399, 2016.

[54] Lionel Guillou, Avin Babataheri, Michael Saitakis, Armelle Bohineust, Stéphanie Dogniaux, Claire Hivroz, Abdul I Barakat, and Julien Husson. T-lymphocyte passive deformation is controlled by unfolding of membrane surface reservoirs. *Molecular biology of the cell*, 27(22):3574–3582, 2016.

[55] Sonja Majstoravich, Jinyi Zhang, Susan Nicholson-Dykstra, Stefan Linder, Wilhelm Friedrich, Katherine A Siminovitch, and Henry N Higgs. Lymphocyte microvilli are dynamic, actin-dependent structures that do not require Wiskott-Aldrich syndrome protein (WASp) for their morphology. *Blood*, 104(5):1396–1403, 2004.

[56] Jianping Fu, Yang-Kao Wang, Michael T. Yang, Ravi A. Desai, Xiang Yu, Zhijun Liu, and Christopher S. Chen. Mechanical regulation of cell function with geometrically modulated elastomeric substrates. *Nat Meth*, 7(9):733–736, 2010.

[57] Thomas D. Pollard and Gary G. Borisy. Cellular motility driven by assembly and disassembly of actin filaments. *Cell*, 112(4):453–465, 2003.

[58] Alex T Ritter, Yukako Asano, Jane C Stinchcombe, N. M. G. Dieckmann, Bi-Chang Chen, C. Gawden-Bone, Schuyler van Engelenburg, Wesley Legant, Liang Gao, Michael W Davidson, Eric Betzig, Jennifer Lippincott-Schwartz, and Gillian M Griffiths. Actin depletion initiates events leading to granule secretion at the immunological synapse. *Immunity*, 42(5):864–876, 2015.

[59] Elena V. Tibaldi, Ravi Salgia, and Ellis L. Reinherz. CD2 molecules redistribute to the uropod during T cell scanning: Implications for cellular activation and immune

surveillance. *Proceedings of the National Academy of Sciences*, 99(11):7582–7587, 2002.

[60] Kristine N Brazin, Robert J Mallis, Dibyendu Kumar Das, Yinnian Feng, Wonmuk Hwang, Jia-huai Wang, Gerhard Wagner, Matthew J Lang, and Ellis L Reinherz. Structural features of the $\alpha\beta$TCR mechanotransduction apparatus that promote pMHC discrimination. *Frontiers in Immunology*, 6, 2015.

[61] Daisuke Mizuno, Catherine Tardin, C. F. Schmidt, and F. C. MacKintosh. Nonequilibrium mechanics of active cytoskeletal networks. *Science*, 315(5810):370–373, 2007.

[62] Derin B. Keskin, Bruce B. Reinhold, Guang Lan Zhang, Alexander R. Ivanov, Barry L. Karger, and Ellis L. Reinherz. Physical detection of influenza A epitopes identifies a stealth subset on human lung epithelium evading natural CD8 immunity. *Proceedings of the National Academy of Sciences*, 112(7):2151–2156, 2015.

[63] Jeffrey T Finer, Robert M Simmons, and James A Spudich. Single myosin molecule mechanics: piconewton forces and nanometre steps. *Nature*, 368(6467):113, 1994.

[64] Coleen T Murphy, Ronald S Rock, and James A Spudich. A myosin II mutation uncouples ATPase activity from motility and shortens step size. *Nature Cell Biology*, 3(3):311, 2001.

[65] Nikolas Hundt, Walter Steffen, Salma Pathan-Chhatbar, Manuel H Taft, and Dietmar J Manstein. Load-dependent modulation of non-muscle myosin-2A function by tropomyosin 4.2. *Scientific reports*, 6:20554, 2016.

[66] Nikolas Hundt, Walter Steffen, Salma Pathan-Chhatbar, Manuel H. Taft, and Dietmar J. Manstein. Load-dependent modulation of non-muscle myosin-2A function by tropomyosin 4.2. *Scientific reports*, 6:20554, 2016.

[67] Tal Ilani, Gaia Vasiliver-Shamis, Santosh Vardhana, Anthony Bretscher, and Michael L. Dustin. T cell receptor signaling and immunological synapse stability require myosin IIA, journal = Nature immunology, volume = 10, number = 5, pages = 531-539, note = , abstract = Immunological synapses are initiated by signaling in discrete T cell receptor (TCR) microclusters and play an important role in T cell differentiation and effector functions. Synapse formation involves orchestrated motion of microclusters toward the center of the contact area with the antigen-presenting cell. Microcluster movement is associated with centripetal actin flow, but the role of motor proteins is unknown. Here we show that myosin IIA was necessary for complete assembly and movement of TCR microclusters and that activated myosin IIA was recruited to the synapse. In the absence of myosin IIA or its ATPase activity, T cell signaling was interrupted downstream of Lck and the synapse was destabilized. Thus, TCR signaling and subsequent immunological synapse formation are active processes dependent on myosin IIA., year = 2009.

[68] Ester San José, Aldo Borroto, Florence Niedergang, Andrés Alcover, and Balbino Alarcón. Triggering the TCR complex causes the downregulation of nonengaged receptors by a signal transduction-dependent mechanism, 2000.

[69] Richard G. Fehon, Andrea I. McClatchey, and Anthony Bretscher. Organizing the cell cortex: The role of ERM proteins. *Nature reviews. Molecular cell biology*, 11(4):276–287, 2010.

[70] Dylan T. Burnette, Lin Shao, Carolyn Ott, Ana M. Pasapera, Robert S. Fischer, Michelle A. Baird, Christelle Der Loughian, Helene Delanoe-Ayari, Matthew J. Paszek, Michael W. Davidson, Eric Betzig, and Jennifer Lippincott-Schwartz. A contractile and counterbalancing adhesion system controls the 3D shape of crawling cells. *The Journal of Cell Biology*, 205(1):83–96, 2014.

[71] Nils Gustafsson, Siân Culley, George Ashdown, Dylan M Owen, Pedro Matos

Pereira, and Ricardo Henriques. Fast live-cell conventional fluorophore nanoscopy with ImageJ through super-resolution radial fluctuations. *Nature Communications*, 7, 2016.

[72] Boryana N. Manz, Bryan L. Jackson, Rebecca S. Petit, Michael L. Dustin, and Jay Groves. T-cell triggering thresholds are modulated by the number of antigen within individual T-cell receptor clusters. *Proceedings of the National Academy of Sciences*, 108(22):9089–9094, 2011.

[73] Peter JR Ebert, Lauren I Richie Ehrlich, and Mark M Davis. Low ligand requirement for deletion and lack of synapses in positive selection enforce the gauntlet of thymic T cell maturation. *Immunity*, 29(5):734–745, 2008.

[74] Marco A. Purbhoo, Darrell J. Irvine, Johannes B. Huppa, and Mark M. Davis. T cell killing does not require the formation of a stable mature immunological synapse. *Nat Immunol*, 5(5):524–530, 2004.

[75] Yuri Sykulev, Michael Joo, Irina Vturina, Theodore J. Tsomides, and Herman N. Eisen. Evidence that a single peptideMHC complex on a target cell can elicit a cytolytic T cell response. *Immunity*, 4(6):565–571, 1996.

[76] Mehdi Roein-Peikar, Qian Xu, Xuefeng Wang, and Taekjip Ha. Ultrasensitivity of cell adhesion to the presence of mechanically strong ligands. *Physical Review X*, 6(1):011001, 2016.

[77] Jia-huai Wang, Alex Smolyar, Kemin Tan, Jin-huan Liu, Mikyung Kim, Zhen-yu J. Sun, Gerhard Wagner, and Ellis L. Reinherz. Structure of a heterophilic adhesion complex between the human CD2 and CD58 (LFA-3) counterreceptors. *Cell*, 97(6):791–803, 1999.

[78] Jun Huang, Veronika I. Zarnitsyna, Baoyu Liu, Lindsay J. Edwards, Ning Jiang,

Brian D. Evavold, and Cheng Zhu. The kinetics of two dimensional TCR and pMHC interactions determine T cell responsiveness. *Nature*, 464(7290):932–936, 2010.

[79] Robert J. Mallis, Ke Bai, Haribabu Arthanari, Rebecca E. Hussey, Maris Handley, Zhenhai Li, Loice Chingozha, Jonathan S. Duke-Cohan, Hang Lu, Jia-Huai Wang, Cheng Zhu, Gerhard Wagner, and Ellis L. Reinherz. Pre-TCR ligand binding impacts thymocyte development before $\alpha\beta$TCR expression. *Proceedings of the National Academy of Sciences*, 112(27):8373–8378, 2015.

[80] Geoff P. O'Donoghue, Rafal M. Pielak, Alexander A. Smoligovets, Jenny J. Lin, and Jay T. Groves. Direct single molecule measurement of TCR triggering by agonist pMHC in living primary T cells. *eLife*, 2:e00778, 2013.

[81] G. Gross, G. Gorochov, T. Waks, and Z. Eshhar. Generation of effector T cells expressing chimeric T cell receptor with antibody type-specificity. *Transplantation proceedings*, 21(1 Pt 1):127–130, 1989.

[82] Michel Sadelain. Chimeric antigen receptors: driving immunology towards synthetic biology. *Current Opinion in Immunology*, 41:68–76, 2016.

[83] Andrea L Szymczak, Creg J Workman, Yao Wang, Kate M Vignali, Smaroula Dilioglou, Elio F Vanin, and Dario AA Vignali. Correction of multi-gene deficiency in vivo using a single 'self-cleaving' 2A peptide–based retroviral vector. *Nature biotechnology*, 22(5):589, 2004.

[84] Hsiu-Ching Chang, Kemin Tan, Jing Ouyang, Emilio Parisini, Jin-huan Liu, Yi Le, Xiasong Wang, Ellis L Reinherz, and Jia-huai Wang. Structural and mutational analyses of a CD8$\alpha\beta$ heterodimer and comparison with the CD8$\alpha\alpha$ homodimer. *Immunity*, 23(6):661–671, 2005.

[85] Hiroshi Hamana, Kiyomi Shitaoka, Hiroyuki Kishi, Tatsuhiko Ozawa, and Atsushi Muraguchi. A novel, rapid and efficient method of cloning functional antigen-

specific T-cell receptors from single human and mouse T-cells. *Biochemical and biophysical research communications*, 474(4):709–714, 2016.

[86] Eiji Kobayashi, Eishiro Mizukoshi, Hiroyuki Kishi, Tatsuhiko Ozawa, Hiroshi Hamana, Terumi Nagai, Hidetoshi Nakagawa, Aishun Jin, Shuichi Kaneko, and Atsushi Muraguchi. A new cloning and expression system yields and validates TCRs from blood lymphocytes of patients with cancer within 10 days. *Nature medicine*, 19(11):1542, 2013.

[87] JL Sebaugh. Guidelines for accurate EC50/IC50 estimation. *Pharmaceutical statistics*, 10(2):128–134, 2011.

[88] Yoseph Ghendler, Rebecca E Hussey, Torsten Witte, Emiko Mizoguchi, Linda K Clayton, Atul K Bhan, Shigeo Koyasu, Hsiu-Chiang Chang, and Ellis L Reinherz. Double-positive T cell receptorhigh thymocytes are resistant to peptide/major histocompatibility complex ligand-induced negative selection. *European journal of immunology*, 27(9):2279–2289, 1997.

[89] Benoît Carpentier, Paolo Pierobon, Claire Hivroz, and Nelly Henry. T-cell artificial focal triggering tools: linking surface interactions with cell response. *PLoS One*, 4(3):e4784, 2009.

[90] Anne Marie Moody, Yi Xiong, Hsiu-Ching Chang, and Ellis L Reinherz. The CD8α β co-receptor on double-positive thymocytes binds with differing affinities to the products of distinct class I MHC loci. *European journal of immunology*, 31(9):2791–2799, 2001.

[91] Tetsuro Sasada, Yuting Yang, Char-Chang Lai, Maki Touma, Linda K Clayton, Jinhuan Liu, Emilio Parisini, Jia-huai Wang, and Ellis L Reinherz. Disparate peptide-dependent thymic selection outcomes in β2m-deficient mice versus TAP-1-deficient

mice: implications for repertoire formation. *European journal of immunology*, 33(2):368–380, 2003.

[92] Tetsuro Sasada, Yoseph Ghendler, Ellis L Reinherz, et al. Thymic selection is influenced by subtle structural variation involving the p4 residue of an MHC class I-bound peptide. *European journal of immunology*, 30(5):1281–1289, 2000.

[93] R Alon, EA Bayer, and M Wilchek. Cell adhesion to streptavidin via RGD-dependent integrins. *European journal of cell biology*, 60(1):1–11, 1993.

[94] Ladan Amin, Erika Ercolini, Rajesh Shahapure, Giacomo Bisson, and Vincent Torre. The elementary events underlying force generation in neuronal lamellipodia. *Scientific reports*, 1:153, 2011.

[95] MH Freedman. Early biochemical events in lymphocyte activation: I. investigations on the nature and significance of early calcium fluxes observed in mitogen-induced T and B lymphocytes. *Cellular immunology*, 44(2):290–313, 1979.

[96] Wayne A Jensen, Christopher M Pleiman, Phillippe Beaufils, Anne-Marie K Wegener, Bernard Malissen, and John C Cambier. Qualitatively distinct signaling through T cell antigen receptor subunits. *European journal of immunology*, 27(3):707–716, 1997.

[97] Susana Moreno-Flores, Rafael Benitez, María dM Vivanco, and José Luis Toca-Herrera. Stress relaxation and creep on living cells with the atomic force microscope: a means to calculate elastic moduli and viscosities of cell components. *Nanotechnology*, 21(44):445101, 2010.

[98] Sonia K Brady, Sarangapani Sreelatha, Yinnian Feng, Shishir PS Chundawat, and Matthew J Lang. Cellobiohydrolase 1 from Trichoderma reesei degrades cellulose in single cellobiose steps. *Nature communications*, 6:10149, 2015.

[99] Marie-Eve Aubin-Tam, Adrian O Olivares, Robert T Sauer, Tania A Baker, and Matthew J Lang. Single-molecule protein unfolding and translocation by an ATP-fueled proteolytic machine. *Cell*, 145(2):257–267, 2011.

[100] Karel Svoboda, Christoph F Schmidt, Bruce J Schnapp, and Steven M Block. Direct observation of kinesin stepping by optical trapping interferometry. *Nature*, 365(6448):721, 1993.

CHAPTER 4

THE $\alpha\beta$TCR COMPLEX RECONFIGURES AND CD45 SEGREGATES THROUGH A PROCESS AKIN TO A PHASE TRANSITION DURING THE FORCE INDUCED TRIGGERING

*Paragraphs related to T-cell receptor α subunit and CD3 dissociation in this chapter are adapted from Kristine N. Brazin, Robert J. Mallis, Andras Boeszoermenyi, Yinnian Feng, Akihiro Yoshizawa, Pedro A. Rech, Pavanjeet Kaur, Kevin Bi, Rebecca E. Hussey, Likai Song, Gerhard Wagner, Hari Arthanari, Matthew J. Lang, and Ellis L. Reinherz, "The T-cell receptor α bipartite transmembrane domain coordinates antigen triggering by regulating bilayer immersion, CD3 association and transcriptomes" under review with the permission of the corresponding author Ellis L. Reinherz.

4.1 Summary

Initial molecular details of cellular activation following $\alpha\beta$T-cell receptor (TCR) ligation by pMHC remain largely unexplored. Locally, our collaborators determined the NMR structure of the TCRα subunit transmembrane (TM) segment revealing a bipartite helix whose segmentation fosters dynamic movement. Positively charged TM residues Arg251 and Lys256 project from opposite faces of the helix, with Lys256 controlling immersion depth. Their modification causes step-wise reduction in associations with T-cell surface CD3$\zeta\zeta$ and CD3$\varepsilon\gamma$/CD3$\varepsilon\delta$, respectively, leading to an activated transcriptome. In this dissertation, optical tweezer assays reveal that Arg251 and Lys256 mutations alter $\alpha\beta$TCR-pMHC bond lifetimes, while mutations within interacting TCRα connecting peptide and CD3δ CxxC motif juxtamembrane elements selectively attenuate signal transduction. Combined with the structural biology, our findings suggest that mechanical forces applied during pMHC ligation initiate T-cell activation by altering the disposition of those

basic sidechains to rearrange TCR complex membrane topology and weaken TCR$\alpha\beta$ and CD3 associations, a phenomena akin to phase transition. Regionally, the asymmetric redistribution of proteins to distinct regions in the plasma membrane is crucial to the cellular function. TCR signaling is proposed to be triggered by the segregation of the phosphatase CD45 from the immune synapse, where the ligation between TCR and pMHC initiates the activation cascade. Using the two-bead assay and single molecule DNA tether technology, we showed the long-range CD45 diffusion (~5 μm maximumly) outside the activation contact zone, a phenomenon different from the size exclusion based kinetic segregation model. Cross-linked CD45 diffusion barrier hinders the TCR triggering in a position and density dependent manner. Meanwhile, optimal external normal force applied through ~1 μm long single anti-TCR tether can trigger the early Ca^{2+} flux. Physical exclusion of CD45 by difference in sizes of innate TCR-pMHC complex was abolished using the tether systems, indicating a mechanosensing facilitated internal molecular rearrangement in the cell membrane during triggering. Discrete structure transitions of TCR were able to visualize for the antibody induced TCR triggering. These results demonstrate that the TCR mechanosensing not only orchestrates the triggering cascade but also facilitates the spatial partitioning of the CD45 from the triggering site.

4.2 Introduction

T-lymphocytes are a critical cellular component of the adaptive immune system responsible for detecting and eliminating aberrant cells in mammals. These motile cells move throughout the body and perform wide-ranging immune surveillance functions to prevent or combat disease states (infections, cancerous transformations, etc.). The $\alpha\beta$ T-cell receptor complex ($\alpha\beta$TCR), a mechanosensor displayed on the T cell surface, mediates T-cell recognition [1, 2, 3, 4, 5, 6]. The TCR is a squat and wide multi-subunit protein complex composed of a disulfide-linked TCR$\alpha\beta$ heterodimer flanked by three sets of non-covalently associated dimeric CD3 subunits: the CD3$\varepsilon\gamma$ and the CD3$\varepsilon\delta$ heterodimers and the CD3$\zeta\zeta$

homodimer [7, 8, 9, 10]. Each TCRα and β chain contains one extracellular variable (V) and constant (C) domain, a membrane proximal connecting peptide (CP), a single transmembrane (TM) domain, and a short cytoplasmic tail [11]. The paired TCR VαVβ extracellular domain module is most distal to the membrane, hence well-positioned to directly interact with a peptide bound to the groove of a major histocompatibility molecule (pMHC) displayed on the surface of an opposing antigen presenting cell (APC). TCR recognition is an exacting process, requiring a given TCR to detect a handful of copies of MHC-bound foreign antigen (i.e. mutant-host or pathogen-derived peptide) arrayed and dispersed amongst 100,000 normal self-peptides on the same APC. Following TCR-pMHC engagement and successive force-driven conformational change and bond lifetime extension that tunes antigen recognition [1], there is an orchestrated set of intracellular T cell signaling responses including tyrosine phosphorylation, a rise in intracellular free calcium and transcriptional activation events that support cytotoxic effector and helper programs in CD8 and CD4 T cells, respectively [12]. The myriad of unique V modules (billions in theory) are parsed out at a clonal T cell level to form a repertoire of diverse T cells sufficient to interrogate the enormous immune peptidome of pathogen- and tumor-derived sequences displayed on the surface membrane of altered cells [13]. Thus, each TCR specifically recognizes only one or a small number of pMHC ligands that it encounters on an APC. Since TCRα and β subunits have extremely short cytoplasmic tails devoid of signaling sequences, the associated CD3 molecules are critical for the transfer of information about a cognate recognition event into the cell despite having no interaction with pMHC [14, 15]. Unlike the TCR α and β subunits, the CD3 molecules are invariant. The CD3 molecules are thought to interact with the TCRα and β subunits through their extracellular and/or the TM domains to foster the relay of TCR-pMHC binding information to the CD3 subunits, including through their long CD3 cytoplasmic tails containing a signaling Immune Tyrosine Activation Motif (ITAM). The CD3$\zeta\zeta$ homodimer contains six ITAMs, three per cytoplasmic tail to amplify activation. Formation of TCR$\alpha\beta$, CD3$\varepsilon\gamma$ and CD3$\varepsilon\delta$ heterodimers is dependent on

the extracellular domain interactions, while in the case of CD3$\zeta\zeta$, an interchain disulfide bond connects the short ectopeptides of the two CD3$\zeta\zeta$ protomers [10, 14, 15]. In contrast, the linkage between the TCR$\alpha\beta$ and CD3 subunits requires interactions in the membrane proximal and TM domains since only weak ectodomain-mediated interactions have been detected [16, 17, 18]. Each of the eight subunits comprising the $\alpha\beta$TCR complex contains a single TM domain marked by the presence of highly conserved charged amino acids. The current hypothesis posits that these charged residues, and their position within the TM, dictate charged-paired interactions between the TCR α and β subunits and CD3 subunits important for surface assembly, expression and signaling [19, 20, 21, 22, 23, 24, 25]. The model suggests that positively charged basic amino acids within the TCRα and β subunits associate with negatively charged acidic residues in each of the CD3ε, γ, and δ TM domains to generate trimeric TCRα-CD3$\varepsilon\delta$ and TCRβ-CD3$\varepsilon\gamma$ sub-complexes. A similar electrostatic charged-based coupling role is proposed for charged TM residues in CD3$\zeta\zeta$ and TCRα [21, 26]. While this assembly hypothesis is attractive, there is no direct molecular evidence supporting it.

Globally, a signaling cascade within the T cell initiated by ligation of TCR and antigen pMHC leads to reorganization of the cytoskeleton and organelles, transcriptional changes, and cell proliferation. The first step in the cascade is the phosphorylation of ITAMs region in TCR complex by Src family tyrosine kinase Lck anchored on the plasma membrane [27], leading to transient rise of cytosolic Ca^{2+}. As the TCR signaling is driven by the Lck based phosphorylation, regulators involved in this process was widely investigated, which includes the abundant membrane protein CD45 that is expressed on T cells and other hematopoietic cells [28, 29]. The function of CD45 draws much attention because of its dual functionality on Lck activation. It not only targets at the phosphorylated ITAMs region in TCR and dephosphorylates them in order to inhibit the triggering cascade, but it also activates inhibitory phosphorylation of Lck, shifting inhibited Lck into the primed state and double active Lck into the single active state. This dual role of CD45 makes it

more difficult to predict the influence of CD45 on the regulation of T cell activation, as it could have an activating as well as an inhibitory effect. The TCR complex does not possess intrinsic kinase activity. Nevertheless, the information of extracellular stimulation needs to be transmitted into the cell and translated into stronger phosphorylation of the ITAMs. Thus, mechanisms either enhancing the phosphorylation of the ITAMs or decreasing in phosphatase activity following TCR stimulation were proposed, in order to interpret the signal propagation. The latter one is termed as the "kinetic segregation" model, which assumes that relevant phosphatases (e.g. CD45 and CD148) are physically excluded from region of TCR-pMHC contact [30]. Specially, CD45 has a very large ectodomain (~28 nm to ~50 nm) [31, 32] that excels the TCR-pMHC complex (~12 nm) in height. Upon the formation of the TCR-pMHC complex, CD45 is pushed out of the region of interaction due to their geometric difference. A second possibility that would exclude phosphatases could be a rearrangement of the cell membrane during TCR triggering. If the amount of phosphatase is reduced in the proximity of the TCR, dephosphorylation is reversed to a much lesser extend and T cells become activated. Recent studies from both real cells and reconstitute system both show that, indeed, CD45 is pushed out of the signaling region where the TCRs accumulate [33]. However, in order to sustain the T cell activation, CD45 needs to be recruited to the immune synapse after a certain time (4.5 to 10 min)[34], make this T cell activation process more sophisticated. Instead of simplifying the T cell-APC interaction as a stagnant contact, during immune surveillance, T cells can scan their environment, physically bind and crawl over structures via cell motility processes. The cell motion itself can generate tensile, shear and compressive stresses over a wide range of forces (pN to nN) [35, 36, 37]. Therefore, to explain the signal pathway from TCR to CD3 molecules, the importance of mechanical forces in TCR signaling has been previously reported [3, 4, 38, 39, 40, 41], which suggested the extracellular mechanical forces can facilitate activation of surface receptors and regulate signaling. Recently, we also showed that the external force induced TCR triggering accompanies with the actomyosin system,

which helps recruitment the pMHC non-ligated TCR to the activation site [6].

To elucidate the mechanistic underpinning of these observations, this chapter firstly focused on the two positively charged, basic amino acids in the TCRα subunit. Combining with the NMR data for TCR transmembrane (TM) and cytoplasmic tail (TMC) domain, we observed that mechanical force operative during pMHC ligation of the TCR in conjunction with lipid alterations and/or post-translational modifications could actuate (toggle) this conformational switch, altering TM immersion topology governed by Lys256 to impact overall $\alpha\beta$TCR subunit associations and T-cell activation. Together, our data provide a model in which TM segments of the TCR complex are loosely interdigitated in the resting state but transfigured under force to dissociate and/or rearrange CD3 homodimers and CD3 heterodimers to initiate TCR complex activation. Consistent with this view, the juxtamembrane elements, the TCRαCP and the CD3δ CxxC motif, interact with each other in the absence of detectable association of their respective TM domains. Based on our results, we present a plausible view of the sequential nature of force driven-rearrangements that are consistent with the selective loss of CD3$\zeta\zeta$ observed in tumor infiltrating lymphocytes linked to persistent inflammation (reviewed in [42]).

On the second part of this chapter, we proposed an external force induced CD45 exclusion from the activation sites. The long-range CD45 diffusion outside the activation contact zone is significant for the TCR triggering. TCR triggering can be interrupted by the cross-linked CD45 fence when the anchored CD45 occupancy is higher than ~400 molecules and the activation site and diffusion barrier is ~2 μm apart. Meanwhile, optimal external normal force applied through ~1 μm long single anti-TCR tether can trigger the T cell. Physical exclusion of CD45 from the close contact zone formed by innate TCR-pMHC complex was abolished using the tether systems, indicating a mechanosensing facilitated molecular rearrangement in the cell membrane during triggering. These results demonstrate that the TCR mechanosensing not only orchestrates the triggering cascade but also facilitates the spatial partitioning of the CD45 from the triggering site.

4.3 Results

4.3.1 Mutations targeting the TCRα-CD3δ interaction site result in signaling defects.

The NMR data provides that the deleterious functional outcomes in the mutant cells (performed by Dr. Brazin in Dr. Ellis L. Reinherz's lab in DFCI) are due to disrupted structural connectivity at the TCRα and CD3δ juxtamembrane interface that undermines force-dependent signal transduction. To test this notion, optical tweezers (OT) were used in a single cell format [6] to characterize the mechanotransduction properties of the WT and mutant $\alpha\beta$TCRs (Fig. 4.1A and B). Concordant with the IL-2 functional results, the OT analysis showed defects in Ca^{2+} triggering for both TCRα-CPmut[7] and CD3δ-SxxS transduced cell lines relative to WT (Fig. 4.1B, top panel). Specifically, the mutant cell lines were unable to trigger Ca^{2+} flux at high pMHC copy number in the absence of force, in contrast to WT TCR expressing cells where internal actomyosin forces pulling on the TCR following pMHC ligation is sufficient to induce activation. Only when substantial triggering force was applied (~21-27 pN for each mutant cell) were the mutant-transduced cell lines able to be activated by pMHC, and this required a high ligand copy number (20,000 molecules of VSV8/K^b per bead-cell interface). Sensitivity of mutant receptor triggering was dramatically compromised compared to the WT TCR expressing cells where just 10 pN/TCR shear force and 2-29 molecules of VSV8/K^b per bead readily induced activation. These data demonstrate that mutations targeting interaction sites identified in the NMR structural studies produce defects in force-coupled signaling.

4.3.2 Antigen recognition sensitivity is enhanced by R251L but abrogated for K256L mutations: linkage to TCR-pMHC bond lifetime alterations

While the observed structural role for the TCRαCP and CD3δ CxxC juxtamembrane region elements is significant, the effects of mutation at R251 and K256 on mechanotransduction were even more striking (Fig. 4.1B, bottom panel). With R251L cells just 2

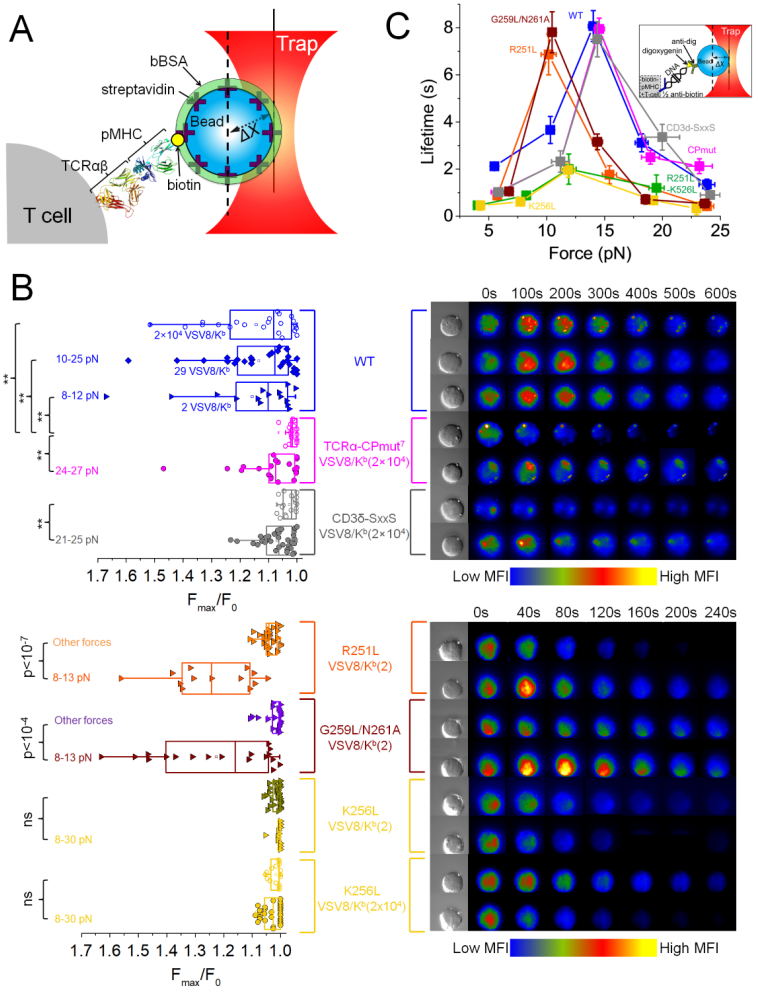

Figure 4.1: **Functional consequences of mutations targeting the TCRα-CD3δ interaction site as assessed by optical trap and fluorescence microscopy.** (A) Diagram depicting the bead-cell contact in the optical trap used for applying force in the TCR triggering experiments as detailed in Chapter 3. (B) T-cell activation analysis of the WT, and mutant gene transduced BW5147 cell lines. Left: Ca^{2+} flux was triggered at the indicated VSV8/K^b densities with applied trapping force (5-35 pN) or without force for the different cell types. The (**) represents P values $\leq$ 0.01. Right: Intracellular Ca^{2+} flux measured over the experiment from representative individual cells. The top corresponds to the analysis of the WT, TCRαCPmut^7 and CD3δ-SxxS cell lines with the time interval of 0-600 seconds vs. the R251L,G259L/N261A and K256L cell lines with the time interval of 0-240 seconds. (C) The catch bond behavior of different TCR-expressing cell types as indicated under force is plotted as bond lifetime vs. force. Error bars represent SEM. The inset represents a cartoon depiction of the single-molecular tether assay for measurement of TCR-pMHC bond lifetimes.

molecules of VSV8/K^b in the OT system led to a response more rapidly than with WT cells, inducing faster calcium flux but with a more rapid return to baseline. The duration of the calcium flux was sustained for 63 +/- 20 sec (10 cells, +/- SD) for the R251L N15 T-cells relative to the much longer response time of 288 +/- 119 sec (8 cells, +/- SD) for WT N15 T-cells both tested with two VSV8/K^b molecules. By contrast, the K256L cells were unresponsive to mechanotransduction at any density of pMHC molecules arrayed on the interacting beads surface and with any pN force applied. Given the loss of all associated CD3 dimers due to the K256L mutation, it is not surprising that the surface membrane TCR$\alpha\beta$ was devoid of signaling activity. By reducing the number of pMHC molecules and extending each from the bead surface using a large DNA tether [1], the OT system can also be used in a single molecule, single cell (SMSC) format to measure individual TCR-pMHC bond lifetimes. Force-bond lifetime dependence in SMSC assays was used to compare the WT and variant lines bearing TCRα mutations that alter the TCRα-CD3δ interaction site or the TCRαTMC membrane immersion depth and assembly (Fig. 4.1C). The WT cell line shows similar force dependence of bond lifetimes as observed previously in OT-based SM and SMSC assays [1, 2]. The individual TCRs all manifest catch bonds, a counter-intuitive behavior in which bond strengthening occurs with application of force relative to 0 force and is manifested as longer bond lifetimes under load, with subsequent bond rupture occurring at higher forces exceeding that of the single bond strength [1, 4]. Despite their impaired ability to facilitate T cell activation (Fig. 4.1B), the CPmut[7] and CD3δ-SxxS mutants display similar force maxima as WT for catch-bond formation, ~15 pN, and maximal lifetime, ~8 s. In contrast, the R251L mutant shows a slightly reduced maximal lifetime, but with the catch bond force maximum shifted downward from the WT to ~10 pN, suggesting that a subunit assembly defect impacts antigen recognition function. Most strikingly, the two K256L bearing mutants show both a large decrease of maximal bond lifetime and attenuation of catch bond formation. Given the normal protein fold of the mutant TCRs as determined by several anti-TCRβ mAbs, the result suggests

an inability of the force-transduction pathways to sustain necessary forces to gate ligand discrimination [1]. This could occur from attenuation of normal TM anchoring, modification of TM tilt geometry upon force-based ligation and/or CD3ζ-linked actin cytoskeletal associations necessary to transduce external force via the $\alpha\beta$TCR complex.

4.3.3 Long-range CD45 phosphatase redistribution during the mechanosensing induced TCR triggering

In Chapter 3, we have already shown that the force-induced TCR clustering before the immune synapse formation formation using the two-bead assay. With the 'pick and place' property of optical trap, here we still inherit the similar scenario, which incorporates two beads with one saturated pMHC coated bead to mechanically induce TCR triggering while the other smaller one with few ligands to label the triggering associated molecules adjacent to the triggering site. The differences between these two assays are the ligand density on the smaller bead surface as well as its position relative to the triggering bead. Here, we systematically explored the long-range CD45 phosphatase redistribution (~5 μm maximumly). Four different positions at four densities were tested, as shown in Fig. 4.2A. Smaller bead (d = 1.09 μm on average) coated with different amount of anti-CD45 antibody molecules was firstly placed on one of the four positions, then the saturated pMHC coated bead was trapped and brought to the T-cell membrane to form the interaction with TCRs. Contour distances between the stimulating bead and smaller inhibiting bead are 2μm, 4μm, 6μm from position 1 to position 3. Position 4 and the position of the stimulating bead represent the two endpoints of the diameter of a circular cell (cell diameter = 8 μm on average). Interestingly, position and antibody density of the CD45 binding bead play a critical role in regulating the early T-cell activation (Fig. 4.2B). With ~2×10^4 copy numbers of anti-CD45 antibody, interference with early T-cell activation by the clustered CD45 becomes apparent when the inhibiting bead is closer to the triggering site (position 2). When the inhibitor bead is ~4 μm relative to the stimulation bead, the triggering is virtually abolished. However, the

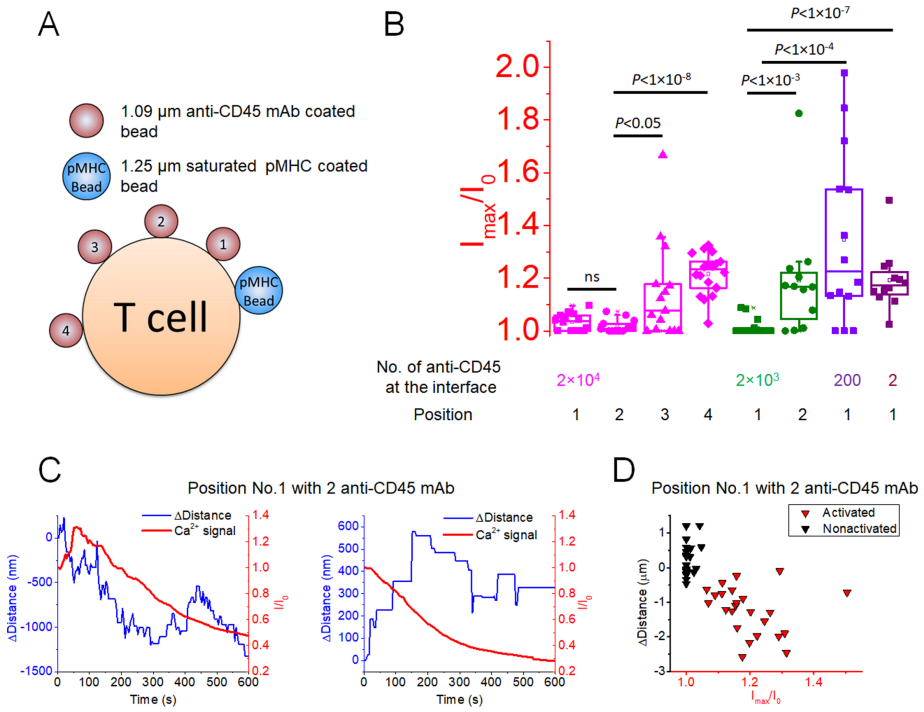

Figure 4.2: **Two-bead assay determines the long-range distribution of CD45 molecule.** (A) The two-bead assay was performed using a triggering stimulating bead coated with saturated VSV8/K^b (2×10^5 per bead) and a second smaller bead coated with different copy numbers of anti-CD45 antibody. The antibody coated bead was also placed at different positions relative to the triggering bead, creating CD45 diffusion barriers with different sizes and distinct distances from the triggering site. (B) Ca^{2+} flux triggered by saturated VSV8/K^b coated bead was tested with the indicated densities and positions of anti-CD45 antibody coated bead. (C) The anti-CD45 antibody coated bead with ~2 molecules at the interface diffused away during the TCR triggering (left). Note in this case the CD45 labeled smaller bead was outside the triggering site, indicating the long-range distribution property of CD45 segregation. On the contrary, smaller bead on the nontriggered T cell did not show dramatical motion and the bead even moved close to the triggering site (right). Smaller bead was sequentially coated with biotin-labeled dye to facilitate the discrimination of triggering bead. (D) Changes of distances between the two beads for activated and non-activated T cells. The two clusters are significantly different at $p \leq 1 \times 10^{-12}$.

triggering can be regained when reducing the number of CD45 molecules anchored down below the smaller inhibiting bead. Calcium flux is unaffected when there are ~400 interfacial CD45 molecules (theoretically one antibody can interact with two antigens, thus 200 anti-CD45 antibody will bind maximumly 400 CD45 molecules) grappled, whose cluster is ~2 μm away from the triggering site. With two anti-CD45 antibody molecules presenting

on the bead surface, we were able to capture the TCR triggering associated CD45 motion at the single molecule level. The motion of CD45 relative to the TCR triggering is shown in Fig. 4.2C. Compared to unligated TCRs co-opt to the triggering site, the CD45 will diffuse away during TCR triggering. Whereas in nontriggered cases CD45 shows limited motion and even close to the stimulation bead at first. The segregation correlating with TCR triggering was also statistically analyzed, as shown in Fig. 4.2D. Relative distance between the CD45 labeling bead and stimulation bead is increased during the TCR triggering whereas the nontriggered T cell shows the inert or opposite motion, revealing the passive diffusion property of CD45 and its complexity of constitutively interaction with F-actin [43].

4.3.4 Force induced TCR triggering by DNA tether technology

In order to test whether TCR-pMHC complexes (ectodomain length = ~12 nm) induced membrane distortion that physically generate the size exclusion of CD45 molecules (ectodomain length = ~50 nm) is necessary for TCR triggering, a 3500-bp single DNA tether (L = ~1 μm) with biotin tag on one end and half-anti-TCRVβ on the other end was used to remotely present the optical trapped bead and TCR on the T-cell surface, as shown in Fig. 4.3A. The half-antibody used here can guarantee the affinity to TCR so under load (<25 pN) bond rupture barely happens [44]. Surprisingly, calcium flux can be initiated by the single anti-TCR tether although the calcium duration is not as long as the pMHC coated bead [6](Fig. 4.3B and C). The stimulation can be generated when using ~10 pN normal force, with the peak Ca^{2+} increment ~1.16. Although the initial touching between bead and cell membrane is still necessary in order to initiate binding to the TCR on T-cell surface, control experiment with a trap held bead pushing cell membrane does not lead to no triggering (Fig. 4.3C, bottom).

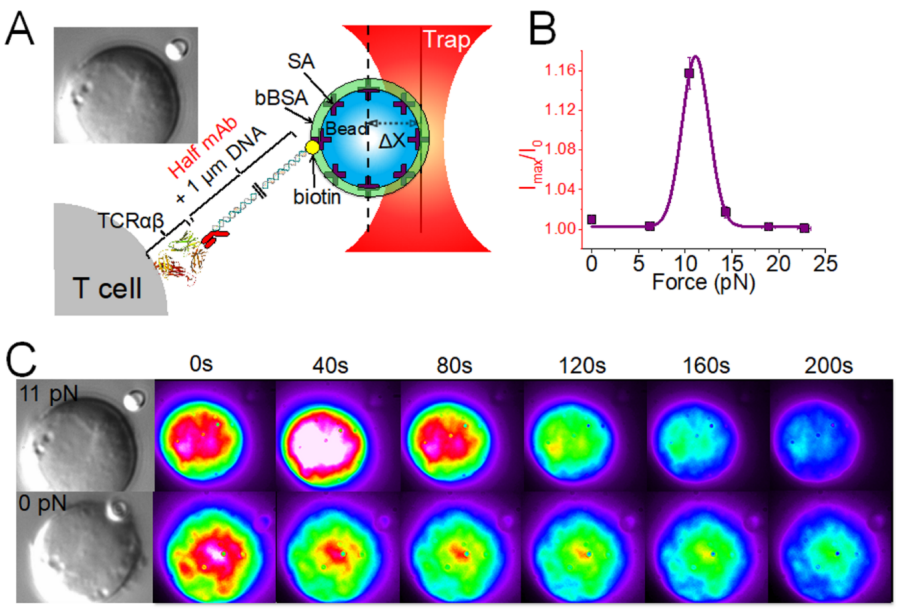

Figure 4.3: **TCR triggering by single DNA tether technology at optimal pulling force.** (A) Cartoon showing the singe tether triggering assay. Instead of using the VSV8/K^b at the DNA end , here we used a anti-TCR Vβ antibody to mimic the interaction between the pMHC and TCR. The stronger interaction between antigen-antibody would guarantee the sustainment of bond at the tested forces. Top left: DIC image of a T cell and a bead separated but bridged by a ~1 μm long DNA tether. (B) Ca^{2+} flux triggered by single tether was tested at different pulling forces. (C) Representative triggering images of T cells at 11 pN (triggered) and 0 pN. Note that at 0 pN, the bead is hold with optical trap in order to make the close contact.

4.4 Discussion

The phase transition after TCR-pMHC ligation is a critical process for thymocyte development and mature T-cell responsiveness to foreign antigens. In this chapter, we have pursued multiple biophysical approaches to understand such phenomena during early T-cell activation.

The single cell activation experiment paralleled with the structural biology data elucidate that the straightened conformation is the active state with force-mediated TCR-pMHC ligation inducing the switch as noted below. A specific juxtamembrane interaction between the CP region of TCRα and the CxxC motif of CD3δ was reported [45], establishing a mechanical link between TCRα and CD3δ subunits in the TCR complex. The TCRα

membrane proximal region was shown to be important for mediating a functional CD3δ interaction with disruption of the TCRαCP FETDxxLN motif reducing positive selection of thymocytes during thymocyte development [46]. Our results reveal residue-specific details of the juxtamembrane interaction between TCRα and CD3δ important for intracellular Ca^{2+} release. Interestingly, TCR-pMHC bond lifetimes of $\alpha\beta$TCRs on T-cells with mutation of the TCRαCP region or CD3δ CxxC were similar to those of WT $\alpha\beta$TCR-expressing T-cells. Hence, the TCRαCP and CD3δ CxxC regions do not control TCR cell surface expression or affect TCR-pMHC bond formation, yet are critical for the translation of mechanical energy across the cell membrane to induce T cell activation. Combined with the structural data provided by our collaborator and optical trap data presented here, we propose a dissociative model for pMHC-triggered $\alpha\beta$TCR complex activation dependent on the distinct roles of TCRαTM Arg251 and Lys256 residues working in tandem as a part of force-driven mechanotransduction. Load on the pMHC-TCR$\alpha\beta$ bond occurs from cell movement during immune surveillance at the time foreign pMHC is first detected and prior to a stop movement signal [reviewed in [47]]. This physical force fosters a structural transition in the TCR$\alpha\beta$ ectodomain to strengthen bond lifetime and energize the TCR, impacting the flanking CD3 heterodimeric ectodomains and inducing TCR complex quaternary change [1, 2]. Force proceeds from subunit ectodomains via their respective connecting peptides and then impacts the TM segments in the cholesterol-rich lipid rafts where TCRs reside largely linked to the actin cystoskeleton [48]. Lipid rafts offer a stiffened platform to suppress mechanical noise while spatially confining force [49]. These events induce changes in lipid composition vicinal to the $\alpha\beta$TCR, including loss of negatively charged phosphatidylserine and phosphoinositides [50]. The lipid changes combined with structural coupling between juxtamembrane connectors, TM and cytoplasmic tail segments, result in the release of the CD3 tethered tails from the inner leaflet of the plasma membrane to expose ITAM phosphorylation sites for signaling initiation [51, 52]. Our dissociative hypothesis is consistent with observations made years ago showing that anti-clonotypic

antibodies which bind to the VαVβ-module recognition surface, akin to pMHC, dissociate the CD3 dimers from the TCR$\alpha\beta$ heterodimer in detergent lysates whereas anti-CD3ε antibodies preserve the integrity of the entire $\alpha\beta$TCR complex [53]. A detailed model is illustrated in Fig. 4.4. In the inactive state, the $\alpha\beta$TCR assembled on the T cell surface is composed of the TCR$\alpha\beta$ heterodimer and non-covalently associated CD3$\varepsilon\gamma$, CD3$\varepsilon\delta$ and CD3$\zeta\zeta$ dimers (Fig. 4.4A). The TCR$\alpha\beta$ and CD3 TM domains are loosely associated, as are the TCRα and β subunit TM domains, with the cytoplasmic tails sequestered on the plasma membrane (Fig. 4.4A, left panel). In the inactive state, the TCRα subunit exists in a predominantly L-shaped configuration with Lys256 snorkeling to associate with lipid head groups. The well-conserved hinge region assists in maintaining the inactive configuration (Fig. 4.4B, left panel). The CD3$\zeta\zeta$ homodimer, including the paired negatively charged Asp residues, may be in contact with the TCRα Arg251 residue. The heterodimeric CD3$\varepsilon\delta$ and CD3$\varepsilon\gamma$ and their respective negatively charged TM residue pairs are potentially interacting with the lipid membrane positively charged choline or amino groups (not shown). Following T cell activation, there is a stepwise disassociation of the complex. An interchange of lipid molecules as noted above occurs in the membrane that causes the cytoplasmic tails to become released from the cell membrane and therefore available for signaling (Fig. 4.4A, right panel). Force transduction through the membrane can initiate key changes causing the TCRαTM to alter its helical tilt, adopting a more straightened configuration, changing the position of the Arg251 sidechain and consequently disrupting an association with CD3$\zeta\zeta$. CD3$\zeta\zeta$ then becomes displaced from the TCR complex resulting in the first stage of activation (Fig. 4.4A and B, right panels). With the subsequent change in TCRα membrane positioning, the Lys256 side chain becomes more embedded in the acyl chains in the membrane. We cannot exclude the possibility that force could transiently extrude the Lys256 sidechain into the cytosol for post-translation modification by acetylation or methylation leading to greater depth in the acyl chain region post-modification [54]. The extremely short TCRα cytoplasmic tail will facilitate such a movement of the straightened

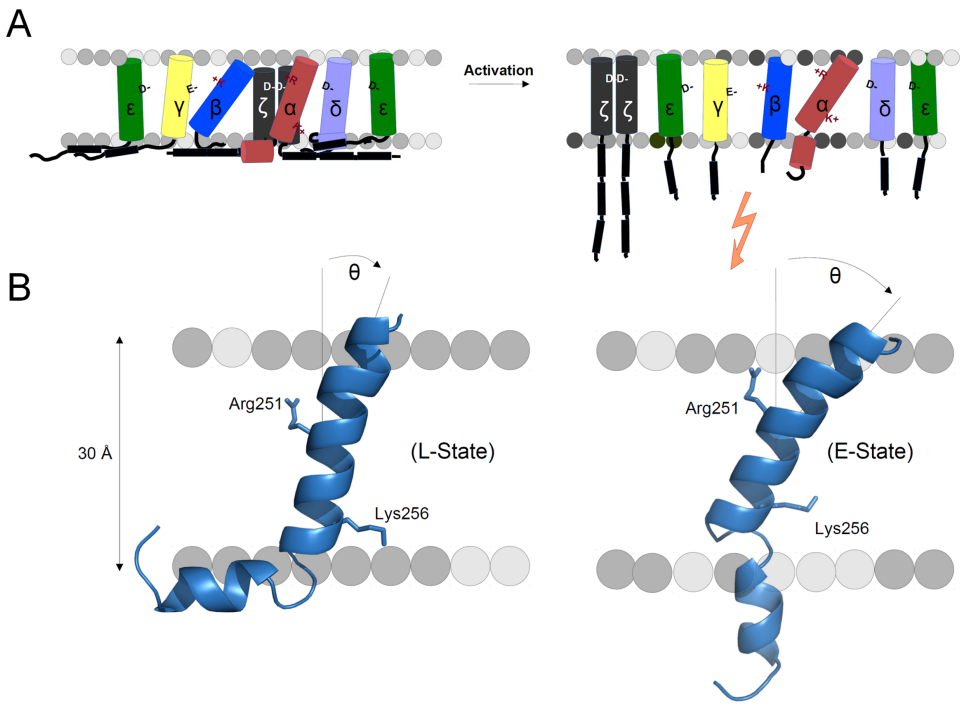

Figure 4.4: **Model of TCR activation involving TM segment conformational change.** (A) The TCR$\alpha\beta$ and dimeric CD3 TMC illustrated in a membrane lipid bilayer. The TM helices are represented as cylinders, flexible regions as black lines, and ITAM motifs as black rectangles. Membrane lipid changes with activation are represented by changes in the headgroup colorization. The lightning bolt signifies an activated cellular state. See text for description of the activation event. (B) The TCRα TMC represented in a lipid bilayer in two conformations, inactive (left) and active (right). The inactive conformer exists primarily in the bent (L)-state conformation and the Arg and Lys residues are only slightly embedded in the membrane and the Lys may be snorkeling through to contact the lipid headgroups. Upon TCR activation and resulting lipid reorganization and potential post-translational modifications, the TCRα TMC then undergoes a change in its helical positioning in the lipid bilayer that then results in the Lys residue to become more embedded within the lipid acyl chains, represented as the active, extended (E)-state conformer. The helical tilt is represented as the angle from the perpendicular membrane axis. This image is granted from Kristine N. Brazin, Robert J. Mallis, Andras Boeszoermenyi, Yinnian Feng, Akihiro Yoshizawa, Pedro A. Rech, Pavanjeet Kaur, Kevin Bi, Rebecca E. Hussey, Likai Song, Gerhard Wagner, Hari Arthanari, Matthew J. Lang, and Ellis L. Reinherz,, "The T-cell receptor α bipartite transmembrane domain coordinates antigen triggering by regulating bilayer immersion, CD3 association and transcriptomes" under review with the permission of the corresponding author Ellis L. Reinherz.

TCRαTM helix. Of note, proteins with short cytoplasmic tails undergoing trogocytosis are fully extracted from the cell membrane [55]. Either possibility could result in the second

stage of activation.

Several lines of evidence suggest that the CD3$\zeta\zeta$ dimer can readily dissociate from the $\alpha\beta$TCR complex. First, loss of CD3$\zeta\zeta$ proteins from human T-cells has been observed in areas of immune inflammation, particularly in associations with cancer [42]. Second, weakening of CD3$\zeta\zeta$ association described above augments the rapidity of mechanotransduction-linked calcium flux. Third, in addition to R251L mutation, other TCRαTM mutations facilitate CD3$\zeta\zeta$ dissociation, underscoring its weak basal level of interaction with the other TCR subunits in the membrane environment. It is noteworthy that $\alpha\beta$TCR triggering is anisotropic, so that direction of force application by pMHC or anti-CD3 mAb determines cellular activation potential [3, 6]. The same must apply for CAR-T cell ligand binding and force transduction through the CAR ectodomain, linker region and TM. Therefore, nuancing of the molecular design of CARs based on evolving principles of mechanotransduction and dissociative $\alpha\beta$TCR complex activation should help to extend the number of targets amenable to this immunotherapy.

A similar phase transition happens in the long-range (L = ~ 5 μm) after CD3$\zeta\zeta$ dissociation. Exclusion of phosphatase such as CD45 and CD148 from the T cell-APC interacting interface has been observed in many in-vivo experiments prior/during immune synapse formation (reviewed in [30]) and even for the reconstituted systems [33]. Based on such phenomena, researchers have proposed a segregation and redistribution model (Fig. 4.5). The brief mechanism in kinetic segregation model is based on the TCR-pMHC interaction [30]. Because the TCR-pMHC complex spans a short length (~12 nm), TCR binding to agonist pMHC traps the TCR/CD3 complex within a close-contact zone as well as size-excluded the inhibitory tyrosine phosphatases with large ectodomain (~50 nm), thereby protecting it from inhibitory tyrosine phosphatases for as long as the TCR remains bound to pMHC. Mechanical pushing forces generated by bending of an ectodomain of CD45 may also applied force (~10 pN) to the TCR-pMHC interaction [43]. Such force magnitude is within the optimal force region that maximizes the catch bond, thus favoring the

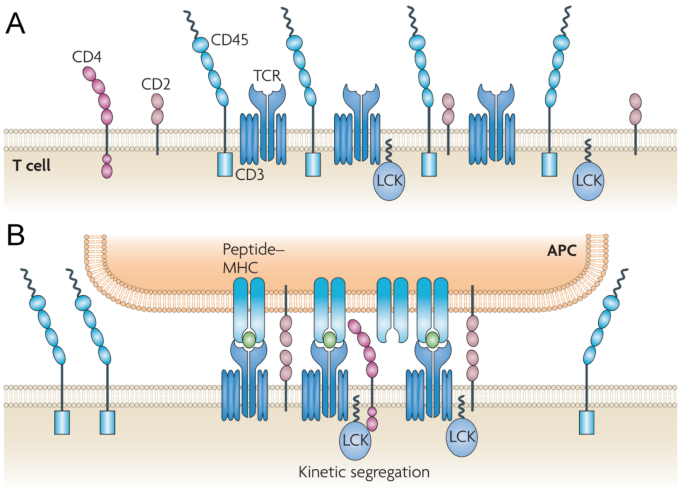

Figure 4.5: **Kinetic segregation model of T cell activation.** (A) Without contact between a T cell and an APC, TCR/CD3 complexes undergo an equilibrium of phosphorylation and de-phosphorylation between kinases (e.g. LCK) and phosphatases (e.g. CD45). Thus, the transient TCR triggering signal will abrogate instantaneously by inhibition of phosphorylation. (B) When TCR-pMHC ligations are formed, CD45 molecules with larger ectodomains are sterically pushed away from the close contact zones. The balance between phosphorylation and de-phosphorylation is broken so that it would favor TCR/CD3 phosphorylation by kinases, thereby accumulating more triggering signals to initiate downstream signaling cascade. This image is reprinted with permission from [56]. Springer Nature Terms and Conditions for RightsLink Permissions

long-lasting of the interaction. In the absence of pMHC, TCR/CD3 complexes that enter a close contact zone will get phosphorylated but this would be too short-lived to result in signaling. They rapidly diffuse out of the close-contact zone where they encounter tyrosine phosphatases and are dephosphorylated.

Several lines of evidence have been provided to support the rationality of kinetic segregation model: first, CD45 and CD148, as two main T cell activation inhibitor are excluded from immune synapse during TCR triggering [57, 58]; second, TCR triggering will be inhibited by truncation of the large CD45 and CD148 ectodomains that eliminates the length difference between TCR-pMHC complex and CD45/CD148 [58, 59], third, elongation of pMHC-I or II complex on the APC abrogates T-cell recognition, thus inhibiting the initial TCR triggering [60, 61]; fourth, when ligand is anchored to a surface, it is more readily to trigger TCR than their soluble tetramer in a 3D environment [62, 63]; and, finally, engi-

neered TCRs show better antigen recognition when the epitope and plasma membrane of the target cell are close to each other [64, 65].

Although experiments mentioned above may support the CD45 redistribution and segregation model, most of the evidence cannot shadow the role of physical force involved in this model. First of all, even though elongation of the pMHC complex inhibits TCR triggering, the longer distance between APC membrane and T-cell surface also transduces lower force compared to the normal case [60, 61, 66]. Using the DNA tether technology interlaced with optical trap, we directly showed that mechanical force applied through a 1 μm spacer between the bead and cell membrane still initiates the triggering signal, in this case the bead surface was kept away from the cell surface during the T-cell triggering (Fig. 4.3). We have previously tested that pMHC coated bead under physiological density fails to trigger TCR without external load, as the same case shown here using the optical trap to hold an anti-TCR tethered bead on the cell surface (Fig. 4.3C, bottom). Second, stochastic distribution of antigen pMHC on the APC will hinder the existence of a handful of identical agonist pMHC molecules in very close location (~10 nm) [67] to sustain the TCR/CD3 complexes entrapment. Considering that the TCR can be triggered by only one pMHC on an APC [68], the tiny membrane bending area generated by single TCR-pMHC catch bond is unlikely to push away CD45 molecules nearby, as the abundance of CD45 over TCR [69]. We have shown that the TCR can be triggered using as low as two pMHC molecules presenting on the bead-T cell interface with optimal shear and normal force [6]. The molecules on the bead surface are statistically separated by a long distance ($\geq$ ~500 nm) and this also revealed by the single molecule TIRF microscopy. Third, the exclusion of CD45/CD148 due to membrane pushing away effect will accumulate more inhibiting signals near the triggering site. Such signals would abrogate the TCR triggering as proved by the two-bead assay (Fig. 4.2). The triggering will only happen if there are less CD45 molecules near the triggering site or the barriers is distal to the triggering site.

Combined with the results in Chapter 3, here we proposed a more general model

for explaining the segregation phenomena happened after the initial CD3$\zeta\zeta$ dissociation (Fig. 4.6). After the force induced TCR-pMHC ligation, the motor system beneath the CD3

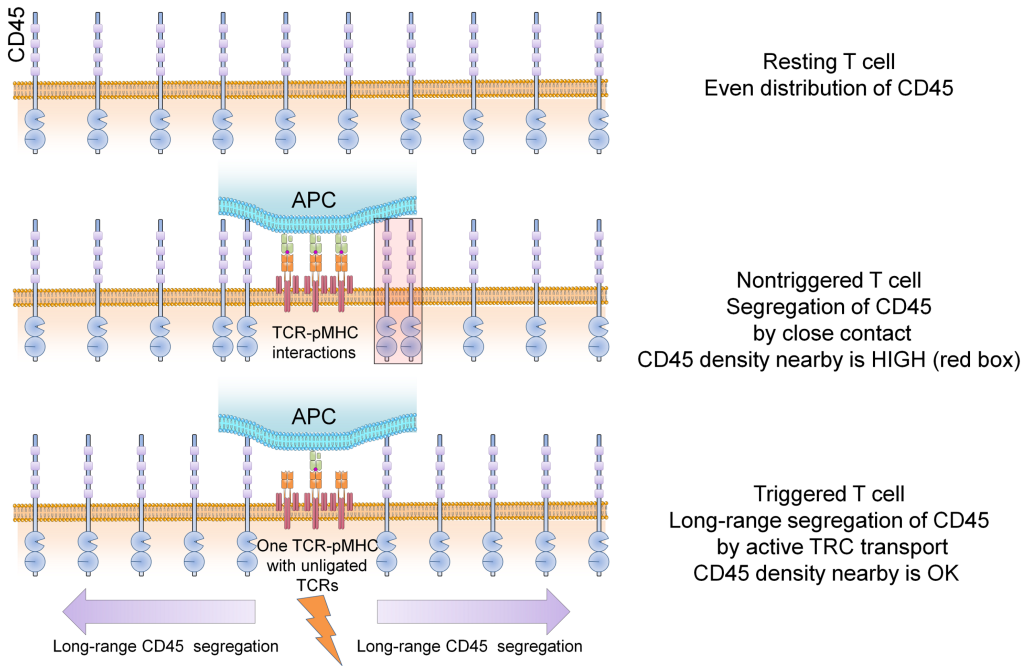

Figure 4.6: **Passive transport of phosphatase CD45 segregation pushed by active TCR accumulation in the T cell/APC contact zone.** Top: Phosphatase CD45 at the resting T cell will undergo an equilibrium distribution. Middle: Sterical exclusion of CD45 by close contact generated membrane protrusion will induce the local enrichment of inhibiting signals near the triggering site (red box), thus would abrogate the TCR triggering. Bottom: Long-range segregation of CD45 could dilute the accumulated inhibiting signals nearby, favoring the TCR triggering. The TCR accumulation driven by cytoskeletal motors will form a compact central supramolecular activation cluster (cSMAC) so that the CD45 would be excluded, a phenomena akin to phase transition.

complex will recruit more TCRs outside the triggering site to participate the formation of immune synapse. During the active transport of TCRs, the passive exclusion of CD45 by the stout and squat TCR complex (12-nm wide $\times$ 8-nm tall) could crowd and eliminate the inhibiting signals near the triggering site.

4.5 Conclusion

Phase transitions are associated with exchange of energy such as crystallization separation [70]. These experiments reveal a non-equilibrium metamorphosis of the TCR upon

activation. In this regard, the $\alpha\beta$TCR is a squat but wide multi-subunit protein complex composed of a disulfide-linked TCR$\alpha\beta$ heterodimer flanked by three sets of non-covalently associated dimeric CD3 subunits: the CD3$\varepsilon\gamma$ and the CD3$\varepsilon\delta$ heterodimers and the CD3$\zeta\zeta$ homodimer [7, 8, 9, 10]. Energizing this receptor system transforms the well-organized complex topology to one that extends the centrally disposed TCR$\alpha\beta$ heterodimer, mandating additional force-directed alterations of CD3 dimers that may trigger new associations/dissociations as well as dissociations yet to be defined and inducing dissociations of negatively charged vicinal phospholipids, as a consequence releasing initiates motility, activates neighboring TCRs and likely releases positively charge tails of CD3 molecules to expose ITAM domains for phosphorylation [47, 52]. These molecular redistribution happening in a long-range not only guarantee recruitment of more TCRs but also for obviating the accumulation of CD45 molecules near the triggering site. Such blossoming changes in the organization are akin to a cellular phase transition (reviewed in [71]) where a solid-like well-organized crystalline system is fluidized and reconfigured as mechanical programs drive formation of structures such as the immune synapse.

4.6 Methods

Cell experiments are identical to Chapter 2&3. Anti-CD45 mAb (clone type: 30-F11, Biolegend) coated bead used here was made based on the method in the Chapter 3. The synthesis of 3500 bps DNA handle with biotin at one end and NH_2 at the other end and then fabrication with cleaved half-anti TCR Vβ at the NH_2 end by sulfo-SMCC are detailed in Chapter 2. The two-bead experiment was elaborated in Chapter 3 and procedures of T cell activation by single tether are similar to the SMSC experiment in Chapter 2.

4.7 Acknowledgements

I gratefully acknowledge Dr. Derin Keskin for technical assistance with early IL-2 screening, Dr. Kristine Brazin for making and purifying the cells, the Jimmy Fund Flow

Cytometry Facility for flow cytometry, and the DFCI Center for Cancer Computational Biology for RNA-seq sequencing. This work is supported by NIH grants PO1 GM047467 to GW and ELR, AI037581 to GW, and R56 AI138489 and R01AI100643 to ELR and MJL. Funding is also provided by the FWF project J3872-B21 to AB, and NSF DMR 1157490 and NHMFL UCGP 5080 grants to LS, NIH Grants R01AI100643, R01AI37581, P01GM047467 and SU2C-AACR-DT13-14 from the SU2C-Farrah Fawcett Foundation. I also thank Sonia K. Brady for helpful discussions and Rebecca E. Hussey for technical assistance.

4.8 Bibliography

[1] Dibyendu Kumar Das, Yinnian Feng, Robert J Mallis, Xiaolong Li, Derin B Keskin, Rebecca E Hussey, Sonia K Brady, Jia-Huai Wang, Gerhard Wagner, Ellis L Reinherz, et al. Force-dependent transition in the T-cell receptor β-subunit allosterically regulates peptide discrimination and pMHC bond lifetime. *Proceedings of the National Academy of Sciences*, 112(5):1517–1522, 2015.

[2] Dibyendu Kumar Das, Robert J Mallis, Jonathan S Duke-Cohan, Rebecca E Hussey, Paul W Tetteh, Mark Hilton, Gerhard Wagner, Matthew J Lang, and Ellis L Reinherz. Pre-T cell receptors (Pre-TCRs) leverage vβ complementarity determining regions (CDRs) and hydrophobic patch in mechanosensing thymic self-ligands. *Journal of Biological Chemistry*, 291(49):25292–25305, 2016.

[3] Sun Taek Kim, Koh Takeuchi, Zhen-Yu J Sun, Maki Touma, Carlos E Castro, Amr Fahmy, Matthew J Lang, Gerhard Wagner, and Ellis L Reinherz. The $\alpha\beta$ T cell receptor is an anisotropic mechanosensor. *Journal of Biological Chemistry*, 284(45):31028–31037, 2009.

[4] Baoyu Liu, Wei Chen, Brian D Evavold, and Cheng Zhu. Accumulation of dynamic catch bonds between TCR and agonist peptide-MHC triggers T cell signaling. *Cell*, 157(2):357–368, 2014.

[5] Robert J Mallis, Ke Bai, Haribabu Arthanari, Rebecca E Hussey, Maris Handley, Zhenhai Li, Loice Chingozha, Jonathan S Duke-Cohan, Hang Lu, Jia-Huai Wang, et al. Pre-TCR ligand binding impacts thymocyte development before $\alpha\beta$TCR expression. *Proceedings of the National Academy of Sciences*, 112(27):8373–8378, 2015.

[6] Yinnian Feng, Kristine N Brazin, Eiji Kobayashi, Robert J Mallis, Ellis L Reinherz,

and Matthew J Lang. Mechanosensing drives acuity of $\alpha\beta$ T-cell recognition. *Proceedings of the National Academy of Sciences*, page 201703559, 2017.

[7] HC Oettgen and C Terhorst. A review of the structure and function of the T-cell receptor-T3 complex. *Critical reviews in immunology*, 7(2):131–167, 1987.

[8] Markus G Rudolph, Robyn L Stanfield, and Ian A Wilson. How TCRs bind MHCs, peptides, and coreceptors. *Annu. Rev. Immunol.*, 24:419–466, 2006.

[9] Jia-huai Wang and Ellis L Reinherz. The structural basis of $\alpha\beta$ t-lineage immune recognition: TCR docking topologies, mechanotransduction, and co-receptor function. *Immunological reviews*, 250(1):102–119, 2012.

[10] Allan M Weissman, Lawrence E Samelson, and Richard D Klausner. A new subunit of the human T-cell antigen receptor complex. *Nature*, 324(6096):480, 1986.

[11] Mark M Davis. T cell receptor gene diversity and selection. *Annual review of biochemistry*, 59(1):475–496, 1990.

[12] Arup K Chakraborty and Arthur Weiss. Insights into the initiation of TCR signaling. *Nature immunology*, 15(9):798, 2014.

[13] Gary W Litman, John P Cannon, Larry J Dishaw, Robert N Haire, Donna D Eason, Jeffrey A Yoder, Jose Hernandez Prada, and David A Ostrov. Immunoglobulin variable regions in molecules exhibiting characteristics of innate and adaptive immune receptors. *Immunologic research*, 38(1-3):294–304, 2007.

[14] Zhen-Yu J Sun, Ki Seok Kim, Gerhard Wagner, and Ellis L Reinherz. Mechanisms contributing to T cell receptor signaling and assembly revealed by the solution structure of an ectodomain fragment of the CD3$\varepsilon\gamma$ heterodimer. *Cell*, 105(7):913–923, 2001.

[15] Zhen-Yu J Sun, Sun Taek Kim, Il Chul Kim, Amr Fahmy, Ellis L Reinherz, and Gerhard Wagner. Solution structure of the CD3$\varepsilon\delta$ ectodomain and comparison with CD3$\varepsilon\gamma$ as a basis for modeling T cell receptor topology and signaling. *Proceedings of the National Academy of Sciences of the United States of America*, 101(48):16867–16872, 2004.

[16] Michael E Birnbaum, Richard Berry, Yu-Shan Hsiao, Zhenjun Chen, Miguel A Shingu-Vazquez, Xiaoling Yu, Deepa Waghray, Suzanne Fischer, James McCluskey, Jamie Rossjohn, et al. Molecular architecture of the $\alpha\beta$ T cell receptor-CD3 complex. *Proceedings of the National Academy of Sciences*, 111(49):17576–17581, 2014.

[17] Identification of the docking site for CD3 on the T cell receptor β chain by solution NMR, author=He, Yanan and Rangarajan, Sneha and Kerzic, Melissa and Luo, Ming and Chen, Yihong and Wang, Qian and Yin, Yiyuan and Workman, Creg J and Vignali, Kate M and Vignali, Dario AA and others, journal=Journal of Biological Chemistry, volume=290, number=32, pages=19796–19805, year=2015, publisher=ASBMB.

[18] Aswin Natarajan, Vidushan Nadarajah, Klara Felsovalyi, Wenjuan Wang, Vivian R Jeyachandran, Riley A Wasson, Timothy Cardozo, Clay Bracken, and Michelle Krogsgaard. Structural model of the extracellular assembly of the TCR-CD3 complex. *Cell reports*, 14(12):2833–2845, 2016.

[19] A Alcover, RA Mariuzza, M Ermonval, and O Acuto. Lysine 271 in the transmembrane domain of the T-cell antigen receptor beta chain is necessary for its assembly with the CD3 complex but not for alpha/beta dimerization. *Journal of Biological Chemistry*, 265(7):4131–4135, 1990.

[20] RS Blumberg, B Alarcon, Jaime Sancho, Francis V McDermott, P Lopez, J Breitmeyer, and C Terhorst. Assembly and function of the T cell antigen receptor. require-

ment of either the lysine or arginine residues in the transmembrane region of the alpha chain. *Journal of Biological Chemistry*, 265(23):14036–14043, 1990.

[21] Matthew E Call, Jason Pyrdol, Martin Wiedmann, and Kai W Wucherpfennig. The organizing principle in the formation of the T cell receptor-CD3 complex. *Cell*, 111(7):967–979, 2002.

[22] Pierre Cosson, Scott P Lankford, Juan S Bonifacino, and Richard D Klausner. Membrane protein association by potential intrarnembrane charge pairs. *Nature*, 351(6325):414, 1991.

[23] C Hall, B Berkhout, B Alarcon, J Sancho, T Wileman, and C Terhorst. Requirements for cell surface expression of the human TCR/CD3 complex in non-T cells. *International Immunology*, 3(4):359–368, 1991.

[24] Nicholas Manolios, Juan S Bonifacino, and Richard D Klausner. Transmembrane helical interactions and the assembly of the T cell receptor complex. *Science*, 249(4966):274–277, 1990.

[25] Nicholas Manolios, Owen Kemp, and Zhan Guo Li. The T cell antigen receptor α and β chains interact via distinct regions with CD3 chains. *European journal of immunology*, 24(1):84–92, 1994.

[26] Matthew E Call, Jason R Schnell, Chenqi Xu, Regina A Lutz, James J Chou, and Kai W Wucherpfennig. The structure of the $\zeta\zeta$ transmembrane dimer reveals features essential for its assembly with the T cell receptor. *Cell*, 127(2):355–368, 2006.

[27] Rebecca J Brownlie and Rose Zamoyska. T cell receptor signalling networks: branched, diversified and bounded. *Nature Reviews Immunology*, 13(4):257, 2013.

[28] Denis R Alexander. The CD45 tyrosine phosphatase: a positive and negative regulator

of immune cell function. In *Seminars in immunology*, volume 12, pages 349–359. Elsevier, 2000.

[29] Nicholas D Huntington and David M Tarlinton. CD45: direct and indirect government of immune regulation. *Immunology letters*, 94(3):167–174, 2004.

[30] Simon J Davis and P Anton van der Merwe. The kinetic-segregation model: TCR triggering and beyond. *Nature immunology*, 7(8):803, 2006.

[31] GR Woollett, AF Williams, and DM Shotton. Visualisation by low-angle shadowing of the leucocyte-common antigen. a major cell surface glycoprotein of lymphocytes. *The EMBO journal*, 4(11):2827–2830, 1985.

[32] MN McCall, DM Shotton, and AN Barclay. Expression of soluble isoforms of rat CD45. analysis by electron microscopy and use in epitope mapping of anti-CD45R monoclonal antibodies. *Immunology*, 76(2):310, 1992.

[33] John R James and Ronald D Vale. Biophysical mechanism of T-cell receptor triggering in a reconstituted system. *Nature*, 487(7405):64, 2012.

[34] Kenneth G Johnson, Shannon K Bromley, Michael L Dustin, and Matthew L Thomas. A supramolecular basis for CD45 tyrosine phosphatase regulation in sustained T cell activation. *Proceedings of the National Academy of Sciences*, 97(18):10138–10143, 2000.

[35] Revathi Ananthakrishnan and Allen Ehrlicher. The forces behind cell movement. *International journal of biological sciences*, 3(5):303, 2007.

[36] Lin Ji, James Lim, and Gaudenz Danuser. Fluctuations of intracellular forces during cell protrusion. *Nature cell biology*, 10(12):1393–1400, 2008.

[37] Xavier Trepat, Michael R Wasserman, Thomas E Angelini, Emil Millet, David A

Weitz, James P Butler, and Jeffrey J Fredberg. Physical forces during collective cell migration. *Nature physics*, 5(6):426–430, 2009.

[38] Zheng Liu, Yang Liu, Yuan Chang, Hamid Reza Seyf, Asegun Henry, Alexa L Mattheyses, Kevin Yehl, Yun Zhang, Zhuangqun Huang, and Khalid Salaita. Nanoscale optomechanical actuators for controlling mechanotransduction in living cells. *nature methods*, 13(2):143, 2016.

[39] Kenneth H. Hu and Manish J. Butte. T cell activation requires force generation. *The Journal of Cell Biology*, 213(5):535–542, 2016.

[40] Julien Husson, Karine Chemin, Armelle Bohineust, Claire Hivroz, and Nelly Henry. Force generation upon T cell receptor engagement. *PLoS One*, 6(5):e19680, 2011.

[41] Ya-Chen Li, Bing-Mae Chen, Pei-Chun Wu, Tian-Lu Cheng, Lung-Sen Kao, Mi-Hua Tao, Andre Lieber, and Steve R. Roffler. Cutting edge: Mechanical forces acting on T cells immobilized via the TCR complex can trigger TCR signaling. *The Journal of Immunology*, 184(11):5959–5963, 2010.

[42] Michal Baniyash, Moshe Sade-Feldman, and Julia Kanterman. Chronic inflammation and cancer: suppressing the suppressors. *Cancer immunology, immunotherapy*, 63(1):11–20, 2014.

[43] Philip P Ostrowski, Sergio Grinstein, and Spencer A Freeman. Diffusion barriers, mechanical forces, and the biophysics of phagocytosis. *Developmental cell*, 38(2):135–146, 2016.

[44] Ulrich Dammer, Martin Hegner, Dario Anselmetti, Peter Wagner, Markus Dreier, Walter Huber, and Hans-Joachim Güntherodt. Specific antigen/antibody interactions measured by force microscopy. *Biophysical journal*, 70(5):2437–2441, 1996.

[45] Kristine N Brazin, Robert J Mallis, Chen Li, Derin B Keskin, Haribabu Arthanari, Yuanwei Gao, Shiaw-Lin Wu, Barry L Karger, Gerhard Wagner, and Ellis L Reinherz. Constitutively oxidized CXXC motifs within the CD3 heterodimeric ectodomains of the T cell receptor complex enforce the conformation of juxtaposed segments. *Journal of Biological Chemistry*, 289(27):18880–18892, 2014.

[46] B Thomas Bäckström, Urs Müller, Barbara Hausmann, and Ed Palmer. Positive selection through a motif in the $\alpha\beta$ T cell receptor. *Science*, 281(5378):835–838, 1998.

[47] Kristine N Brazin, Robert J Mallis, Dibyendu Kumar Das, Yinnian Feng, Wonmuk Hwang, Jia-huai Wang, Gerhard Wagner, Matthew J Lang, and Ellis L Reinherz. Structural features of the $\alpha\beta$TCR mechanotransduction apparatus that promote pMHC discrimination. *Frontiers in immunology*, 6:441, 2015.

[48] Steve Caplan, Shlomit Zeliger, Lynn Wang, and MicHAL Baniyash. Cell-surface-expressed T-cell antigen-receptor zeta chain is associated with the cytoskeleton. *Proceedings of the National Academy of Sciences*, 92(11):4768–4772, 1995.

[49] Andriy Anishkin and Ching Kung. Stiffened lipid platforms at molecular force foci. *Proceedings of the National Academy of Sciences*, 110(13):4886–4892, 2013.

[50] Etienne Gagnon, David A Schubert, Susana Gordo, H Hamlet Chu, and Kai W Wucherpfennig. Local changes in lipid environment of TCR microclusters regulate membrane binding by the CD3ε cytoplasmic domain. *Journal of Experimental Medicine*, 209(13):2423–2439, 2012.

[51] Dikran Aivazian and Lawrence J Stern. Phosphorylation of T cell receptor ζ is regulated by a lipid dependent folding transition. *Nature Structural and Molecular Biology*, 7(11):1023, 2000.

[52] Chenqi Xu, Etienne Gagnon, Matthew E Call, Jason R Schnell, Charles D Schwieters, Christopher V Carman, James J Chou, and Kai W Wucherpfennig. Regulation of

T cell receptor activation by dynamic membrane binding of the CD3ε cytoplasmic tyrosine-based motif. *Cell*, 135(4):702–713, 2008.

[53] Stefan C Meuer, David A Cooper, James C Hodgdon, Rebecca E Hussey, Kathleen A Fitzgerald, Stuart F Schlossman, and Ellis L Reinherz. Identification of the receptor for antigen and major histocompatibility complex on human inducer T lymphocytes. *Science*, 222(4629):1239–1242, 1983.

[54] Kerri A Mowen and Michael David. Unconventional post-translational modifications in immunological signaling. *Nature immunology*, 15(6):512, 2014.

[55] Linda M Wakim and Michael J Bevan. Cross-dressed dendritic cells drive memory CD8+ T-cell activation after viral infection. *Nature*, 471(7340):629, 2011.

[56] Arup K Chakraborty and Jayajit Das. Pairing computation with experimentation: a powerful coupling for understanding T cell signalling. *Nature Reviews Immunology*, 10(1):59, 2010.

[57] Rajat Varma, Gabriele Campi, Tadashi Yokosuka, Takashi Saito, and Michael L Dustin. T cell receptor-proximal signals are sustained in peripheral microclusters and terminated in the central supramolecular activation cluster. *Immunity*, 25(1):117–127, 2006.

[58] Joseph Lin and Arthur Weiss. The tyrosine phosphatase CD148 is excluded from the immunologic synapse and down-regulates prolonged T cell signaling. *The Journal of cell biology*, 162(4):673–682, 2003.

[59] Claudine Irles, Antony Symons, Frédérique Michel, Talitha R Bakker, P Anton van der Merwe, and Oreste Acuto. CD45 ectodomain controls interaction with GEMs and Lck activity for optimal TCR signaling. *Nature immunology*, 4(2):189, 2003.

[60] Kaushik Choudhuri, Mathew Parker, Anita Milicic, David K Cole, Michael K Shaw, Andrew K Sewell, Guillaume Stewart-Jones, Tao Dong, Keith G Gould, and P Anton van der Merwe. Peptide-major histocompatibility complex dimensions control proximal kinase-phosphatase balance during T cell activation. *Journal of Biological Chemistry*, 284(38):26096–26105, 2009.

[61] Kaushik Choudhuri, David Wiseman, Marion H Brown, Keith Gould, and P Anton van der Merwe. T-cell receptor triggering is critically dependent on the dimensions of its peptide-MHC ligand. *Nature*, 436(7050):578, 2005.

[62] TD Geppert and P Ei Lipsky. Accessory cell independent proliferation of human T4 cells stimulated by immobilized monoclonal antibodies to CD3. *The Journal of Immunology*, 138(6):1660–1666, 1987.

[63] Zhengyu Ma, Kim A Sharp, Paul A Janmey, and Terri H Finkel. Surface-anchored monomeric agonist pMHCs alone trigger TCR with high sensitivity. *PLoS biology*, 6(2):e43, 2008.

[64] Claudia Bluemel, Susanne Hausmann, Petra Fluhr, Mirnalini Sriskandarajah, William B Stallcup, Patrick A Baeuerle, and Peter Kufer. Epitope distance to the target cell membrane and antigen size determine the potency of T cell-mediated lysis by BiTE antibodies specific for a large melanoma surface antigen. *Cancer immunology, immunotherapy*, 59(8):1197–1209, 2010.

[65] Scott E James, Philip D Greenberg, Michael C Jensen, Yukang Lin, Jinjuan Wang, Brian G Till, Andrew A Raubitschek, Stephen J Forman, and Oliver W Press. Antigen sensitivity of CD22-specific chimeric TCR is modulated by target epitope distance from the cell membrane. *The Journal of Immunology*, 180(10):7028–7038, 2008.

[66] Zhengyu Ma, Paul A Janmey, and Terri H Finkel. The receptor deformation model of TCR triggering. *The FASEB Journal*, 22(4):1002–1008, 2008.

[67] Jennifer R Cochran, Thomas O Cameron, Jennifer D Stone, Jodi B Lubetsky, and Lawrence J Stern. Receptor proximity, not intermolecular orientation, is critical for triggering T-cell activation. *Journal of Biological Chemistry*, 276(30):28068–28074, 2001.

[68] Jun Huang, Mario Brameshuber, Xun Zeng, Jianming Xie, Qi-jing Li, Yueh-hsiu Chien, Salvatore Valitutti, and Mark M Davis. A single peptide-major histocompatibility complex ligand triggers digital cytokine secretion in CD4+ T cells. *Immunity*, 39(5):846–857, 2013.

[69] Veronica T Chang, Ricardo A Fernandes, Kristina A Ganzinger, Steven F Lee, Christian Siebold, James McColl, Peter Jönsson, Matthieu Palayret, Karl Harlos, Charlotte H Coles, et al. Initiation of T cell signaling by CD45 segregation at 'close contacts'. *Nature immunology*, 17(5):574, 2016.

[70] John William Mullin. *Crystallization*. Elsevier, 2001.

[71] Yongdae Shin and Clifford P Brangwynne. Liquid phase condensation in cell physiology and disease. *Science*, 357(6357):eaaf4382, 2017.

CHAPTER 5

CONCLUSIONS AND FUTURE WORK

*Section about CARs and future works in this chapter are adapted from Yinnian Feng, Ellis L. Reinherz, and Matthew J. Lang, "$\alpha\beta$ TCR mechanosensing forces out serial engagement" under review.

The ultra-high sensitivity and specificity of $\alpha\beta$TCR recognition determines the precise operation of immune system. Since the signaling cascade starts from the TCR-pMHC ligation, many TCR triggering models have been proposed from the molecular perspective besides serial engagement model, involving TCR aggregation, conformation change, kinetic proofreading with synergy of coreceptor, signaling amplification by endogenous pMHC, TCR-mediated Lck activation, ITAM sequestration and kinetic segregation (reviewed in [1, 2]). Artificial aggregation of TCR by pMHC tetramer or antibody is sufficient for triggering the cascade , but low density of pMHC on APC casts doubt on this model physiologically. Crystallography studies to date have provided some controversial evidences for conformational change upon pMHC ligation, thus still suffering issue of authenticity [1]. Kinetic proofreading and signaling amplification by endogenous pMHC were suggested based on the intermediate off-rate difference between agonist-pMHC and self-pMHC measured by biacore kinetics, recent OT and BFP experiment, however, clearly shows the amplification of such difference by mechanical force [3, 4]. Specific force-loaded TCR-pMHC ligation can sustain their catch bond linkage even at 2 interactions/interface for a long time, such that consecutive mechanical work stored by TCR structural transition can be transduced to the CD3 complexes then generate the their phase transition, pushing the equilibrium system to a non-equilibrium stage with the help of underlying cytoskeletal motors. The surrounded adhesion molecule could also assist TCR-pMHC at single molecule level, thus one pMHC may be enough to activate the T cell [5]. Helps from endogenous pMHC

are doubtful, as bead coated with L4/K^b shows immediate bond rupture and no triggering at physiological density (29 L4/K^b at interface). The TCR mechanosensing model clearly shows the presentation, reception, transmission and transduction manners of TCR, exclude the models (TCR-mediated Lck activation and ITAM sequestration) that only consider it as a digital switch. The ITAM sequestration may happen after receiving the energy, similar to a spring relay. Kinetic segregation has been popular and seems to be required and it has been observed even in a reconstituted system [6], the size-exclusion could be alternatively induced by passive transport of longer phosphatases [7], and reducing their length causes decrease of molecular weight will alter the diffusion rate. On the other side, elongation of pMHC on APC could buffer the force generated from the T-cell crawling and/or retrograde so that T-cell activation could be hindered by no mechanosensing. Moreover, from the molecular side, compared to wt T cell with 2 pMHCs at the interface, H57 Fab treated T cell only shows transient Ca^{2+} flux with high load, but with the identical properties such as interacting area and molecular size difference between TCR and phosphatases. All the clues mentioned above make kinetic segregation as an amplification factor of TCR triggering, not the initiator. A recent intriguing work publish by Taylor et al. have also indicated the involvement of mechanical force during the TCR triggering [8]. The DNA based chimeric TCR complex can sense force generated during hybridization [9], although the authors seem to focus more on discrimination and TCR clustering. From our perspective, thus, mechanosensing model provides fidelity to explain intensive investigation we have been observed.

In this dissertation, the whole T-cell mechanome for early T-cell activation has been investigated. Here we list the novelty of the thesis as follows:

1. The mechanical works exerted at the TCR$\alpha\beta$/pMHC interface are able to be transduced into the TCR$\alpha\beta$ transmembrane domain through the energized reversible structural transitions preserved by FG loop in TCR constant β domain.

2. The works (100-150 pN·nm) would facilitate the allosteric change of the TCRα cy-

toplasmic tail from a "L" shape to a extended state, favoring the the rearrangement of local CD3 complex and finally release the membrane associated ITAM regions into cytoplasm to initiate the phosphorylation cascade.

3. Certain amount of CD45 inhibitors ($\geq$ 4000 interficial copy numbers) presented close to the pMHC bead-T cell stimulation site ($\leq$ ~4 μm apart) could deactivate the phosphorylation reaction. Thus, the long-range CD45 diffusion away from the triggering site is crucial for sustaining the T-cell activation.

4. T cell uses the underlying active motor system to transport pMHC-unligated TCRs into the triggering site so that the crowded and clustered TCRs would squeeze out the CD45 inhibitors, a phenomenon akin to the crystallization purification.

5. The motor system also synergizes with the external forces loaded by microvilli protrusion or general T-cell immunosurveillance in order to balance the trigger in a optimal window, where sustained and reversible TCR structural transitions may happen.

The contributions of the author are also listed below:

1. The author at first has performed a novel single molecule on single cell (SMSC) assay that proves the catch bond phenomenon within the interaction of TCR and agonist pMHC as well as the functions of CD8 coreceptor and FG loop in stabilizing such interaction.

2. Using the single cell (SC) activation assay, the author has investigated the physiochemical threshold of the TCR triggering as well as the active motor transport system underlying the TCR. Thus, a synergistic mechanosensing model based on nonequilibrium is proposed to explain the acuity of T-cell recognition. This model rules out the possibility of TCR serial engagement (either the traditional or repetitive force facilitated version) in the early T-cell activation.

3. The two-bead assay the author has built may reveal the traffic network for transportation of pMHC unligated TCRs to the triggering site by motor system.

4. With the advantage of SMSC and SC assays, the author has shown the importance of Arg251 to sustain the reversible transitions of TCRα cytoplasmic tail that favors the CD3 complex rearrangement.

5. Again, using the two-bead assay and the DNA tether technology, the author has shown that CD45 molecules as T-cell activation inhibitors will segregate away from the T cell/APC contact area where TCRs are accumulated.

In a nutshell, the T cell functions as a precise mechanosensing machine, in which the optimal mechanical force (both in magnitude and direction) loaded on the TCR$\alpha\beta$ facilitates the peptide discrimination, TCR$\alpha\beta$ and CD3 conformational changes, early T-cell activation (Ca_{2+} flux), active $\alpha\beta$TCR transport by motor system, and long-range CD45 segregation.

In this regard, it is noteworthy that chimeric antigen receptors (CARs) are recombinant proteins transduced into T cells with ligand binding activity distinct from the TCR, often employing a scFv ectodomain, a CP linker and TM segment unrelated to $\alpha\beta$TCR components and a cytoplasmic tail consisting of an amalgam of CD3$\zeta\zeta$ and one or more costimulatory receptor domains [10]. In these constructs CD3$\zeta\zeta$ is separated from TCR subunits. Given that the TM segment is not TCR-related, the lipid associations are likely distinct from the raft localized $\alpha\beta$TCR components. While CARs do not form associations with endogenous TCRs in CAR-T cells, their ligation to targets induces cellular cytolytic activity and cytokine production, presumably by force-dependent release of ITAMs akin to the normal physiology described above. It is noteworthy that $\alpha\beta$TCR triggering is anisotropic, so that direction of force application by pMHC or anti-CD3 mAb determines cellular activation potential [11, 12]. The same must apply for CAR-T cell ligand binding and force transduction through the CAR ectodomain, linker region and TM. Therefore,

nuancing of the molecular design of CARs based on evolving principles of mechanotransduction and dissociative $\alpha\beta$TCR complex activation should help to extend the number of targets amenable to this immunotherapy. Although this dissertation here has systematically investigated the TCR triggering from single molecule to the single cell level, it is worth pointing out that there are still lot of undiscovered areas, as listed below to enlighten the future works:

1. Is the TCR-pMHC bond lifetime force curve a key indicator of TCR quality linked to protective biology as opposed to conventionally measured functional avidity or tetramer staining?

2. From the molecular perspective, how does force-dependent transition in the TCR$\alpha\beta$ heterodimer influence the quaternary structure of the $\alpha\beta$TCR complex and conformations of the CD3 cytoplasmic domains to initiate signaling?

3. What is the structure of the extended and force-loaded relative to the compact and unloaded $\alpha\beta$TCR complex?

4. Can adhesion molecules stabilize a single TCR-pMHC bond to facilitate the T-cell activation in a digital manner? What is the precise molecular identification of the biochemistry, physiology and associated protein interactions of the motor protein activated by TCR-pMHC bond formation?

5. On the APC side, how does viscoelasticity of the pMHC embedded in the membrane affect the TCR mechanosensing and force-induced T-cell activation?

6. Is this altered when dendritic cells go from an immature to a mature state?

7. How does the mechanical force applied on the TCR-pMHC interface initiate the actomyosin activity?

5.1 Bibliography

[1] Arup K Chakraborty and Arthur Weiss. Insights into the initiation of TCR signaling. *Nature immunology*, 15(9):798, 2014.

[2] P Anton Van Der Merwe and Omer Dushek. Mechanisms for T cell receptor triggering. *Nature Reviews Immunology*, 11(1):47, 2011.

[3] Dibyendu Kumar Das, Yinnian Feng, Robert J Mallis, Xiaolong Li, Derin B Keskin, Rebecca E Hussey, Sonia K Brady, Jia-Huai Wang, Gerhard Wagner, Ellis L Reinherz, et al. Force-dependent transition in the T-cell receptor β-subunit allosterically regulates peptide discrimination and pMHC bond lifetime. *Proceedings of the National Academy of Sciences*, 112(5):1517–1522, 2015.

[4] Baoyu Liu, Wei Chen, Brian D Evavold, and Cheng Zhu. Accumulation of dynamic catch bonds between TCR and agonist peptide-MHC triggers T cell signaling. *Cell*, 157(2):357–368, 2014.

[5] Jun Huang, Mario Brameshuber, Xun Zeng, Jianming Xie, Qi-jing Li, Yueh-hsiu Chien, Salvatore Valitutti, and Mark M Davis. A single peptide-major histocompatibility complex ligand triggers digital cytokine secretion in CD4+ T cells. *Immunity*, 39(5):846–857, 2013.

[6] John R James and Ronald D Vale. Biophysical mechanism of T-cell receptor triggering in a reconstituted system. *Nature*, 487(7405):64, 2012.

[7] Eva M Schmid, Matthew H Bakalar, Kaushik Choudhuri, Julian Weichsel, Hyoung Sook Ann, Phillip L Geissler, Michael L Dustin, and Daniel A Fletcher. Size-dependent protein segregation at membrane interfaces. *Nature physics*, 12(7):704, 2016.

[8] Marcus J Taylor, Kabir Husain, Zev J Gartner, Satyajit Mayor, and Ronald D Vale. A DNA-based T cell receptor reveals a role for receptor clustering in ligand discrimination. *Cell*, 169(1):108–119, 2017.

[9] Mukta Singh-Zocchi, Sanhita Dixit, Vassili Ivanov, and Giovanni Zocchi. Single-molecule detection of DNA hybridization. *Proceedings of the National Academy of Sciences*, 100(13):7605–7610, 2003.

[10] Jessica Hartmann, Martina Schüßler-Lenz, Attilio Bondanza, and Christian J Buchholz. Clinical development of car T cellschallenges and opportunities in translating innovative treatment concepts. *EMBO molecular medicine*, page e201607485, 2017.

[11] Yinnian Feng, Kristine N Brazin, Eiji Kobayashi, Robert J Mallis, Ellis L Reinherz, and Matthew J Lang. Mechanosensing drives acuity of $\alpha\beta$ T-cell recognition. *Proceedings of the National Academy of Sciences*, page 201703559, 2017.

[12] Sun Taek Kim, Koh Takeuchi, Zhen-Yu J Sun, Maki Touma, Carlos E Castro, Amr Fahmy, Matthew J Lang, Gerhard Wagner, and Ellis L Reinherz. The $\alpha\beta$ T cell receptor is an anisotropic mechanosensor. *Journal of Biological Chemistry*, 284(45):31028–31037, 2009.

APPENDIX A

PROTOCOLS

A.1 Medium/Buffer Recipes

1. Complete DMEM Medium
   To be used in cell culturing of BW5147 cell line in Chapter 3 and 4

   Materials:
   High glucose DMEM medium
   fetal bovine serum (FBS)
   100 U/ml penicillin and streptomycin
   2 mM glutamine
   1% (v/v) Non-essential amino acid
   0.1% (v/v) 2-mercaptoethanol

   (a) Prepare 125 mL of Complete DMEM Medium by mixing:
   96.125 ml DMEM
   25 mL FBS
   1.25 ml penicillin and streptomycin
   1.25 ml glutamine
   1.25 ml Non-essential amino acid
   0.125 ml 2-mercaptoethanol

   (b) Add the above mixture to the Corning Disposable Sterile Filter Systems and then do the vacuum facilitated filtration.

2. Selective Complete DMEM Medium
   To be used in cell culturing of BW5147 cell line in Chapter 3 and 4

   Materials:
   High glucose DMEM medium
   fetal bovine serum (FBS)
   100 U/ml penicillin and streptomycin
   2 mM glutamine
   500 μg/ml G418
   500 μg/ml Hygromycin B
   1% (v/v) Non-essential amino acid

0.1% (v/v) 2-mercaptoethanol

(a) Prepare 125 mL of Complete DMEM Medium by mixing:
93.625 ml DMEM
25 mL FBS
1.25 ml penicillin and streptomycin
1.25 ml glutamine
1.25 ml G418
1.25 ml Hygromycin B
1.25 ml Non-essential amino acid
0.125 ml 2-mercaptoethanol

(b) Add the above mixture to the Corning Disposable Sterile Filter Systems and then do the vacuum facilitated filtration.

3. DMEM colorless Medium
To be used in cell activation and bond lifetime measurement of BW5147 cell line in Chapter 3 and 4

Materials:
Colorless DMEM Medium
100 U/ml penicillin and streptomycin
2 mM glutamine
1% (v/v) Non-essential amino acid

(a) Prepare 50 mL of DMEM colorless Medium by mixing:
48.5 ml DMEM
0.5 ml penicillin and streptomycin
0.5 ml glutamine
0.5 Non-essential amino acid

(b) Add the above mixture to the Corning Disposable Sterile Filter Systems and then do the vacuum facilitated filtration. Remember never add the 2-mercaptoethanol inside this medium, the 2-mercaptoethanol will reduce the disulfide bond and antibodies.

4. Complete RMPI 1640 Medium
To be used in cell culturing of 58 cell line in Chapter 2 and naïve cell in Chapter 3

Materials:
RPMI 1640

fetal bovine serum (FBS)
100 U/ml penicillin and streptomycin
2 mM glutamine
and 0.1% (v/v) 2-mercaptoethanol

(a) Prepare 125 mL of Complete RPMI 1640 Medium by mixing:
108.625 ml RPMI 1640
12.5 mL FBS
1.25 ml penicillin and streptomycin
1.25 ml glutamine
1.25 ml Non-essential amino acid
0.125 ml 2-mercaptoethanol

(b) Add the above mixture to the Corning Disposable Sterile Filter Systems and then do the vacuum facilitated filtration.

5. Selective Complete RMPI 1640 Medium
To be used in cell culturing of 58 cell line in Chapter 2 and naïve cell in Chapter 3

Materials:
RPMI 1640
fetal bovine serum (FBS)
100 U/ml penicillin and streptomycin
2 mM glutamine
500 μg/ml G418
500 μg/ml Hygromycin B
1% (v/v) Non-essential amino acid
and 0.1% (v/v) 2-mercaptoethanol

(a) Prepare 125 mL of Complete DMEM Medium by mixing:
106.125 ml RPMI 1640
12.5 mL FBS
1.25 ml penicillin and streptomycin
1.25 ml glutamine
1.25 ml G418
1.25 ml Hygromycin B
1.25 ml Non-essential amino acid
0.125 ml 2-mercaptoethanol

(b) Add the above mixture to the Corning Disposable Sterile Filter Systems and then do the vacuum facilitated filtration.

6. RPMI 1640 colorless Medium
   To be used in bond lifetime measurement of 58 cell line in Chapter 2 and cell activation of naïve cell in Chapter 3

   Materials:
   Colorless DMEM Medium
   100 U/ml penicillin and streptomycin
   2 mM glutamine
   1% (v/v) Non-essential amino acid

   (a) Prepare 50 mL of DMEM colorless Medium by mixing:
   48.5 ml DMEM
   0.5 ml penicillin and streptomycin
   0.5 ml glutamine
   0.5 Non-essential amino acid

   (b) Add the above mixture to the Corning Disposable Sterile Filter Systems and then do the vacuum facilitated filtration. Remember never add the 2-mercaptoethanol inside this medium, the 2-mercaptoethanol will reduce the disulfide bond and antibodies.

7. 0.1 M MES buffer with 0.01% tween-20, pH 4.5
   To be used in the preparation of anti-DIG beads using EDC chemistry.

   Materials:
   MES
   Tween-20

   (a) Prepare 100 mL of buffer by mixing the following:
   1.95 mg MES
   10 μL Tween-20 deionized water up to 100 mL total volume
   (b) pH adjust the solution to 4.5.

8. 0.1 M borate buffer, pH 8.5
   To be used in the preparation of anti-DIG beads using EDC chemistry.

   Materials:
   Boric Acid
   Deionized water

(a) Prepare 100 mL of buffer by mixing the following:
0.618 g boric acid
deionized water up to 100 mL total volume

(b) pH adjust the solution to 8.5 using NaOH.

9. reaction buffer, pH 7.5-8.0
To be used in the preparation of half-antibody.

Materials:
1X PBS
EDTA

(a) Prepare 100 mL of buffer by mixing the following:
292.24 mg EDTA
1X PBS up to 100 mL total volume

(b) pH adjust the solution to 7.5-8.0 using 1M NaOH.

A.2 anti-DIG functionalized beads by EDC chemistry

This protocol is slightly adapted from a protocol developed by Marie Eve Aubin-Tam, a former post-doctoral researcher in the lab.

Materials:
MES buffer with 0.01% tween-20 (pH = 4.5)
Borate buffer with 0.01% tween-20 (pH 8.5)
PBST (1X PBS with 0.01% tween-20)(pH 7.4)
Carboxy polystyrene beads (0.99 μm)
EDC crosslinker
anti-Dig polyclone antibody
BSA
Ethanolamine
Cup sonicator
Rotator
Microcentrifuge

1. Make MES (0.1 M), borate (0.1 M, pH 8.5), and PBST (pH 7.4) buffers according to the recipes in section A.1.
2. Mix 100 μL of 1 μm carboxy polystyrene beads with 100 μL of MES buffer.
3. Spin down (12000 rpm for 2 minutes) and resuspend in 200 μL MES buffer (repeat 5x).
4. Sonicate using a cup sonicator for 4 minutes at 40% with ice.
5. Add 200 μL of freshly made EDC solution 2% w/v (corresponds to 10 mg EDC in 500 μL MES buffer).
6. Incubate the bead mixture for 3.5 hours at room temperature on a rotator.
7. Spin down (12000 rpm for 2 minutes) and resuspend the bead mixture in 1 mL of borate buffer.
8. Spin down (12000 rpm for 2 minutes) and resuspend the bead mixture in 400 μL of borate buffer.
9. Sonicate using a cup sonicator for 3 minutes at 40% with ice.
10. Add 80 μL of 200 μg mL^{-1} anti-DIG in borate buffer.
11. Rotate overnight at 4°C.
12. Stop the reaction by adding 10 μL of 0.25 M ethanolamine (0.25 M solution of ethanolamine corresponds to 10 μL ethanolamine + 650 μL borate buffer).

13. Incubate and mix the bead mixture on at rotator for 30 minutes at 4°C.
14. Spin down the beads (12000 rpm for 2 minutes) and resuspend in 400 μL of PBST buffer.
15. Sonicate the bead mixture in a cup sonicator for 1 minute at 25% with ice.
16. Store the beads at 4°C and rotating gently.

A.3 anti-DIG functionalized beads by protein G method

This protocol is slightly adapted from a protocol developed by Marie Eve Aubin-Tam, a former post-doctoral researcher in the lab.

Materials:
1X PBS (pH = 7.5)
PBST (1X PBS with 0.01% tween-20)(pH 7.4)
Protein G coated beads (0.89 μm)
anti-Dig polyclone antibody
DMSO
Ethanolamine
Cup sonicator
Rotator
Microcentrifuge

1. Pipette 25 μL of bead slurry into a 1.6 mL microcentrifuge tube.
2. Wash the beads with 500 μL PBST (repeat 2x).
3. Resuspend the bead in the 100 μL 1X PBS buffer.
4. Sonicate using a cup sonicator for 3 minutes at 30% with ice.
5. Add 80 μL of 200 μg mL^{-1} anti-DIG in the bead slurry.
6. Allow antibody to bind to beads for 1 h at RT with continuous mixing.
7. After 1 h, wash the beads by adding 500 μl PBST (repeat 3x)
8. Prepare a fresh made 100 mM DSS solution by weighting out 2 mg of DSS and dissolving in 54 μl DMSO.
9. Once dissolved, dilute to 5 mM by adding 646 μl 1X PBS buffer. (Solution becomes cloudy.)
10. Add 250 μl of 5 mM DSS solution to the bead slurry.
11. Sonicate the slurry 2 min at 20% and incubate with end-over-end mixing for 1h at room temperature.
12. Stop the reaction by adding 250 μL of 50 mM ethanolamine in PBS and incubate for 30 mins at room temperature with end-over-end mixing.
13. Wash with 500 μl PBST (repeat 3x) and put the tube in 4 ^{o}C with end-over-end mixing. *Note: The protein G bead used here can guarantee that the orientation of all the coated anti-DIG antibody molecules are point outward whereas anti-DIG bead made by EDC chemistry can not. You need to pay attention to the affinity between*

the antibody you use and protein G. There are other protein A and protein L coated bead for antibodies from different animal species. The anti-DIG antibody used in this protocol is from goat so its affinity to protein G is high.

A.4 pMHC coated bead

This protocol can be applied to VSV8/K^b, L4/K^b, SEV9/K^b, VSV8/$K^b{}_m$, NP366/$D^b{}_m$, biotin labeled half anti-TCRVβ, biotin labeled anti-CD45, biotin labeled 17A2 coated bead in Chapter 3 and 4.

Materials:
PBST (1X PBS with 0.01% tween-20)(pH 7.4)
Streatavidin coated beads (1.09 μm)
pMHC (from Ellis lab or NIH tetramer core)
biotin-BSA
Cup sonicator
Rotator
Microcentrifuge

1. Pipette 5 μL of bead slurry into a 0.6 mL microcentrifuge tube.
2. Wash the beads with 100 μL PBST (repeat 3x).
3. Sonicate using a cup sonicator for 2 minutes at 20%.
4. Resuspend the bead in the 5 μL PBST buffer.
5. Add certain amount of pMHC solution in to the bead slurry and rotate for 1h at room temperature.
6. After 1 h, wash the beads by adding 100 μl PBST (repeat 3x)
7. For T-cell triggering, bead surfaces were blocked by adding 5 mg/ml 20 μl biotin-BSA in the pMHC coated bead slurry.
8. Rotate for 1 h at room temperature and then wash three times by 100 μl PBST. The BSA on the bead surface eliminates potential non-specific binding of the bead to the cell membrane.
9. Resuspend in 100 μl PBST. Each time take ~0.7 μl for experiment.

A.5 PCR Protocol for Phusion

This protocol can be applied to make DNA with certain length based on M13M18 plasmid in Chapter 3 and 4.

Materials:
TE buffer (pH=8.0)
20μM forward primer
20μM backward primer
25 mM dNTPs in dd water
50 ng/μL M13mp18 plasmid (in TE buffer)
5X GC buffer
dd water
Phusion polymerase
PCR machine

Prepare 100 μL of solution by mixing:
25 μL of 20uM forward primer
25 μL of 20uM backward primer
8 μL of 25 mM dNTPs
5 μL of 50 ng/μL M13M18 plasmid
200 μL of 5X GC buffer
10 μL Phusion polymerase
727 μL dd water
Put 100 μL of that solution in 10 tubes and follow the Phusion procedure:

1. 98 ^{o}C during 30 sec
2. 98 ^{o}C during 10 sec
3. 49 ^{o}C during 30 sec
4. 72 ^{o}C during 90 sec
5. repeat steps 2-3-4 for a total of 35X
6. 72 ^{o}C during 10 min
7. keep at 4 ^{o}C
8. Then you purify with the Qiagen kit.

A.6 DNA gel electrophoresis

This protocol will allow determination of DNA length and quality by running the DNA out on an agarose gel. This is useful to check products made using the protocol in PCR Phusion.

Materials:
10 mM TE buffer (pH = 7.5)
5X TBE buffer
6X gel loading buffer
1 kB ds DNA ladder mixture (200uL 6X gel loading buffer, 750uL 10mM TE buffer pH 7.5, 50uL stock DNA solution)
Agarose
SybrGreen 10,000X

1. Combine 60 mL 5X TBE buffer with 540 mL of DI water to make 1X TBE.
2. In a 250 mL Erlenmeyer flask combine 0.8 g Agarose with 100 mL 1X TBE buffer and microwave for 4 minutes on High power level (Watch the flask and pause heating if solution begins to boil over.).
3. Allow agarose solution to cool for 4 mins.
4. Add 8 μL of SybrGreen.
5. Prepare electrophoresis chamber for gel pouring and align comb.
6. Pour the agarose solution in the chamber and allow 30 minutes to cool.
7. Rotate the chamber so that the combs are proximal to the cathode (black terminal).
8. Fill the electrophoresis apparatus with the remainder of the 1X TBE buffer (~500 ml).
9. Remove the comb and inspect the well walls.
10. Combine for each PCR sample (1.8 μL PCR sample, 16.2 μL TE buffer, 3 μL 6X gel loading buffer).
11. Add 6 μL of the DNA ladder mixture to the well.
12. Place 16 μL of the PCR sample/loading buffer into a well, repeat for each sample to be run.
13. Replace the gel box cover and begin run at 110V.
14. Run until the marker lines (blue and yellow) near the anode side of the gel (Between 1.5 and 2.5 hs).
15. View bands on Alpha Innotech Fluor Chem 8900 machine.
16. Dispose of the gel in appropriate container.

A.7 Calcium flux assay using flow cytometry protocol

Materials:
2C11(145-2C11) (0.5 mg/ml in PBS+0.02%NaN_3)
DyLight 649 Goat anti-hamster (Armenian) IgG Antibody (0.5 mg/ml in PBS+0.02%NaN_3)
T hybridoma cells (from Ellis lab)
FBS
Asante Calcium Red (ACR) (2 mM in DMSO)
Imaging buffer (140 mM NaCl, 1.5 mM Na_2HPO_4, 50 mM HEPES, 0.8 mM $MgCl_2$, 1.6mM $CaCl_2$) or DMEM colorless medium
F-127 (3% in PBS)

1. Count the cell density.
2. Wash the cells with PBS 1X and then change the medium to RPMI 1640 colorless medium. Add the ACR (final conc 2 μM), FBS (3%), F-127 (final conc. 0.02%), make the cell density to 2 millions/mL.
3. Incubate the sample at 37C for 40 mins. Resuspend the sample every 10 mins.
4. Wash the sample with DMEM+3%FBS 2X. (1 mL each time).
5. Resuspend the sample in imaging buffer(or DMEM)+3% FBS. Make the cell density to 1×10^6 cells/mL. Total volume is ~1 mL.
6. Rest the cell for 15 mins at RT before collection. (Walk to medical center north)
7. Choose the Qdot655 to measurement the fluorescence change.
8. The cell will be collected for 1 min at first to set the baseline. Then add the 2C11 antibody (10 μL) to the sample and then run this for 1min, following adding anti-hamster IgG (10 μl) and collect events for 7 mins.
9. Add the Ionomycin (0.2 μL) and then run another 1 mins.

A.8 Ca^{2+} flux dye loading for single cell activation using optical trap

Materials:
T hybridoma cells (from Ellis lab)
FBS
Quest Rhod-4, AM (2 mM in DMSO)
colorless DMEM medium for hybridoma or colorless RPMI 1640 for naïve cells
F-127 (3% in PBS)

1. Cells were washed, resuspended at 2 million cells/ml in either colorless DMEM medium (Sigma-Aldrich) for cell lines or colorless RPMI 1640 (Life technology) for naïve cells, and loaded with Quest Rhod-4 at 2 μM for 40 mins in the presence of 3% (v/v) FBS, 0.02% (v/v) Pluronic F-127 (Sigma-Aldrich) in PBS at 37 ^{o}C.

2. Cells were gently pipetted every 10 min. T cells were then washed by 1 mL colorless DMEM medium, resuspended in 800 μL colorless DMEM (cell line) or colorless RPMI 1640 (naïve cell) with 3% (v/v) FBS and transferred to a cover glass flow cell for 1 h incubation at 37 ^{o}C, 5% CO_2 to allow for cell attachment to the cover glass surface.

3. After coating the surface with blocking buffer containing 5 mg/ml BSA in colorless DMEM medium for 10 min, pMHC-coated beads in A.4 in blocking buffer were flowed into the sample.

4. After 1h incubation at 37 ^{o}C, 5% CO_2, the slide was ready for manipulation using an optical trap combined with fluorescence.

A.9 Freezing cell protocol

This protocol will allow cleavage of hinge region in IgG antibody so that it only has one antigen binding site that can be used in Chapter 2, 3 and 4.

Materials:
FBS
DMSO
T-hybridoma
30 MBS desalting column

1. When cells have reached late log phase, determine cell density using Coulter counter. Calculate total number of cells in flask, and determine amount of freeze medium needed. (Cells should be resuspended in freeze medium at 1,500,000 2,000,000 cells/mL.).

2. Centrifuge cells in 15mL Falcon tube at 1200rpm for 5 minutes at 37 ^{o}C.

3. While cells are spinning, make freeze medium (e.g. 90% culture media, 10% DMSO). Label cryogenic vials with date, cell type, and users initials.

4. Suction away supernatant from centrifuged cells and add freeze medium. Triturate cells until homogeneous.

5. Quickly aliquot 1 mL of freeze stock per cryogenic vial. Screw each vial closed.

6. Store overnight cryo-freezing container to -80 ^{o}C freezer.

7. Next day, put cells into appropriate rack in liquid N_2 tank.

A.10 Cell thaw procedure

Materials:
Freezing cells in A. 11
Cell culturing medium
70% ethanol in DI water

1. Slowly remove appropriate tray rack from liquid N_2 tank. Remove long safety pin and take out one vial from appropriate tray.
2. Put tray back in slot and put safety pin back in place. Return tray rack to liquid N_2 tank again.
3. Rapidly thaw vial in 37 ^{o}C water bath until only a small ice pellet remains. Spray down vial with 70% ethanol, wipe, and place into hood.
4. Slowly add 9 mL of warm (37 ^{o}C) culture medium.
5. Since freeze medium contains (DMSO), spin down cells and resuspend in fresh medium (37 ^{o}C, 4-5 ml) in new T25 flask.

A.11 FBS deactivated

Materials:
FBS from sigma (500 ml)

1. Remove 500 mL bottle of FBS from -80 ^{o}C freezer and place in refrigerator to thaw overnight. Complete thawing of serum the following day by placing serum in a 37 ^{o}C water bath with a water level higher than the serum level in the bottle. Mix by inversion.

2. Once serum is completely thawed, incubate for an additional 15 min to allow serum to equilibrate with the 37 ^{o}C bath.

3. Raise the temperature setting of the bath to 56 ^{o}C. Use a timer to measure the 35 min needed for the temperature of the bath and serum to come to 56 ^{o}C. During this incubation, invert the bottle to mix the serum every 10 min. If necessary, allow and additional 5 min for bath to reach 56 ^{o}C.

4. Once bath reaches 56 ^{o}C, incubate serum for 30 min. Invert bottle every 10 min.

5. Remove serum from water bath and allow to cool at room temperature for 30 min. Reset water bath to the 37 ^{o}C mark.

6. Aliquot 20 mL of treated serum into conical tubes and store at 4 ^{o}C (short-term use) or freeze at -20 ^{o}C (long-term use) .